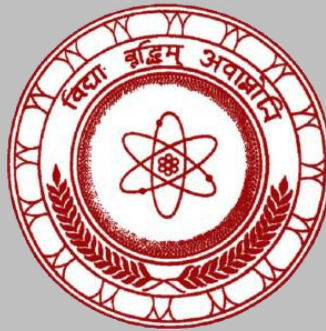# Journal of the Sri Lanka Association for the Advancement of Science

Founded in 1944 and incorporated by the Act of Parliament No 11 of 1966.

JSLAAS

TABLE OF CONTENTS

Assessment of the chemical facies of groundwater using factor analysis in the Chunnakam aquifer, Jaffna Peninsula

S. Arasalingam,[1] H. Manthrithilake,[1] S. Pathmarajah,[2] T. Mikunthan,[3*] and M. Vithanage[4]

[1]*International Water Management Institute, Sunil Mawatha, Battaramulla, Sri Lanka*
[2]*Department of Agricultural Engineering, Faculty of Agriculture, University of Peradeniya, Sri Lanka.*
[3]*Department of Agricultural Engineering, Faculty of Agriculture, University of Jaffna, Sri Lanka.*
[4]*Chemical and Environmental Systems Modeling Research Group, Institute of Fundamental Studies, Kandy, Sri Lanka.*

Abstract

The Jaffna Peninsula has four main types of aquifer systems, namely,Chunnakam (in the Valikamam area), Thenmaradchi, Vadamaradchi, and Kayts. The water resources of the Valikamam region depend totally on rainfall recharge to the Miocene limestone aquifer. Valikamam is an intensified agricultural and high population density area in the Jaffna Peninsula. Groundwater is an extremely valuable resource and the pollution of groundwater resources is a matter of serious concern in the Jaffna Peninsula. Therefore, this study examines the hydro-chemical facies of groundwater in the Chunnakam aquifer using factor analysis. Forty four wells were selected to represent the entire Chunnakam aquifer during the months of January, March, April, July and October 2011 to denote various rainfall regimes within a year. Samples were analyzed for Electrical Conductivity (EC), pH, chloride, nitrate as nitrogen, calcium, magnesium, carbonate, bicarbonate, sulfate, sodium and potassium concentration based on Sri Lankan Standard (SLS) procedure. Groundwater was classified based on the Chadha diagram and factor analysis was performed using software XLSTAT 2012. Interpretation of the hydro-chemical analysis reveals that the groundwater of Chunnakam aquifer is alkaline in nature. All water quality parameters except EC, NO_3^- as N, and SO_4^{2-} are within the Sri Lankan Standard for drinking purposes. Two major hydro-chemical facies Ca^{2+}-Mg^{2+}-Cl^- and Na^+-Cl^--SO_4^{2-} were identified using the Chadha diagram and permanent hardness and salinity problems were deemed probable. Salinization, water–soil/rock interaction, and anthropogenic activities are identified in the factor analysis. Salinity development and high nitrate as nitrogen content in drinking water are problems identified in the Chunnakam aquifer.

Keywords:Chunnakam aquifer, factor analysis, groundwater, salinity, Jaffna Peninsula.

1. INTRODUCTION

The suitability of groundwater for drinking, irrigation, and other domestic purposes depends on its quality. Naturally, changes in groundwater quality are due to variations in climatic conditions, the duration of the presence of aquifer material in the water, and soil inputs during percolation

---

*Corresponding author. E-mail:tmikunthan@yahoo.co.in

(Krishnakumar*et al.*, 2008). Anthropological activities have become a major reason for groundwater pollution in recent times. In particular, the haphazard disposal of urban and industrial waste, overuse of agrochemicals, and the unplanned disposal of human waste are the main sources of groundwater pollution in many countries. The Jaffna Peninsula lies in the northern most part of Sri Lanka and its population depends entirely on groundwater resources to meet all of their water requirements (drinking, irrigation, etc.). The Peninsula has four main aquifer systems, namely, Chunnakam (Valikamam area), Thenmaradchi, Vadamaradchi, and Kayts (Punthakey and Gamage, 2006). All four aquifers depend on rainfall recharge, which is their only source of fresh water. Groundwater is an extremely valuable resource and the pollution of groundwater resources is a matter of serious concern. Among the major threats to groundwater from which drinking water supplies are obtained are leachates from human and animal waste matter along with other chemical pollutants. Agricultural leachates often contribute significantly to groundwater pollution.

Understanding groundwater characteristics is important for groundwater management in the Jaffna Peninsula. Early studies on the characterization of groundwater facies and chemical evolutionary history utilized the graphical representation of major ionic compositions of groundwater (Piper, 1944; Stiff, 1951). These schemes were useful in visually describing differences in major ion chemistry in groundwater and in classifying water compositions into identifiable groups (Freeze and Cherry, 1979), which are usually of similar genetic history. Recently, factor analysis has been used with remarkable success as a tool in the study of groundwater chemistry. Therefore, this study aimed to characterize the hydro-chemical quality of groundwater in the Chunnakam aquifer using factor analysis and relating them to specific geochemical processes to ensure the better water resource management.

2. EXPERIMENTAL

Description of the studied area

The major rainy season in the Peninsula occurs during the North-East monsoon from October to December.The South-West monsoon provides rainfall in April and May but the amount of rainfall is less compared to that of the North-East monsoon. The period between the South-West monsoon and the North-East monsoon is the dry season and extends from June to September. The major soils are the calcic red-yellow latosols which are shallow (less than 2m deep), fine textured and well-drained and have a very rapid infiltration rate (De Alwis and Panabokke, 1972).Agriculture is the main source of livelihood for 65% of the population and about 34.2% of the land is cultivated intensively for commercial purposes with high value cash crops (Thadchagini and Thirudchelvam, 2005).The land in the Jaffna Peninsula can be characterized as flat with less than a 5% slope. The Chunnakam aquifer feeds most parts of the Valikamam area, which is highly populated and practises intensive agriculture.

Selection of wells

Forty-four wells were selected for long- term water quality monitoring in a systematic manner, to represent the entire Chunnakam aquifer. An identification number was painted on each well. These wells were selected to represent different uses such as wells used solely for domestic purposes, those with domestic and home gardening uses, public wells for drinking, and farm wells. Figure 1shows the locations of the wells selected for the monitoring.
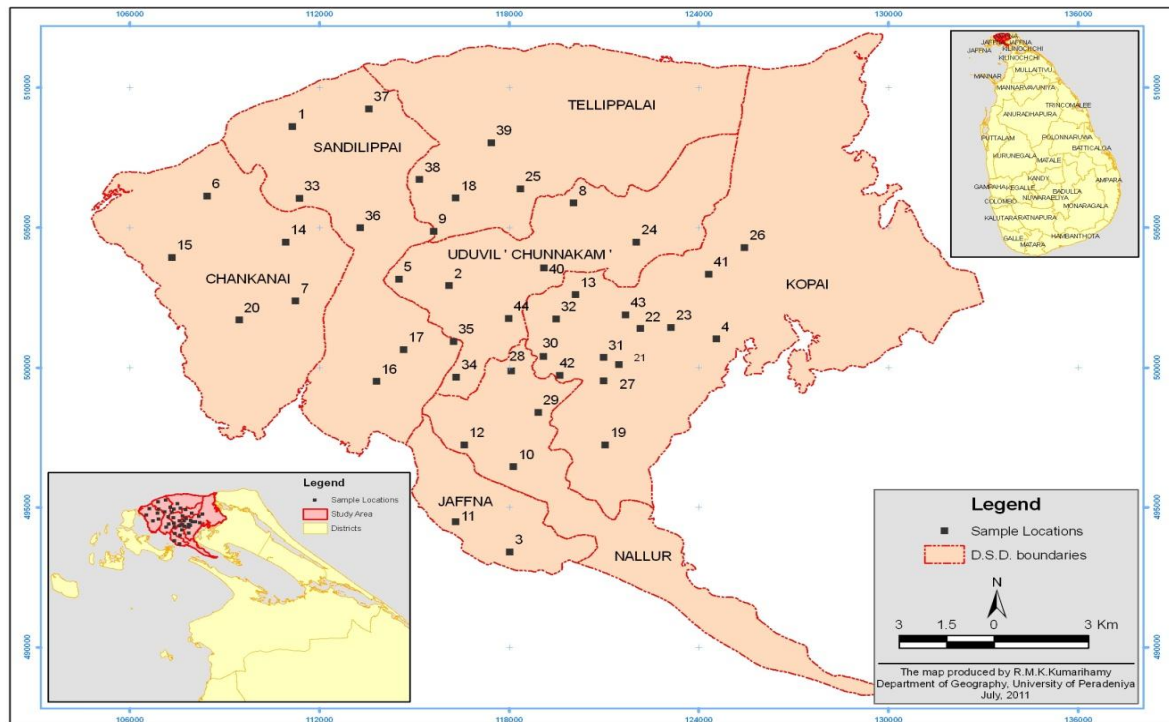
Figure 1: Location of selected wells with different uses in the Chunnakam aquifer

Collection of water samples

Water samples were collected for chemical analysis five times during the year, to cover various rainfall regimes: mid-January, early March, mid-April, mid-July, and mid October, 2011. Each sample was poured into 1 liter plastic bottles, which had been rinsed several times with the same well water. These bottles were tightly closed, labeled, and transported to the laboratory of the National Water Supply and Drainage Board (NWS&DB), Jaffna, for analysis within 48 hours of collection.

Analytical techniques

Samples were analyzed for electrical conductivity (EC), pH, chloride, nitrate as nitrogen, calcium, magnesium, carbonate, bicarbonate, sulfate, sodium and potassium concentrations. Conductivity meters and pH meters were used to measure the EC and pH respectively. Chloride concentration was measured by silver nitrate titration. Nitrate-N concentration was estimated using a colorimetric spectrophotometer. The calcium and magnesium content was determined by EDTA titration using the Eriochrome black T as the indicator. The carbonate and bicarbonate content was measured by acid-base titration. The sulfate content was estimated by the turbidimetric method using a turbidity meter. Sodium and potassium contents were determined by using a flame photometer at the National Institute of Fundamental Studies (NIFS), Hantana, Kandy. The procedures of the analysis were based on Sri Lankan Standard 614 (SLS, 1983).

Groundwater was classified based on the Chadhadiagram (Chadha, 1999). This technique examines the relationships between variables (such as chemical parameters in groundwater), shown in a number of cases (such as sampling points).Factor analysis was performed using software XLSTAT 2012. The principal factor method was applied iteratively to generate several factors enhanced by the selection of

varimax rotation to facilitate interpretation of the results. The variance of a factor is described by the factor's Eigen value. Eigen values of 1.0 or greater are considered significant (Kim and Mueller, 1987). The output of factor analysis is a list of significant factors, with each factor grouping several chemical parameters. Once the factors have been determined, factor scores can be calculated for each case. In considering groundwater quality, factor scores calculated for each case (sampling point) can be plotted on contour diagrams to get the distribution of factors within an aquifer (David *et al*., 2004). The interpretation was based on rotated factors, rotated loadings and rotated Eigen values. Spatial distribution maps for different factors were developed using ArcGIS 10. Here, the Inverse Distance Weighted interpolation technique was used to develop the maps.

3. RESULTS AND DISCUSSION

Hydro-chemical characteristics

The chemical compositions of the groundwater samples were statistically analyzed and the obtained results are summarized in Table 1. The EC of the water samples is an indicator of their salinity. The values of EC ranged from 556 to 4701 µS/cm, with a mean of 1534µS/cm. This behavioral response was used to determine the nature of salinity in the studied area. The chloride concentrations of water samples were between 153.9 mg/L and 1146 mg/L and the mean value was 327.4 mg/L. All values of measured wells were below the permissible level of the Sri Lankan Standard (SLS) for drinking. All wells were suitable for drinking. The results revealed that pH ranged from 7.20 to 8.26 and all groundwater samples were found to be below the desirable SLS level for the pH value of drinking water with a mean of 7.53 and slight alkalinity.

Table 1: Statistical summary of the hydro chemical parameters of groundwater

Variable	Minimum	Maximum	Mean	Std. deviation	SLS for drinking water	
					Max Des	Max Per
EC	556.0	4701.0	1534.3	1045.7	750	3500
Cl^-	153.9	1146	327.4	246.2	200	1200
pH	7.20	8.26	7.53	0.17	7-8.5	6.5-9.0
NO_3^- -N	0.28	13.9	4.9	4.0	-	10
Ca^{2+}	58.9	203.1	95.5	35.7	100	240
Mg^{2+}	4.27	20.9	10.2	3.5	30	150
CO_3^{2-}	11.7	61.4	28.2	9.5	-	-
HCO_3^-	158.5	545.8	258.7	91.0	-	-
Na^+	17.7	763	149	172	-	-
K^+	0.39	92.0	9.14	15.0	-	-
SO_4^{2-}	35.2	499.5	151.0	106.7	200	400

Except pH and EC (µS/cm), the others parameters are expressed in mg/L**.**

SLS: Sri Lankan Standard

The nitrate- N concentration ranged from 0.28 to 13.9 mg/L. The values of all domestic, domestic with home garden and public wells were recommended for drinking because the average value of nitrate-N was below the limit of the Sri Lankan drinking water standard. Some of the farm wells exceeded the limit of the Sri Lankan drinking water recommended level of 10 mg/L and was not suited for drinking.

The farmers practiced applying excessive amounts of inorganic fertilizer, which leaches out to the shallow groundwater. But all farm wells were below the irrigation requirement of 30 mg/L. The concentration of calcium values of selected wells varied from 58.9 mg/L to 203.1 mg/L and magnesium values of selected wells varied from 4.27 mg/L to 20.9 mg/L. All wells measured were below the desirable SLS level for drinking water. The concentration (mg/L) of other ions varied as CO_3^{2-} from 11.7 to 61.4; HCO_3^- 158.5 to 545.8; Na^+ 17.7 to 763; K^+ 0.39 to 92.0; and SO_4^{2-} 35.2 to 499.5.

Classification of groundwater based on chemical facies

The Chadha diagram is a somewhat modified version of the Piper diagram (Piper, 1944) and the expanded Durov diagram (Durov, 1948).This diagram is used to classify the groundwater and identify hydro-chemical processes (Chadha, 1999). In Chadha's diagram (Figure 2), the difference in the milliequivalent percentage between alkaline earths (Ca^{2+} + Mg^{2+}) and alkali metals (Na^+ + K^+) expressed as percentage reacting values is plotted on the X axis, and the difference in the milliequivalent percentage between weak acidic anions (CO_3^{2-} + HCO_3^-) and strong acidic anions (Cl^- + SO_4^{2-}) is plotted on the Y axis.

From this diagram, 68 % of groundwater samples fall within the field of 6 which belong to Ca^{2+}-Mg^{2+}-Cl^- type hydro-chemical facies. Such water has permanent hardness and does not deposit residual sodium carbonate in irrigation use. Another 32% of groundwater samples fall within the field of 7, which belong to Na^+-Cl^--SO_4^{2-} hydro-chemical facies and represent Na^+-dominant Cl^- -type or Cl^--dominant Na^+ -type waters. Such water generally creates salinity problems both in irrigation and drinking use.

1. Alkaline earth exceeds alkali metals.
2. Alkali metals exceed alkaline earth.
3. Weak acidic anions exceed strong acidic anions.
4. Strong acidic anions exceed weak acidic anions.
5. Represent Ca^{2+} -Mg^{2+}-HCO_3^- type.
6. Represents Ca^{2+} -Mg^{2+}-Cl^- type.
7. Represent Na^+-Cl^-- type, Na_2SO_4-type.
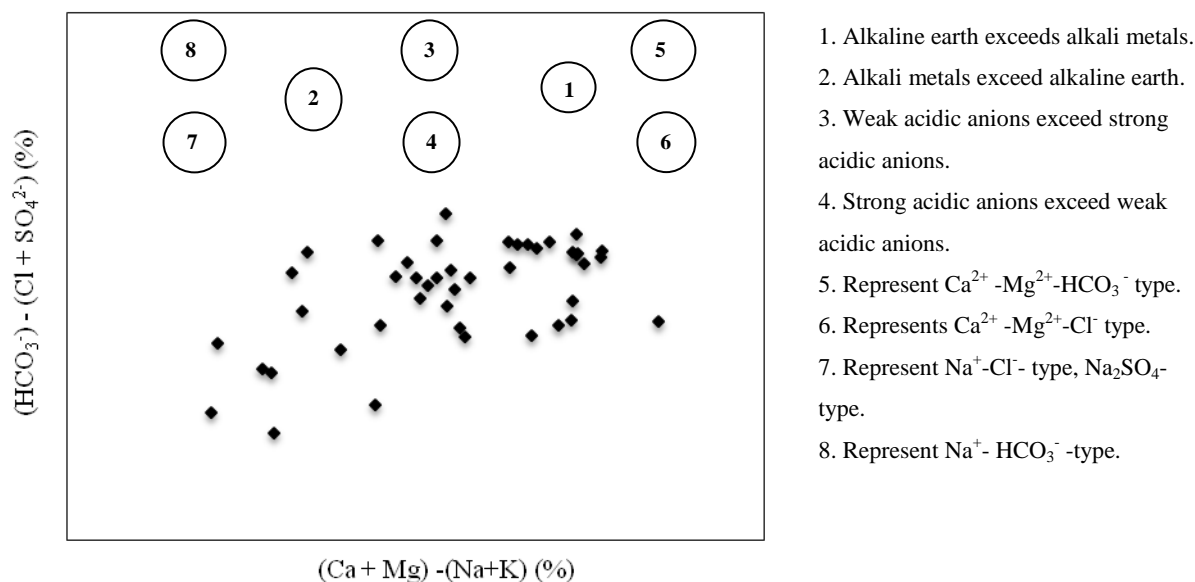8. Represent Na^+- HCO_3^- -type.

Figure 2: Groundwater quality plotted on Chadha diagram

Factor analysis

Factor analysis is a useful tool for interpreting commonly collected groundwater quality data and relating them to specific geochemical processes. Its aim is to reduce the complex patterns of correlation among many parameters to simpler sets of 'factors', which are then interpretable.

Correlation matrixes of chemical data for the groundwater of the Chunnakam aquifer are given in Table 2. High correlation (> 0.80) is observed between EC and Cl^- (0.95), EC and Na^+ (0.94), EC and Ca^{2+} (0.88), EC and SO_4^{2-} (0.87) as well as EC and HCO_3^- (0.84), due to sea water intrusion. The EC of groundwater is the most efficient water quality parameter used in detecting salinity. It was found that significant correlation exists between salinity and major components of seawater (Na^+, Cl^- and SO_4^{2-}). This is an indication of seawater influence on groundwater salinity. High correlation is also observed between Cl^- and Na^+ (0.92) as well as Cl^- and Ca^{2+} (0.87), which also contributed to the salinity and hardness of groundwater. Certain areas of the Jaffna Peninsula also experience salinity in groundwater as a result of over extraction (Navaratnarajah, 1994). In general, there were two main factors that played an important role in the quality of the water in the aquifer: (i) anthropogenic factors: over abstraction of freshwater from the aquifer, and (ii) natural factors: mixing of seawater and freshwater at the sharp interface (Aris, *et al*., 2007).

Table 2: Pearson Correlation matrix of the groundwater aquifer

Variables	EC	Cl^-	pH	NO_3^-	Ca^{2+}	Mg^{2+}	CO_3^{2-}	HCO_3^-	Na^+	K^+	SO_4^{2-}
EC	1										
Cl^-	**0.95**	1									
pH	-0.18	-0.13	1								
NO_3^-	-0.34	-0.36	0.00	1							
Ca^{2+}	**0.88**	**0.87**	-0.20	-0.16	1						
Mg^{2+}	0.50	0.48	-0.22	-0.17	0.55	1					
CO_3^{2-}	0.38	0.35	0.05	-0.57	0.20	0.21	1				
HCO_3^-	**0.84**	0.76	-0.24	-0.44	0.74	0.45	0.48	1			
Na^+	**0.94**	**0.92**	-0.06	-0.40	**0.77**	0.43	0.42	**0.79**	1		
K^+	0.61	0.56	-0.25	-0.18	0.69	0.60	0.26	0.50	0.45	1	
SO_4^{2-}	**0.87**	0.76	-0.17	-0.26	**0.78**	0.51	0.43	0.74	**0.79**	0.71	1

The rotated factor loading, Eigen values, percentages of variance, and cumulative percentages of variance associated with each factor for principal factor analysis are summarized in Table 3. Two factors with respective eigen values closer or greater than one were identified which account for above 65 % of the total chemical parameters in the original data set.

The pairs of factors are plotted on the bi-plot diagram (Figure 3), which explains the positive and negative loading of the parameters on each factor. It is clear from the diagram that most of the parameters have positive loading on factor 1 and factor 2.

Table 3: Factor pattern after Varimax rotation in the Chunnakam aquifer

Variables	F1	F2
EC	**0.888**	0.419
Cl^-	**0.828**	0.406
pH	-0.264	0.085
NO_3^-	-0.074	**-0.716**

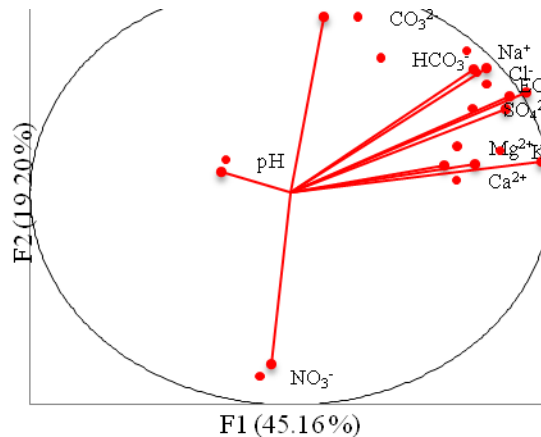|		
Ca^{2+}	**0.947**	0.129
Mg^{2+}	0.580	0.114
CO_3^{2-}	0.127	**0.734**
HCO_3^-	0.693	0.519
Na^+	**0.739**	0.524
K^+	0.698	0.122
SO_4^{2-}	**0.811**	0.352
Eigenvalue	6.110	0.969
Variability (%)	45.157	19.201
Cumulative variance %	45.157	64.358

Figure 3: Factor loading (F1 and F2:64.36 %) after varimax rotation

The following factors are indicated:
Factor 1: EC, Cl⁻, Na^+, Ca^{2+} and SO_4^{2-}
Factor 2: CO_3^{2-} and NO_3^- as N

Factor 1 has a high loading of EC, Cl⁻, Na^+, Ca^{2+} and $SO_4^{2-}$and explains 45 % of the total variance (Table 3). The concentration of Na^+, Cl⁻, and SO_4^{2-} in seawater is much greater than in continental water. This factor can be ascribed to the intrusion of seawater into the aquifer system, which increases the concentration of these ions and hence the values of the dissolved solids. Figure 4 shows a similar pattern between the score of factor 1 and EC. Therefore, *Factor 1* is defined as the salinization factor and is an indication of seawater intrusion in the studied aquifer.

The spatial distribution of factor 1 parameters is presented as an iso-scores map, shown in Figure 5. The high values are indicated with dark grey representing high salinization regions, and the low values are shown with light grey denoting low salinization regions. This indicates the intensity of saltwater activity to be more prevalent closer to the coast and decreasing inland in the Jaffna Peninsula.Several wells once used to supply potable water are not in use now due to the increase of salinity in the Jaffna Peninsula

(Nandakumar, 1983). Puvaneswaran (1985) reported that the salinity of groundwater in a location at the Valukaiaru drainage basin of the Valikamam area is inversely related to its distance from the sea.
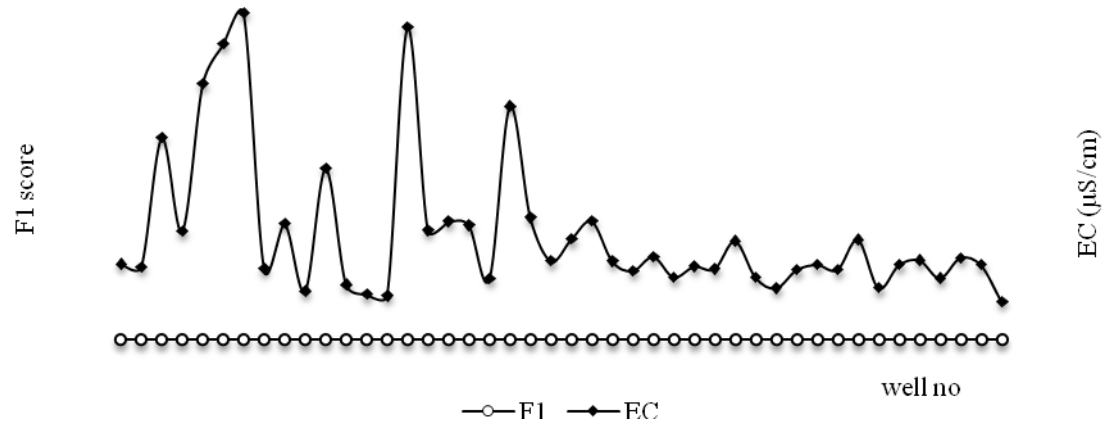
Figure 4: Relationship between the F1 score and EC of groundwater
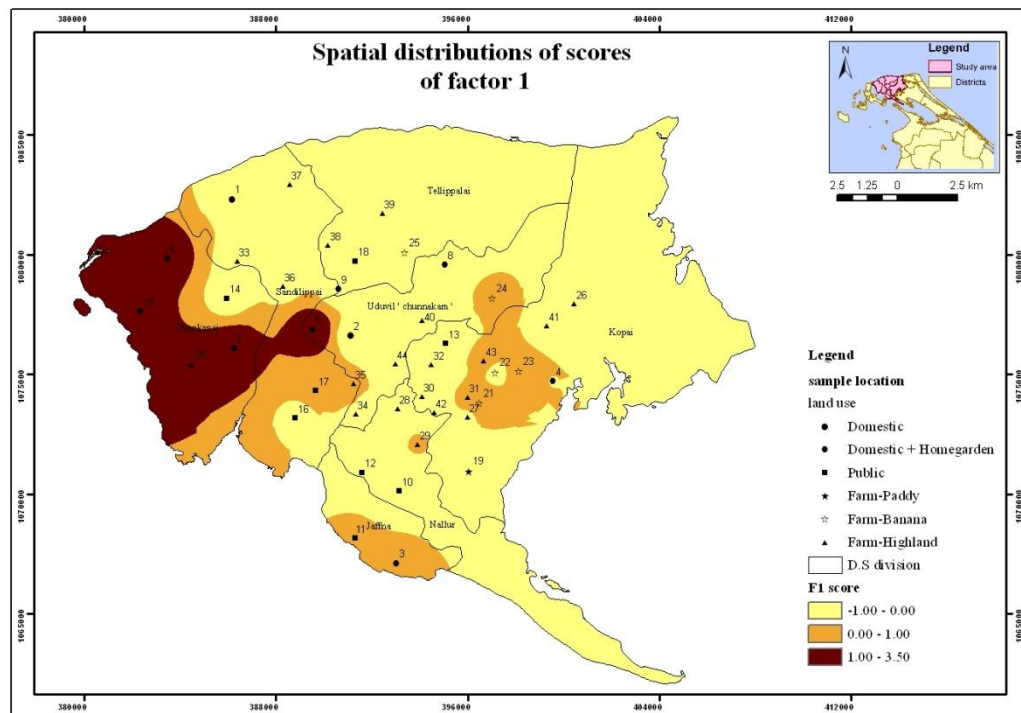
Figure 5: Spatial distribution scores of Factor 1 in Chunnakam aquifer

A significant factor that has contributed to increased salinity in the well water has been the indiscriminate extraction of water from underground aquifers. This has been exacerbated by the increase in population in the region and the rapid rate of extraction using pumps, both electric and petrol- driven, for domestic and agricultural purposes (Navaratnarajah, 1994).

Factor 2, which explains 19 % of the total variance, has a strong positive loading on CO_3^{2-} (Figure 6) and a negative loading on NO_3^- as N (Figure 7). The negative loading of NO_3^- as N on factor 2 confirms that the concentration of NO_3^- as N in the groundwater does not contribute significantly to CO_3^{2-} values.
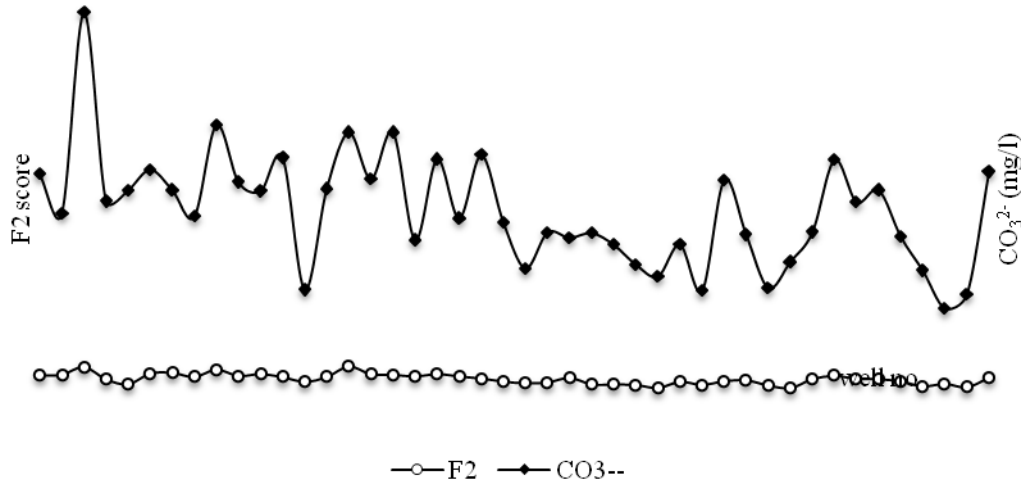
Figure 6: The relationship between F1 score and CO_3^2 of groundwater
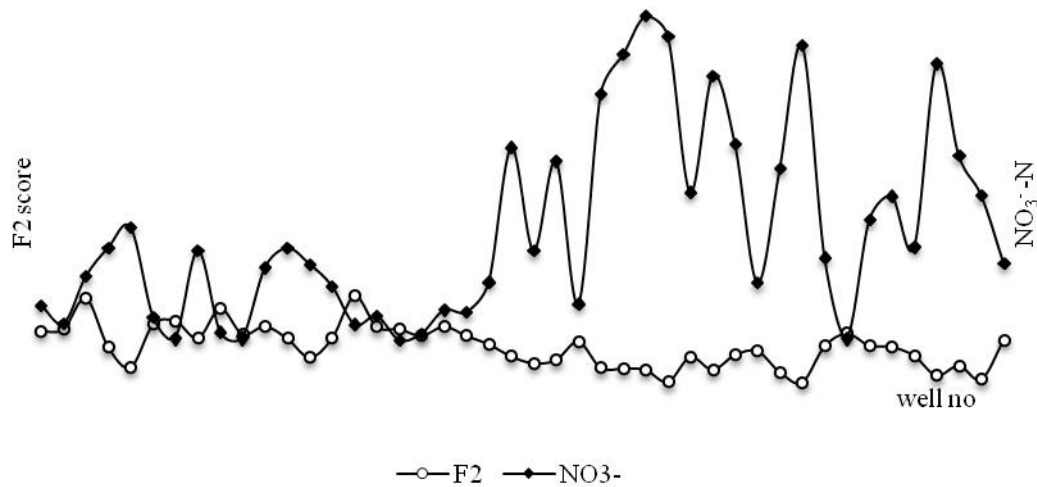
Figure 7: Relationship between F1 score and NO_3^- of groundwater

The limestone aquifer is rich in carbonates. Hence water flowing through limestone brings the carbonate to the groundwater, which increases the alkalinity. The main sources of natural alkalinity are rocks, which contain carbonate, bicarbonate and hydroxide compounds. Further, the high concentration of NO_3^- as N may be derived from the continuous use of fertilizer chemicals in the agricultural fields. This is due to the fact that nitrate as nitrogen has no significant lithologic source and must be associated with the anthropogenic activities (Belkhiri*et al*., 2010). Therefore, Factor 2 reflects the signatures of water-soil/ rock interaction and anthropogenic activities.

Figure 8 shows the spatial distribution of the scores of Factor 2. The high scores are shown with dark grey, indicating water-soil/ rock interaction and a high alkalinity aquifer. The negative low scores are indicated with light grey, revealing a high nitrate-N-polluted aquifer. These areas come under intensified agriculture. Dissanayake and Weerasooriya (1985) pointed out in the hydro geochemical atlas of Sri Lanka that the Jaffna Peninsula has the highest nitrate content of groundwater in Sri Lanka. They also mentioned that the major factors responsible for poor water quality in the Jaffna Peninsula are the abundant use of agricultural fertilizers, mainly urea, use of cattle manure and the discharge of human excreta in the form of soakage pits.
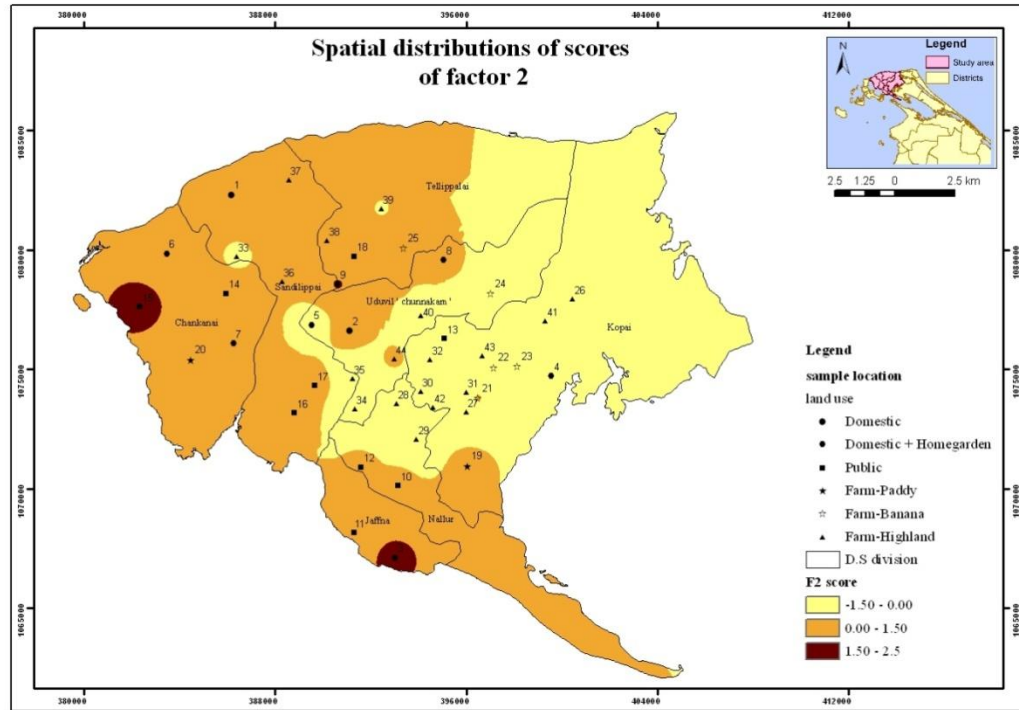
Figure 8: Spatial distribution scores of factor 2 in Chunnakam aquifer

4. CONCLUSION

This study demonstrates the effectiveness of factor analysis in assessing the hydro-chemical processes of groundwater and also provides preliminary assessment of groundwater quality, that will serve as a data base for the future investigations and monitoring of groundwater quality in the study area. Interpretation of hydro-chemical analysis reveals that the groundwater of the study area is alkaline in nature. Except for EC, NO_3^- as N and SO_4^{2-} values, all the others parameters of groundwater quality are within the Sri Lankan Standard (SLS) for drinking purposes. Two major hydro-chemical facies,Ca^{2+}-Mg^{2+}-Cl^- and Na^+-Cl^--SO_4^{2-}, were identified using the Chadha diagram. Accordingly, permanent hardness and salinity problems are probable. In factor analysis, the first salinization factor accounts for 45% of the total variance and includes the variables of EC, Cl^-, Na^+, Ca^{2+}, and SO_4^{2-}. The second signature of water-soil/rock interaction and anthropogenic activities factor specifies 19% and contains the variables of a strong positive loading on CO_3^{2-} and a negative loading on NO_3^- as N. It follows that

either naturally occurring processes or human activities may have a significant impact on the water quality of the Chunnakam aquifer.

REFERENCES

1. Aris, A. Z., Abdullah, M. H., Ahmed, A. and K. K. Woong. (2007). Controlling factors of groundwater hydrochemistry in a small island's aquifer. *International Journal of Environmental Science and Technology,* 4 (4): 441-450.

2. Belkhiri1, L., Boudoukha, A., and L. Mouni. (2010). Groundwater quality and its suitability for drinking and agricultural use in AinAzel plain, Algeria, *Journal of Geography and Regional Planning.* 3(6): 151-157.Available online at http://www.academicjournals.org/jgrp

3. Chadha, D. K.(1999). A proposed new diagram for geochemical classification of natural waters and interpretation of chemical data.*Hydrogeologial Journal* 7: 431-439.

4. David, L., Dieter, H., Amos, A., and Roumiana, H. (2004). Factor analysis as a tool in groundwater quality management: two southern African case studies. *Physics and Chemistry of the Earth.*29: 1135–1143.

5. De Alwis, K. A., and Panabokke, C. R. (1972).*Handbook of soils of Sri Lanka (Ceylon).*Soil science society, Ceylon. 2:1-97.

6. Dissanayake, C.B., and Weerasooriya, S.V.R. (1985).*The hydro geochemical atlas of Sri Lanka*.Natural resources, energy and science authority of Sri Lanka, Colombo, pp: 17-26.

7. Durov, S.A. (1948). Natural waters and graphic representation of their compositions.*AkademiyaNauk SSSR Doklady.*59: 87-90.

8. Freeze, R.A. and Cherry, J.A., (1979).*Groundwater.*Prentice- Hall, Englewood Cliffs, New Jersey. pp 604.

9. Kim, J. O. and Mueller, C. W.(1978a). Introduction to factor analysis: What it is and how to do I. Sage University paper series on quantitative applications in the social sciences, series no. 07-013, Beverly Hills, CA: Sage Publications.

10. Krishnakumar, S., Rammohan, V., Sahayam, J. D., and Jeevanandam, M. (2009).Assessment of groundwater quality and hydrogeochemistry of Manimuktha River basin, Tamil Nadu, India.*Environmental Monitoring Assessment*.159(1-4):341-351.

11. Nandakumar, V. (1983).Natural environment and groundwater in Jaffna Peninsula, Sri Lanka.*Climatological notes*, Tsukuba, Japan. 33:155-164.

12. Navaratnarajah, V. (1994).Water problems in the Jaffna Peninsula.Paper presented at the '20th WEDC conference in affordable water supply and sanitation'. Colombo, Sri Lanka.

13. Piper, A.M. (1944). A graphic procedure in geochemical interpretation of water analyses.*American Geophysical Union Transactions*.25: 914-923.

14. Punthakey, J. F., and Nimal, P.D. (2006). Coupled flow and salinity transport modelling and assessment of groundwater availability in the Jaffna Peninsula, Sri Lanka. 32nd WEDC International Conference. 2006. Colombo, Sri Lanka. pp 326-327.

15. Puvaneswaran, P. (1986). Geomorphology of the Valukkaiaru drainage basin, Sri Lanka.*Journal of South Asian studies*. 1:43-58.

16. Rajasooriyar, L., Mathavan, V., Dharmagunawardhane,H. A., and Nandakumar, V.(2002). Groundwater quality in the Valigamam region of the Jaffna Peninsula, Sri Lanka.*Sustainable Groundwater Development.*Geological Society, London.193:181-197.

17. Sri Lanka Standard 614: Part 1 (1983). Specification for potable water physical and chemical requirements.pp 5-10.

18. Stiff, H.A., Jr. (1951).The interpretation of chemical water analysis by means of patterns.*Journal Petroleum Technoogy.*3(10): 15-17.

19. Thadchayini, T. and Thiruchelvam, S. (2005). An economic evaluation of drip irrigation project for banana cultivation in Jaffna district.*In*Galagedara, L.G. (Ed).*Water resources research in Sri Lanka.* Symposium proceedings of the water professionals' day- 2005.

Nutritional assessment of pre-school children of aged between 3-5 years in Kattankudy D.S.division of Batticaloa district

M. R. Roshana[*] and T. Mahendran

Department of Agricultural Chemistry, Faculty of Agriculture, Eastern University, Sri Lanka.

Abstract

The study was conducted in Kattankudy D.S.Division of Batticaloa district of Sri Lanka to assess the nutritional status of pre-school children. The study sample consisted of 100 children between 3 and 5 years of age. A pre-tested questionnaire was used to collect information on socio-economic status, dietary assessment, household information, anthropometric measurements, and nutritional knowledge of the mothers. Anthropometric measurements of weight, height, mid-upper-arm, head and chest circumference were collected using a standardized procedure. From those measurements anthropometric indices of height-for-age, weight-for-height, and weight-for-age were generated. The height and weight of the children were measured using properly calibrated equipment. The study revealed that 72% of the children are in normal nutritional status, 19.2% of the children are wasting and underweight, and 8.6% of the children are stunted. When educational levels of parents are concerned, it was satisfactory as 77% of mothers and 81% of fathers had secondary education. Also there were mothers with tertiary education (16%) and fathers with tertiary education (10%).The average income of the 38% of the total families was more than Rs. 40,000 per month.Only 7% of the families earn less than Rs.10,000 per month. They consume rice as the main meal, and with that, they use all types of meat (other than pork), fish, egg and green vegetables.It is concluded that the nutritional status among pre-school children between 3-5 years in Kattankudy D.S. division of Batticaloa district is satisfactory. Nutritional status of the children of this area can be furtherimproved by providing nutritional interventional programmes.

Key words:*Anthropometric measurements, malnutrition, nutritional assessment,*

1.INTRODUCTION

Nutrition of pre-school children is very important, because the foundation for lifetime health, strength and intellectual vitality is laid during this period. A significant proportion of deaths of young children worldwide is due to malnutrition and efforts to reduce malnutrition should be animportant task (Caulifield*et al*., 2004). The level of childhood malnutrition is exceptionally high in South Asia, ranging from 45-48% in India, Bangladesh and Nepal to 38% in Pakistan and 30% in Sri Lanka. The underlying

---

[*]Corresponding author. E-mail: mrroshana30@gmail.com

causes of malnutrition include poverty, low levels of education, and poor access to health services (Khan and Bano, 2007).Growth monitoring is globally used to assess nutritional status and the health and development of individual children, and also to assess the overall nutritional status and health of the populations. Compared to other health assessment tools, measuring child growth is a relatively inexpensive, easy to perform, and non-invasive process.

Malnutrition in Sri Lanka continues to prevail at relatively higher levels. About 2.3% of children under five (40,000) suffer from Severe Acute Malnutrition. Poor nutrition also negatively affects school participation and performance. Sri Lanka Demographic and Health Survey highlighted (2016) that 17%, 4%, 15%, 3%, 21%, and 4% of Sri Lankan children are stunted, severely stunted, wasted, severely wasted, underweight, and severely underweight, respectively (Department of Census and Statistics, 2016). Regarding micronutrient deficiencies, nearly 19% of the population was diagnosed as iodine deficient. About 45% of pre-school childrenand 58% of children 5 to 11 years old suffer from anemia. More than 30% of pre-school children have marginal serum values of vitamin A (WHO, 2009).Adequate nutrition and health care during the first several years of life is fundamental to the attainment of the Millennium Development Goals (MDGs) for child survival and the prevention of malnutrition (Lutter, 2003).

Nutritional abnormalities in children are not only affected by food intake, but also by access to health services with support and quality of care for the children and pregnant mothers, as well as good hygiene habits.Although inadequate food intake is a basic cause of under-nutrition, several other factors such as living standards, water and sanitation, birth weight, birth interval and parity, weaning practices, and mother's education have been identified as contributing to incidence of malnutrition among preschool children.

There are several factors that can influence children's eating practices. Parents are one of the factors that play an important role for the development of their children. Research done by Vareecken and Maes (2010) found that children's eating practices were influenced by their mother's nutritional knowledge. The parenting attitudes had an influence on the children's weight and dietary intake. Khandare*et al*. (2008) identified that health status of the mothers, dietary and socio economic factors can influence the nutrient intake among children. Chang *et al*. (2010) reported that low nutritional status in childhood can affect brain development. This will cause under-nutrition and poor nutritional status of the children, and can become a risk to develop a disease in their later life.

One approach to studying nutrition is to assess nutritional status on the basis of anthropometric indicators. These are based on physical body measurements such as height and weight (Jeffrey, 2006).Anthropometric indices represent the cumulative effect of access to food, nutrition practices, health, education of parents and environmental health conditions. Therefore, the nutritional status is a powerful indicator of nutrition status and well-being of an individual, and reflects the nutritional and poverty situation of a household. The nutritional status of pre-school children is a sensitive indicator, because children are most vulnerable to nutritional imbalances.

Indices of protein energy malnutrition (PEM) needs to be linked to simple anthropometric parameters. There is a need also to compare mental and academic performance of this group of children with their nutritional status, hence the need for this work.This study was carried out to determine the nutritional status of children between 3 and 5 years of age in Kattankudy D.S Division of the Batticaloa district to

find the correlation between anthropometric indicators and issues of malnutrition among primary school children.

2. METHODOLOGY

2.1 Selection of Samples

The study population included children aged 3-5 years in the Kattankudy area. Data collection was carried out at the primary school level. Ten pre-school children were selected from each of 10 pre-schools in the Kattankudy area. The total number of samples was 100 children. Simple random sampling method was used for the selection of the study population. Children 3 to 5 years old and free from any medical disorder such as asthma, congenital heart failure, diabetes mellitus, and kidney diseases were considered for this study. Children <3 years or >5 years old were excluded from this study.

2.2 Data collection

A questionnaire was designed which includes socio- economic and health related questions and anthropometric measurements such as weight, height, and age. Questionnaires were pre-tested before collecting data to adjust the questionnaire adequately and to avoid systemic errors. After that the questionnaires were finalized and printed. Interviews with parents were used to obtain general information about nutritional status of children. Data was collected from the children's mothers, who belong to various socio-economic groups. Written informed consent was obtained from all the participants of this study.

2.3 Anthropometric measurements

Anthropometric measurements were undertaken for all subjects, such as height, weight, mid-arm circumference, chestcircumference, and head circumference. For measuring weight, the children were asked to stand straight in the middle of the scale's platform without touching anything and the eyes are looking at the horizontal line. For the height measurement, the children were asked to stand straight and look straight in a horizontal plane while the top of thestadiometer was lowered to the top of the head. Mid-upper-arm circumference is a measure of the diameter of the upper arm, and gauges both fat reserves and muscle mass. It is primarily used for children. It was measured by a flexible measuring tape. Measurements were taken on left hand at the level of the midpoint between acromion and olecranon, with the elbow flexed.For head circumference measurement, the tape was firmly placed over the glabella and supra-orbital ridges anteriorly and that part of the occiput posteriorly that gives maximal circumference of the head.Chest circumference was taken at mid inspiration at the level of xiphoid cartilage or sub sternal notch, in the plane at right angles to the vertebral column.

3. RESULTS AND DISCUSSION

3.1Distribution of Children by Gender and Age

Distribution of children by gender and age are shown in Figure 1. According to the survey, the children aged 3–5 years includes 48% males and 52% females in the Kattankudy area.Out of 100 children, 21

were three years, 37were four years, and 42 were five years of age. Most of the mothers participated in the survey. This helped this survey to get more household and dietary information.
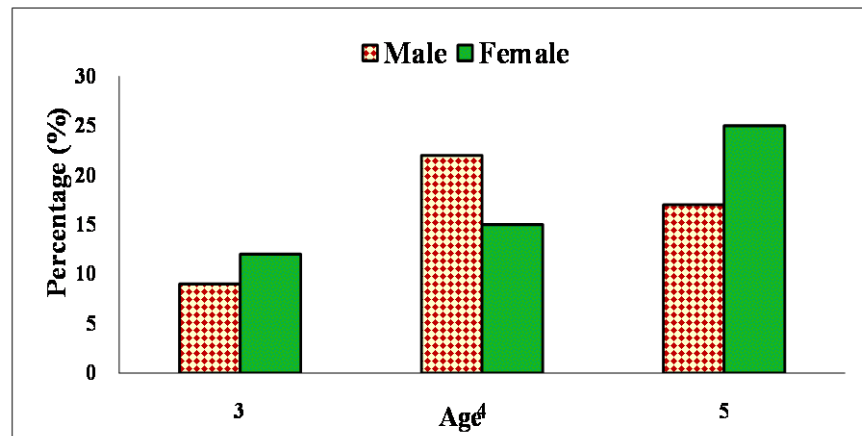

Figure 1: Distribution of Children by Gender and Age

3.2 Food Intake

The consumption of food items which are eaten by the children was surveyed. They consume rice as the main meal, and also with that, they select all types of meat (except pork), fish, eggs and green vegetables. They consume meat three times per week. Parents with high socioeconomic status can afford first class proteins like milk, egg, meat, etc., which are sourced mainly from animals. This study showed that there is moreconsumption of proteinrich animal foods in this area. Protein rich foods directly affect the malnutrition situation of children. The children in this area are also consuming more vegetable and dairy products. Therefore, we can significantly reduce the anemia and iron deficiency which are associated with low nutritional status.The habitual intake of chocolates, soft drinks and fast foods like tip tip were higher among preschool children. It was also observed that 79% of the children had snacks consisting of three main meals which included chocolates (68.3%), soft drinks (14.3%) and tip tip (17.4%). According to the data, children in this area eat more chocolates and fast food items.Most of the children (87%) consumed their breakfast at pre-school and they consume milk and biscuitsbefore going to school. Others (13%) take their breakfast at home.

3.3Malnutrition

Under nutrition is increasingly recognized as a prevalent and important health problem in many developing countries including India. This problem has serious long term consequences for the child and adversely influences development of a nation(Nyaruhucha*et al*., 2006).Stunting and wasting are widespread among pre-children in developing countries (Jeffrey, 2006). Wasting refers to a low weight-for-height that is below 2SD of the median value of the WHO International weight-for-height reference. Underweight is defined as low weight-for-age at below 2SD of the median value of the WHO International reference for weight-for-age. Stunting refers to shortness that is a deficit or a linear growth that has failed to reach an individual's genetic potential, and it is technically defined as low height for age at below 2SD of the median value of the WHO International Growth Reference.

The nutritional status of the children (Figure 2) was evaluated using age and sex specific values of height and weight from the WHO data.The indices of under nutrition such as stunting, underweight and wasting were calculated by Z-score using the reference values of height-for-age, weight-for-age and weight-for-height of WHO standards. Three Z-scores were calculated for height-for-age Z-score (HAZ), weight-for-age Z-score (WAZ) and weight-for-height Z-score (WHZ).
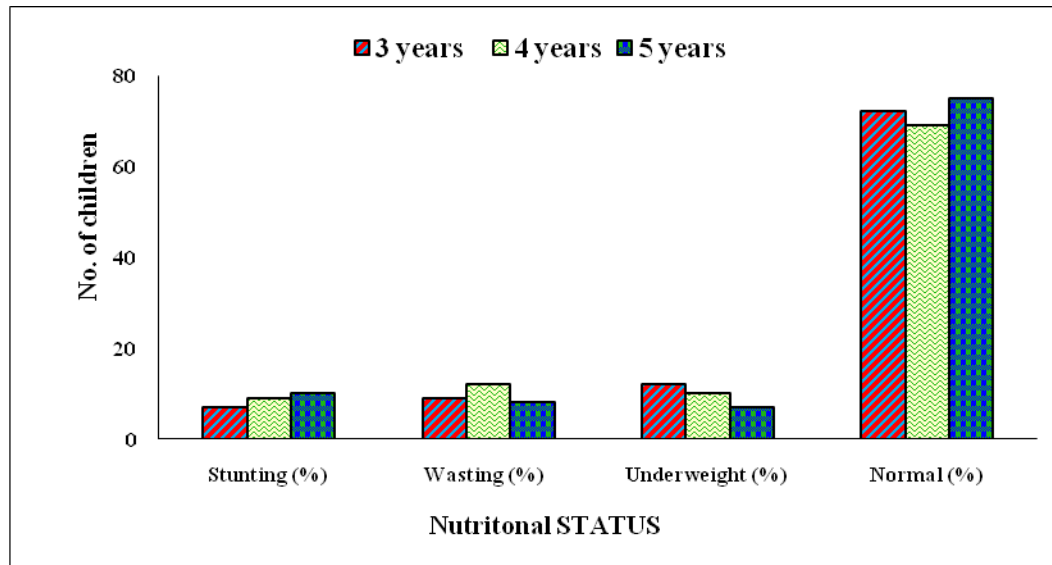

Figure 2: Nutritional Status of Children by age group in the Kattankudy D.S. Division of the Batticaloa District

As shown in Figure 2, the average nutritional status of children revealed that 72% of the children are in normal nutritional status, 19.2% of the children are wasting and underweight and 8.6% of the children are stunting. Latest estimates on child stunting at country level shows that Sri Lanka is doing much better than all the other south Asian region countries (De Onis*et al*., 2012). According to the national survey 2018, stunting levels of the India, Pakistan, Maldives, Nepal, Bhutan, Afghanistan, Bangladesh and South Asia are 38.4%, 45%, 20.3%, 35.8%, 21.2%, 40.9%, 36.1% and 35% respectively. But stunting level of Sri Lanka is 17.3%. According to this survey, this division shows a better stunting level (8.6%).

In this area, the nutritional status of the children is much better. This condition is due to the consumption of more animal protein food items such as meat, fish, egg and milk. The primary cause of normal nutrition status observed in the present study are good socioeconomic status, proper vaccination and medicine, hygienic conditions, sanitation, life style, and better education. Insufficient breast feeding, type of weaning food and welfare of the household are some of the important factors that play a role in the malnutrition of children.According to the survey, breastfeeding between 1 to 6 months is 39% and breastfeeding between 7 months to a year is 33%. There were 14% who reported breastfeeding between 13 and 19 months and 6% reported breastfeeding between 20 to 24 months. Breastfeeding for less than 1 month was reported to be 8%.

3.4 Growth status by mid-upper-arm circumference, chest circumference, and head circumference

On the basis of observations obtained after careful measurements of circumferences of head, chest, and mid-upper-arm, the average chest circumference and head circumferenceareshown in Table 1.

Table 1: Average Chest Circumference and Head Circumference

Age	Chest circumference (cm)	Head circumference (cm)
3	51.98	49.02
4	53.10	49.58
5	55.54	49.72

Between the age of 6 months to 5 years, if chest/head circumference ratio is less than 1, that may be due to failure to develop or wasting of muscle and fat in the chest wall. In our survey 100% of the children are in the normal level,which means that all children have chest/head circumference ratio higher than 1. Mid-upper-arm circumference is an importantanthropometric measurement to identify acute malnutrition. Normally children with mid-upper-arm circumference less than 11cm are in a malnutrition condition. According to the survey, 89% of children are in the normal level and 11% of children are malnourished.The mean value of the mid-upper-arm circumference also shows an increase with increasing age on both sexes.

3.5Members of the Family and Living Status of Children

This study showed that most families consist of four to five members,*i.e*., there are two to three children in each family. Ninety-six percent of families depend on the father,whileother families are headed by the motherwhile the fathers are abroad. One hundred percent of the children are living with their parents. This information helps to analyze the family background and check their living standard.
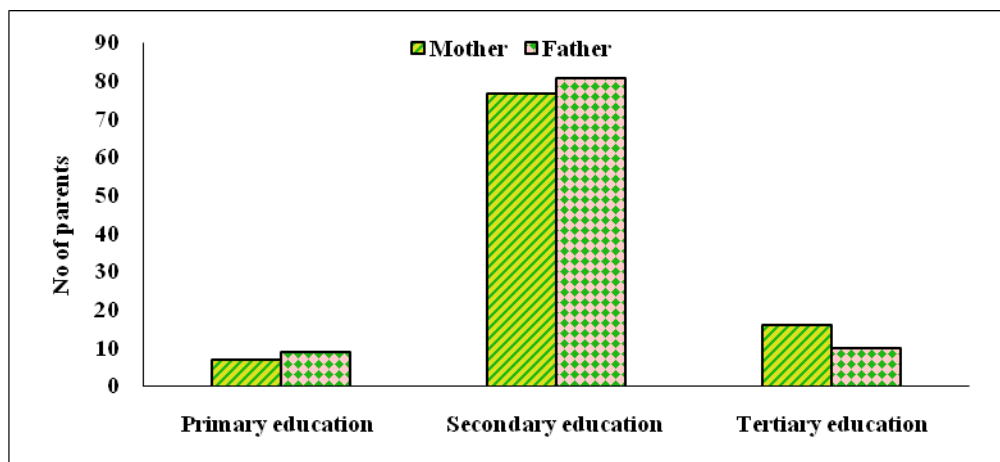
3.6Education levels of parents

Figure 3: Educational Pattern of Parents

Education levels of parents are shown in Figure 3. The educational status in this area was satisfactory, as 77% of mothers and 81% of fathers had secondary education. Also there were mothers with tertiary education (16%) and fathers with tertiary education (10%). Mothers with only primary education (7%) andfathers with only primary education (9%) were few. When the educational level of the parents was compared with the nutritional status of the child, a significant($p < 0.05$) relationship was found between those factors. The nutritional status of the family directly affects the nutritional status of the child. In particular, mothers are the important persons in selecting food for the child.

3.7 Income Levels of Family

The income level of the families in this area was fairly good. Income Levels of the family are shown in Figure 4. The income of 38% of the families is more than Rs. 40,000 per month, while 13%, 28% and 14% of the families earnRs.30,000 – 40,000, Rs.20,000 – 30,000, and Rs.10,000 – 20,000 per month, respectively. Only 7% of the families get less than Rs.10,000 per month.
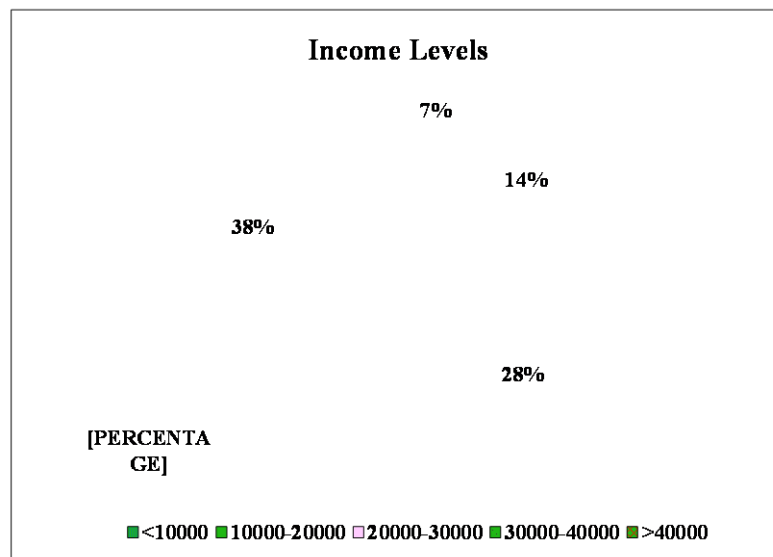

Figure 4: Income Levels of Family

The main income source in this area is business,while some have government or non- government jobs. Food stamp is one of the income sourcesfor those with income less than Rs.10,000; they also work as labourers in private shops. In this area, most of the people have sufficient money for their family members to consume nutritional foods. Therefore, they can maintain the nutritional status of their children at a good level. According to the findings regarding income, only 7% of households in the Kattankudy area are in the category of poor households. They face difficulties in intake of sufficient food as well as nutritious food. Parents in ahigh income range can normally afford more nutritious food for their children than those in a low income range.This survey shows a positive relationship between nutritional status and family income.

4. CONCLUSIONS

The present study provides a summary of the nutritional status of pre-school age childrenin the Kattankudy D.S. division of the BatticaloaDistrict.Several factors affect the nutritional status of pre-school children in communities. Food habits, socio-economic capacity, available health facilities, environmental sanitation and geographical disparity in terms of economic development are some of the factors that should be considered in formulating the nutrition programs for children. Nutritional status and dietary habits of the children are satisfactorydue to proper food intake,better education and income level of parents, and living status.Possible interventions should include a health and nutrition education program that facilitate the promotion of children's nutrition at home, physical activity, capacity building, sanitation, and hygiene in the community.

REFERENCES

1. Caulifield, L. E., De Onis, M., Blössner, M., and Black, R.E. (2004). Undernutrition as an underlying cause of child deaths associated with diarrhoea, pneumonia, malaria, and measles. *American Journal of Clinical Nutrition*. 80:193-198.

2. Chang, S. M., Walker, S. P., Grantham, S. M., and Powell, C. A. (2010). Early childhood stunting and later fine motor abilities. *Developmental. Medicine and Child Neurology*. 52:831-836.

3. De Onis, M., Blössner, M. and Borghi, E. (2012). Prevalence and trends of stunting among pre-school children, 1990–2020. *Public Health Nutrition.* 15:142-148.

4. Department of Census and Statistics. (2016). Sri Lanka Demographic and Health Survey 2016. Ministry of Healthcare and Nutrition, Colombo, Sri Lanka.

5. Jeffrey, B. (2006). The assessment of the nutritional status of a community. WHO, Geneva. 50-76.

6. Khan, A. A., and Bano, N. (2007). Child Malnutrition in South Asia. *South Asian Survey*. 14(1):129-145.

7. Khandare, A. L., Siruguri, V., Rao, A., Venkaiah, K., Reddy, G., and Rao, G. S. (2008). Diet and nutrition status of four tribal blocks of thane district of Maharashtra, India (Nutritional Status of Children). *Pakistan Journal of Nutrition*. 7:485-488.

8. Lutter, C. (2003). Meeting the challenge to improve complementary feeding. In: Moreira (Ed.). Meeting the challenge to improve complementary feeding. SCN News. UN Systems Standing Committee on Nutrition, Lavenhem Press, UK. pp. 4-10.

9. Nyaruhucha, C. N. M., Mamiro, P. S., Kerengi, A. J., and Shayo, N. B. (2006). Nutritional status of under five children in a pastoral community in Simanjiro district, Tanzania. *Tanzan Health Research Bulletin*. 8(1):32-36.

10. Vareecken, C., and Maes, L. (2010). Young children's dietary habits and associations with the mothers' nutritional knowledge and attitudes. *Appetite*. 54:44-51.

11. WHO. (2009). Global prevalence of vitamin A deficiency in populations at risk 1995-2005: WHO Global Database on Vitamin A Deficiency. Geneva.

Analysis of factors controlling acoustic absorption ofcommercial flexible polyurethane foams

K.W.N.S. Samaranayake and R.V. Coorey[*]

Department of Physics, University of Colombo, Colombo 03

Abstract

In Sri Lanka, commercial flexible (CF) polyurethane (PU) foams are used for many purposes including sound absorption and noise reduction. The main factors that control sound absorption are thickness, density and flow resistivity of PU foam materials. The primary aim of the study is to experimentally determine frequency-dependant normal incidence acoustic absorption coefficients (NIAACs) of PU foams of densities in the range (12.0 kg m^{-3} to 21.0 kg m^{-3}) and thicknesses in the range (5.08 cm to10.16 cm) of PU foam materials,using the impedance tube method according to ASTM C384-04 standard. The studied foam materials exhibit excellent acoustic properties with high NIAACs of more than 0.70 in the high frequency range above 1 kHz. For fixed density of these materials, NIAACs increased with increasing foam thickness. However, for fixed thickness of these materials, the NIAACs were found to be independent of the foam density. The air flow resistivity dependency on thickness and density of PU foams were determined based on simulated NIAACs as a function of frequency using the Dunn &Davern model. For fixed thickness of foam materials, the flow resistivity increased with increasing density of foam materials. However, for fixed density of foam materials, the variation between flow resistivity and thickness of foam materials were found to be inconsistent, indicating inhomogeneity / heterogeneity of CFPU foams.

Keywords:absorption coefficients,Dunn & Davern, flow resistivity,polyurethane.

1. INTRODUCTION

A wide range of materials is used as sound absorption materials where it is necessary to reduce the noise and the reflected sound (Asdrubali*et.al*., 2012).Materials which have nonporous solid surfaces, cannot absorb sound because the incident sound energy reflects back to the environment. However, if a surface is highly porous, the incident sound wave causes air molecules to vibrate within the cavities, channels, or pores present in these materials (Kuczmarski& Johnston, 2011) and lose some of its original sound energy. In the vibrational process, energy of air molecules is converted to heat due to frictional losses within the material (Arenas & Crocker, 2010). In porous materials, the pores can be either "open pores,"

---

[*]Corresponding author: Email: rvcoorey@gmail.com

forming a continuous 3-dimensional cell structure which is open to external surface of the material, or "closed pores," where pores are isolated discrete pores surrounded by material. Porous absorbing materials are also classified as cellular (foam), fibrous, or granular, based on their microscopic configurations (Arenas & Crocker, 2010).

Polyurethane (PU) is the most popular and most commonly used polymeric material in acoustic absorption because this material also could be used in thermal insulation and many other technological applications (Defonseka, 2013). PU foam materials come in two forms, namely, flexible PU foams and rigid PU foams. Open cell flexible PU foams have a higher sound absorption property than rigid PU forms (Ancuţa-Elena*et al*. 2014). Flexible PU foams are made with densities ranging from 12 to 50 kg m^{-3}(Defonseka, 2013). PU foams are generally formed by a chemical reaction between di- or poly-isocyanates and polyols (Gwon*et al*. 2016) and small amounts of blowing agents are added to design low density foams (Jain *et al*., 2013).Since isocyanates are highly toxic materials, in order to mitigate environmental and health issues, numerous research studies have been carried out to determine how environment-friendly materials could be used to replace these materials and to enhance the sound absorption property of PU materials (Caillol*et al*. 2012). Polyols are petroleum-based materials and continuing research is in progress to use natural products such as soya and other sources to produce eco-friendly polyols to make these foams more cost-effective (Defonseka, 2013).

The absorption coefficient in porous materials depends on the frequency of sound, the angle of incidence, and density and thickness of material (Sagartzazu*et al.*, 2008). The most important non-acoustic property of porous materials of interest in sound absorption is flow resistivity which depends on micro-structural parameters such as porosity and tortuosity of the material, which is closely related to size and distribution of pores (Yamashita*et al*., 2008; Stinson &Champoux, 1992). Flow resistivity of a porous material gives a measure of the extent the material offers resistance to a fluid flow through the material. In processing porous materials, flow resistivity is an important parameter because specific air flow needed to be measured during development of sound absorbing materials and for their quality control during manufacture. Flow resistivity is usually determined experimentally and is defined as the ratio of the pressure difference across the sample of the material to the velocity of flow of air through that sample. Joshi *et al*. have observed flow resistivity values range from (11,000 to 31,000) N s m^{-4} for polyurethane foams of densities in the range 22 – 36kg m^{-3} (Joshi *et al*., 2011). Various theoretical models have been proposed to simulate sound absorption coefficients of porous absorbing materials. The Delany-Bazley model considers characteristic wave impedance as a function of flow resistivity and it has been studied for fibrous materials (Delany &Bazley, 1970). The Dunn-Davern model utilizes the same technique and it has been tested for PU foam materials (Dunn &Davern, 1986).

Only few research studies have been carried out in Sri Lanka to find acoustic absorption properties of materials. These studies were restricted to natural fibre-polymer composites such as coir fibres (Hapuarachchi, 2004; Priyadharshana*et al*., 2015) and granular materials such as rice bran (Priyadharshana*et al.*, 2015).

The present study investigates the effectiveness of commercially available flexible PU materials as acoustic absorber material. The frequency-dependent acoustic absorption coefficients of PU foams has been investigated as a function of thickness and density of PU foams. The Dunn-Davern model has been used to simulate experimental acoustic absorption data and to generate the flow resistivity values

of PU materials (depends on micro-structural parameters) and to study how flow resistivity depends on thickness and density of PU foam materials.

2. METHODOLOGY

2.1 Experimental Measurement using Impedance Tube Method

Measurements were carried out at the Industrial Technology Institute, Colombo 7, Sri Lanka, using a Brüel&Kjaer type 4002 Standing Wave Apparatus, according to the ASTM C384-04 standard. The standing wave tube (SWT) (also known as an impedance tube) consisted of an acoustic source (a signal generator to produce a sinusoidal signal at a desired frequency) at one end and an acoustic load (test sample of the absorptive material) mounted at the other end of the tube. A probe movable microphone was used to locate the positions throughout the tube corresponding to pressure maxima and minima, which are detected by the sound level meter (Figure 1).
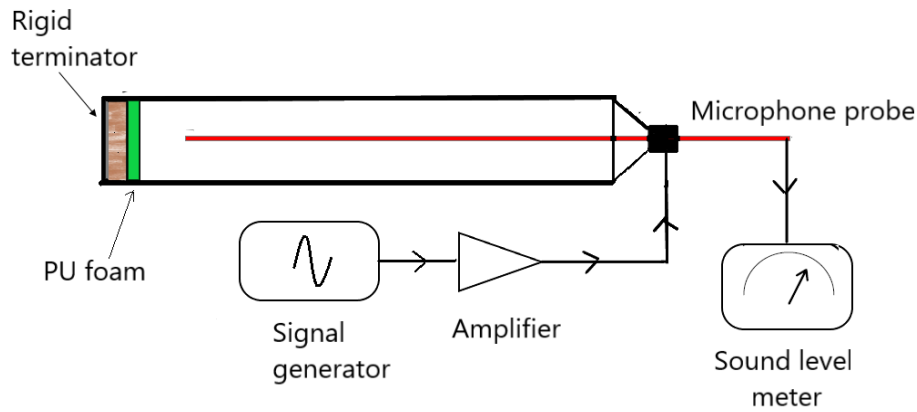

Figure 1: The standing wave tube for measuring absorption coefficient of polyurethane foams at normal incidence

2.2 Theoretical basis for measurement

Theoretically, a standing wave is established in the tube, as the result of incident and reflected pressure wave. The resulting pressure $p\ (x,t)$ can be represented as,

$$p(x,t)= p_0\left(e^{i(2\pi ft+kx)} - R\,e^{-i(2\pi ft-kx)}\right) \tag{1}$$

where x is the distance from the sample, f and p_0 are the frequency and complex pressure amplitude of the wave respectively, k is the wave number, and R is the complex reflection coefficient
The standing wave ratio is given by

$$SWR = \frac{p_{max}}{p_{min}} = \frac{1+R}{1-R} \tag{2}$$

Experimentally, the sound level measured has the following relationship to rms pressure:

$$Level_{dB} = 20\log p_{rms} \tag{3}$$

$$p_{rms} = 10^{(Level_{dB}/20)}$$

Thus sound absorption coefficient α can be calculated using the relation,

$$\alpha = 1 - |R|^2 \tag{4}$$

2.3 Materials and Methods

PU foam materials of densities 12.0, 16.0 and 21.0 kg m^{-3} with commercial standard thicknesses of 2.0″ (5.08 cm), 2.5″ (6.35 cm) and 4.0″ (10.16 cm) were purchased from local manufacturers and were used in acoustic absorption measurements. All experiments were carried out at a constant temperature of 21.0°C.

In choosing the proper length of the SWT tube for measurements of absorption coefficients over the frequency range of interest, ASTM C384-04 standards were adopted. According to the standard, the minimum frequency f_{min} and maximum frequency f_{max} limits were determined subjected to the conditions given by (5).

$$f_{min} = \frac{0.75\,c}{L - d}$$
$$f_{max} = 0.586\,c/d \tag{5}$$

where L is the length of the tube and d is the diameter of the tube and c is the speed of sound in air (m s^{-1}).

A long SWT (length 120 cm and diameter 14.5 cm) and short SWT (length 100 cm and diameter 6.5 cm) were used to measure frequencies in the ranges of 200 Hz – 1250 Hz and 1000 Hz – 4000 Hz, respectively.

3. RESULTS AND DISCUSSION

3.1 Frequency Dependent NIAACs as a Function of Foam Thickness

Frequency-dependent normal incidence absorption coefficients (NIAACs) of commercial PU foams as a function of thickness (for density value of 21.0 kg m^{-3}) are illustrated in Figure 2. In the frequency range below 1 kHz, NIAACs increase linearly from zero to values in the range of 0.60 - 0.80 (for different thicknesses). At frequencies above 1 kHz, NIAACs vary in the range of 0.70 and 0.95 (for different thicknesses). Therefore, it could be seen that PU foams studied exhibit excellent acoustic properties in the high frequency range. The frequency *vs*. NIAACs variation trends of PU foams studied are similar to those documented in literature (Joshi *et al*., 2011).

For foam thickness of 5.08 cm, the mean NIAACs values calculated for the frequency range below 1 kHz, vary in the range of 0.53 - 0.61 (Figure 3). However, for a larger foam thickness of 10.16 cm, mean NIAACs increase significantly to the range of 0.76 - 0.83.
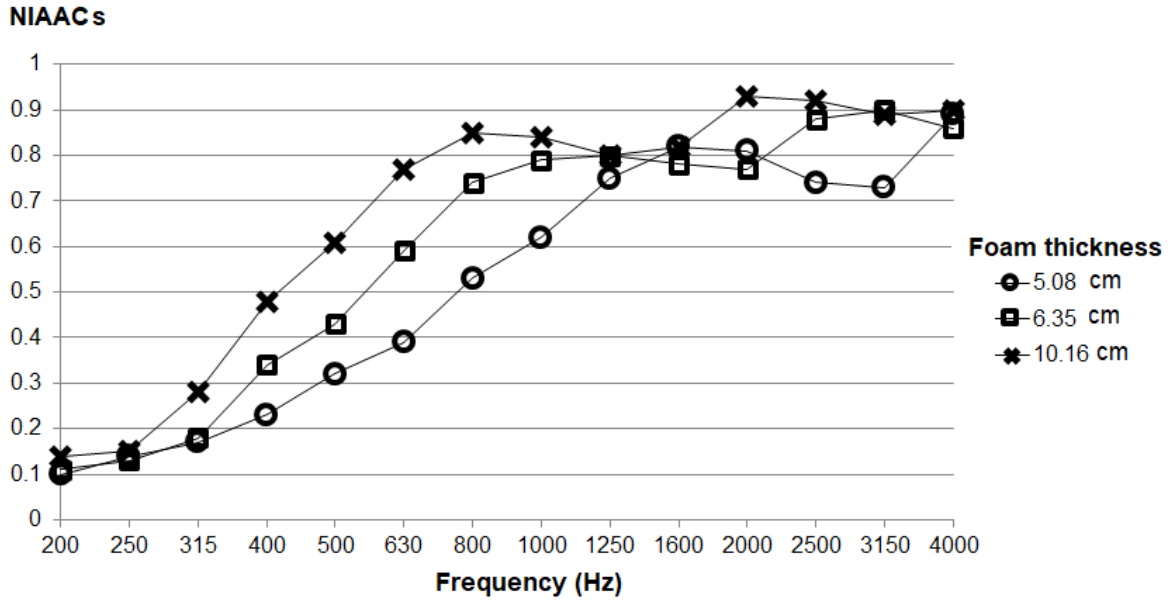
Figure 2. The frequency dependence of normal incidence absorption coefficients of PU foams as a function of thickness values of 5.08, 6.35 and 10.16 cm for fixed density value of 21.0 kg m^{-3}.
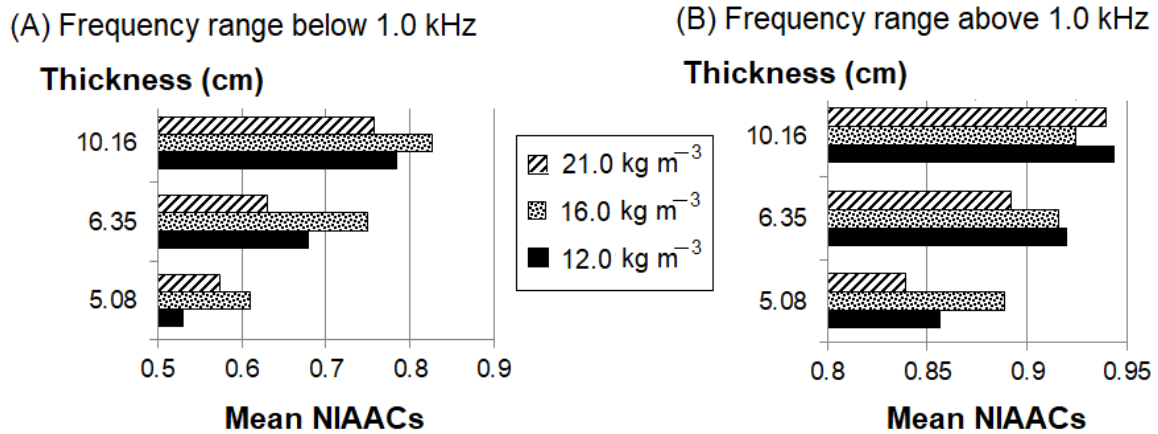

Figure 3. The variation of mean NIAAC for PU foams of thickness values of 5.08, 6.35 and 10.16 cm and density values of 12.0, 16.0 and 21.0 kg m^{-3} in the (A) frequency range below 1.0 kHz and (B) frequency range above 1.0 kHz.

In the frequency range above 1 kHz, the increase in corresponding mean NIAACs are from the range of 0.84 - 0.89 to 0.92 - 0.94. These results show that even though in the frequency range below 1 kHz, NIAACs significantly increase as a function of increasing thickness values, at frequencies above 1 kHz the increase is not significant. These results agree with previously published work on acoustic absorption of fibrous materials (Ibrahim &Melik 1978).

3.2 Frequency Dependent NIAACs as a Function of Foam Density

Frequency-dependent normal incidence absorption coefficients (NIAACs)as a function of density (for fixed thickness of 10.16 cm) are illustrated in Figure 4.The increase in frequency-dependent NIAACs is found to be almost independent of density in the low frequency range below 1 kHz.
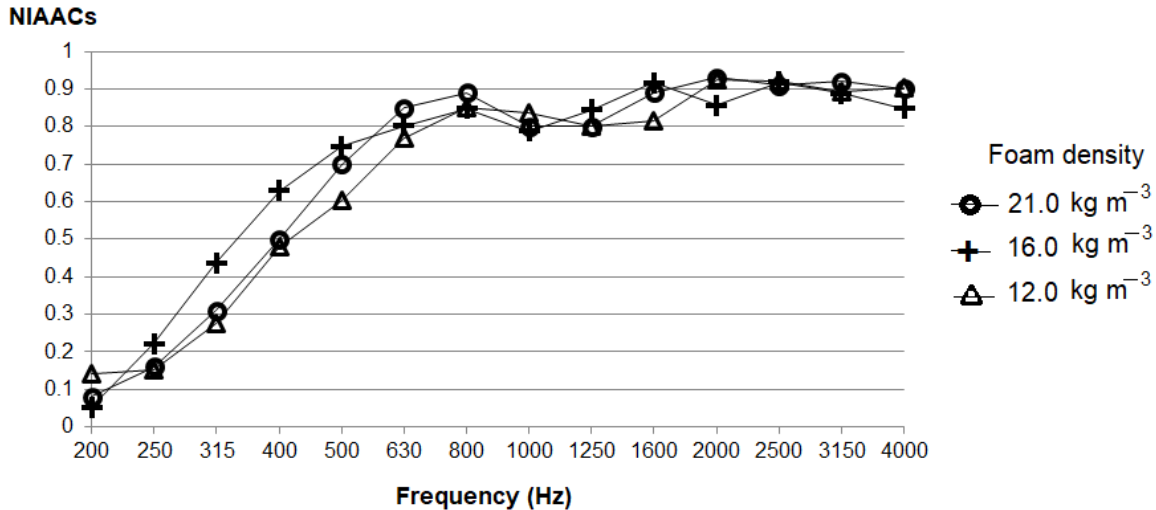

Figure 4. The frequency dependence of normal incidence absorption coefficients of PU foams as a function of density values of 12.0, 16.0 and 21.0 kg m^{-3} for fixed thickness value of 10.16 cm.

Figure 3 shows that for foam density of 12.0 kg m^{-3}, 16.0 kg m^{-3} and 21.0 kg m^{-3}, the mean NIAACs vary in the ranges 0.53 - 0.78, 0.61 - 0.83,and 0.57 - 0.75, respectively, for frequency range below 1 kHz. These NIAACs do not show a significant increase with increasing density. In the frequency range above 1 kHz, for a fixed thickness of the material, NIAACs are in the range of 0.84 - 0.94 (frequency-dependentNIAACs are almost independent of the foam density range studied). However, examining the published literature by other investigators shows otherwise. Lee *etal*.(2012) reported that with increasing density of PU/nano-silica nanocomposite foams, the cell size would decrease and the sound absorption would increase. Koizumi *et al*.(2002) reported that the sound absorption coefficient of natural bamboo fibres increases in the middle and higher frequencies with increasing sample density.

The inconsistency of present results with previous studies performed with porous materials can be attributed to inhomogeneity of the studied commercial PU foams. Since the foam density of commercially manufactured porous materials depends on their manufacturing process, materials could be inhomogeneous—the local density of the materials could vary throughout the material. Published results report that various filler reinforcementagents (inert inorganic compounds) are usually added to PU foams in order to make them suitable for various industrial applications (Ekici*et al*. 2012). Chemical properties of commercial PU foams are modified by adding such agents, which could result in inhomogeneity of such materials. Inhomogeneity/heterogeneity in commercial PU foams manufactured across India have already been reported by Jain *et.al*.(2013).

In the present study a check for homogeneity in the density of foam materials has not been investigated. However, since flow resistivity is the major parameter which depends on micro-structural parameters governing the acoustic behaviour in porous materials (Dragonetti*et.al.*, 2011), a study has been carried out to determine flow resistivity using the experimental NIAACs and to investigate how it depends on density and thickness of studied foam materials.

3.3 Simulation of Flow Resistivity from Measured NIAACs

The surface impedance Z is given by the ratio of pressure $p(x,t)$ and the particle velocity $u(x,t)$ normal to the surface.

$$Z = \frac{p(x,t)}{u(x,t)} \qquad (6)$$

With the surface at $x = 0$, from (1), the combined pressure and speed normal to the surface are given by

$$p(0,t) = p_0(1+R)e^{j2\pi ft} \qquad (7)$$

$$u(0,t) = \frac{p_0}{\rho_0 c}(1-R)e^{j2\pi ft} \qquad (8)$$

where ρ_0 is the density of air (kg m^{-3})

From (6), (7) and (8), the surface impedance in terms of reflection coefficient can be expressed as,

$$Z = \rho_0 c \frac{1+R}{1-R} \qquad (9)$$

where $\rho_0 c$ is characteristic acoustic impedance of air and c_0 are the density without the presence of absorbent material.

From (4) and (9), the normal incidence acoustic absorption coefficient α as function of the surface impedance Z can be obtained.

$$\alpha = 1 - \left(\frac{Z-\rho_0 c}{Z+\rho_0 c}\right)^2 \qquad (10)$$

The surface impedance Z of a rigidly backed layer of thickness b of absorbent is given by Cox&d'Antonio(2009),

$$Z = Z_c \coth(\gamma b) \qquad (11)$$

where γ is the propagation constant, and Z_c the characteristic impedance of the absorbent .

According to the Dunn &Davern model (Dunn &Davern, 1986), the flow resistivity can be estimated with following empirical relationships for open-cell foams (Mirowska&Czyźevski, 2007):

$$Z_c = \rho_0 c_0 \left[1 + 0.0571 B^{-0.754} - j\, 0.087 B^{-0.732}\right]$$

$$\gamma = \frac{2\pi f}{c_0}\left[(0.168 B^{-0.715}) - j(1 + 0.136 B^{-0.494})\right] \qquad (12)$$

where$B$ is a dimensionless frequency-dependent variable:

$$B = \frac{2\pi f \rho_0}{R_f} \; ; \; (0.01 < B < 0.1)$$

(13)

where$R_f$is the air flow resistivity (Pa s m^{-2}).

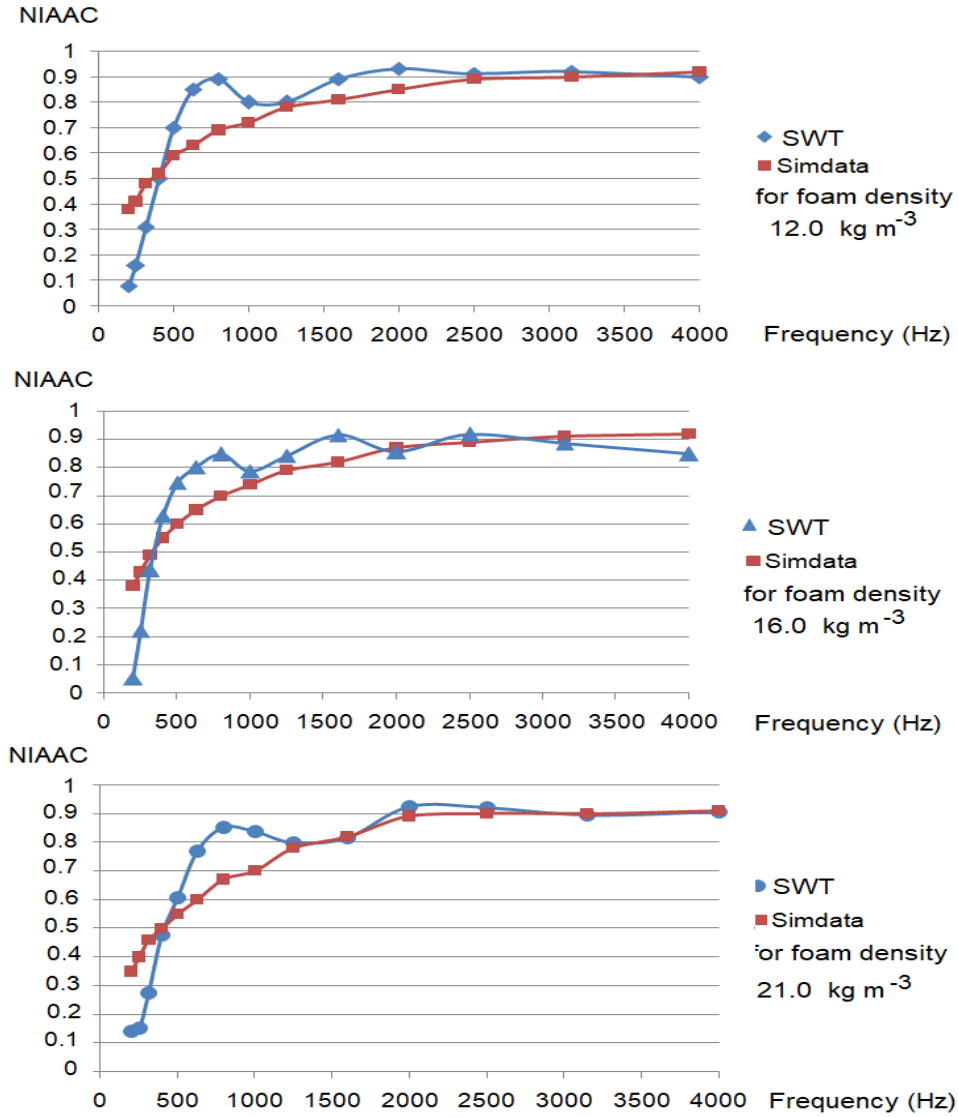### 3.4 Flow Resistivity as a Function of Foam Thickness and Density

Figure 5. The best-fit between frequency-dependent measured NIAAC and simulated NIAAC (using the empirical relationships developed for open cell foams by Mirowska&Czyźevski, based on Dunn &Davern model) for PU foams of thickness 10.16 cm and density values of 12.0 kg m^{-3} (R_f = 14790 N s m^{-4}), 16.0 kg m^{-3} (R_f = 17450 N s m^{-4}) and 21.0 kg m^{-3} (R_f = 19550 N s m^{-4}) are illustrated.

Using MATLAB coding, the measured normal incidence acoustic absorption coefficients (NIAACs) as a function of frequency were fed to (12) and (13) - empirical relationships developed for open cell

foams by Mirowska&Czyźevski(2007)based on the Dunn &Davern model. Thereby, NIAACs simulated data were generated considering flow resistivity as a variable. Flow resistivity values were varied until the best-fit between experimental (SWT) and simulated (Simdata) NIAACs *vs*. frequency curves was achieved (Figure 5).

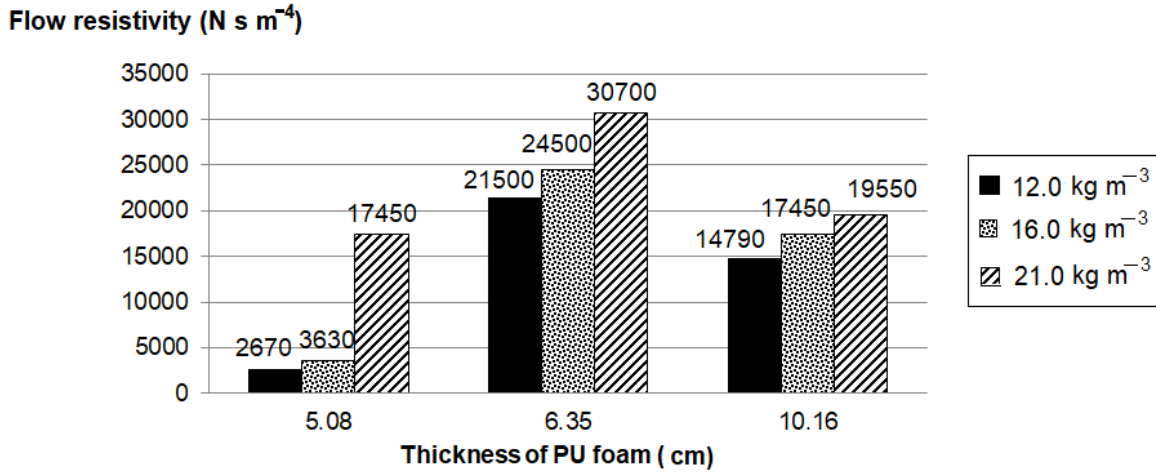**Flow resistivity (N s m^{-4})**

Figure 6: Optimum flow resistivity values for different thicknesses and densities of PU foam materials are shown. Optimum flow resistivity values increase with increasing density of PU foam materials

The best-fitbetween SWT and Simdata curves generate the optimum flow resistivity values showed in Figure 6 for considered density and thickness values of PU foam materials. Figure 6 shows that there is no consistent relationship between optimum flow resistivity values and thickness of foam materials for fixed density of foam materials. However, for a fixed thickness of foam materials, there is an increase in optimum flow resistivity values with increasing density of foam materials.

These results agree with already published work on experimentally measured flow resistivity of porous materials such as melamine and glass wool (Joshi *et al*, 2011; Cuenca *et al.,* 2014). Van der Kelen, (2011) in uni-directional flow resistivity measurements in melamine foams has shown that, due to a local increase in foam density, there is a possibility that the flow resistivity could increase. Since frequency-dependent NIAACs as a function of macroscopic properties of PU foams have similar trends to that in melamine foams (Joshi *et al*, 2011), the increase flow resistivity as a function of density is likely due to local effects in the material. Further research is needed to investigate this hypothesis. Furthermore, since flow resistivity depends on microscopic parameters such as porosity and tortuosity, further research is in progress to study these parameters in commercial PU foam materials.

4. CONCLUSIONS

The commercial flexible PU foams studied exhibit excellent acoustic properties with high normal incidence acoustic coefficients (NIAACs) of more than 70% in the high frequency range above 1 kHz**.** The NIAACs dependence on thickness of PU foams are found to be in conformity with those reported in the literature. However, for a constant thickness of PU foam materials, the frequency-dependent

NIAACs are found to be independent of the foam density range studied, which was an unexpected result. The air flow resistivity increased with increasing density of foam materials. However, for fixed density of foam materials, the variation between flow resistivity and thickness of foam materials were found to be inconsistent, indicating inhomogeneity/heterogeneity of commercial flexible PU foams.

ACKNOWLEDGMENT

REFERENCES

1. Ancuţa-Elena, T.I.U.C., Vasile, O., Anamaria-Didona, U.S.C.Ă., Gabor, T., &Vermeşan, H. (2014). The analysis of factors that influence the sound absorption coefficient of porous materials,*Rom J of AcoustVib*, XI(2), 105–108.

2. Arenas, J.P.,& Crocker, M.J., (2010) Recent Trends in Porous Sound-Absorbing Materials, *Sound and Vibration*, Vol.44, No. 7 pp. 12-17.

3. Asdrubali, F., Schiavoni, S.,&Horoshenkov, K.V. (2012) A review of sustainable materials for acoustic applications, *Buil. Acoust*. 19, 283–312.

4. ASTM C384-04 (2004) Standard test method of acoustical materials by impedance tube method. (New York) American National Standard Institute.

5. Caillol, S., Desroches, M., Boutevin, G., Loubat, C., Auvergne, R., &Boutevin, B. (2012) Synthesis of new polyester polyols from epoxidized vegetable oils and biobased acids, *Eur. J. Lipid Sci. Technol*. 114, 1447-1459.

6. Cox, T., &d'Antonio, P. (2009). *Acoustic absorbers and diffusers: theory, design and application*. 2nd Ed., Taylor & Francis.

7. Cuenca, J., Van der Kelen, C., &Göransson, P. (2014). A general methodology for inverse estimation of the elastic and anelastic properties of anisotropic open-cell porous materials - with application to a melamine foam, *Journal of Applied Physics* 115, 084904.

8. Defonseka C. (2013) Practical guide to flexible polyurethane foams, SmithersRapra.

9. Dunn, I. P., &Davern, W. A. (1986). Calculation of acoustic impedance of multi-layer absorbers. *Applied acoustics*, *19*(5), 321-334.

10. Delany, M.E.,&Bazley, E.N. (1970) Acoustic properties of fibrous absorbent materials, *Applied Acoustics*, **3**, 105 - 116.

11. Dragonetti, R., Ianniello, C., & Romano, R. A. (2011). Measurement of the resistivity of porous materials with an alternating air-flow method. *J. Acoust. Soc. Am.*, 129(2), 753-764.

12. Ekici, B.*,* Kentli, A.*,* &Kucuk, H. (2012) Improving sound absorption property of polyurethane foams by adding tea-leaf fibers. *Archives of Acoustics*. 37(4): 515–520.

13. Gwon, J.G., Kim, S.K., & Kim, J.H. (2016) Sound absorption behavior of flexible polyurethanefoams with distinct cellular structures, *Mater. Des*. 89, 448-454.

14. Ibrahim, M. A.,&Melik, R. W. (1978). Physical Parameters Affecting Acoustic Absorption Characteristics of Fibrous Materials, *Proceedings of the mathematical and physical society of Egypt,* 46, 126-130.

15. Hapuarachchi, S.S.K. (2004). A study on characterization of sound absorption properties of locally available absorption materials, MSc Thesis, University of Colombo, Sri Lanka.

16. Jain, S.K., Joshi, M., Shravage P., &Karanth, N.V. (2013 November 10-15). A study on homogeneity and heterogeneity of polyurethane foams – an Indian scenario. Paper presented at ACOUSTIS2013, New Delhi, India.

17. Joshi, M.P., Shravage, P., Jain S.K. &Karanth, N.V. (2011) A comparative study on flow resistivity for differentpolyurethane foam samples, *Journal of Acoustical Society of India*, 38, 153 - 157.

18. Koizumi, T., Tsujiuchi, N.,& Adachi, A. (2002). The Development of Sound Absorbing Materials Using Natural Bamboo Fibers, High Performance. Ashurst Lodge, Southampton: W.I.T Press, pp.157–166.

19. Kuczmarski M.A. & Johnston, J.C. (2011). Acoustic Absorption in Porous Materials paper of NASA, NASA/TM –2011-216995.

20. Lee, J., Kim, G. H., & Ha, C. S. (2012). Sound absorption properties of polyurethane/ nano-silica nanocomposite foams. *J ApplPolym Sci.*, 123(4), 2384-2390.

21. Mirowska, M. &Czyźevski, K., (2007), "Estimation of sound absorption coefficients of porous materials", ICSV14, Cairns, Australia.

22. Priyadharshana, P.A.N.S., Abeywarna, U.K., &Pannila, A. S. (2015). Investigation of sound absorption coefficient of materials using tube impedance method. In Proceedings of the Technical Sessions, Vol. 31, Institute of Physics, Sri Lanka, pp. 61-68.

23. Sagartzazu, X., Hervella-Nieto, L. &Pagalday, J. (2008) Review in sound absorbing materials, *Arch. Comput. Meth. Eng.* 15, 311-342.

24. Stinson, M.R., &Champoux, Y. (1992) Propagation of sound and the assignment of shape factors in model porous materials having simple pore geometries, *J. Acoust. Soc. Am.* 91, 685-695.

25. Van der Kelen C. (2011) Characterization of Anisotropic Acoustic Properties of Porous Materials-Inverse Estimation of Static Flow Resistivity, Licentiate thesis, Stockholm, Sweden.

26. Yamashita, T., Suzuki, K., Nishino S. &Tomota, Y. (2008) Effect of microscopic internal stractures on sound absorption properties of polyurathane foam by X-ray computed tomography observations, *Materials Transactions*, 49 (2) 345 – 351.

Acoustic performance testing of Sri Lankan *pirith* chants: Insights for vowel distribution

Shantha S.N. Gamage[*] and M.A.C.P. Gunawardana

Department of Physics, University of Sri Jayewardenepura, Sri Lanka

Abstract

Pirithis a special type of chanting in Pali language and is believed to be a protective doctrine preached by the Lord Buddha. This work is dedicated to developing a phonetic picture ofPirith chants and analyse acoustic properties using computer-aided tools. The motive of this study is to investigate vowel distribution of Pirith chants with the aim of special pattern recognition. Generally, voice signals consist of the fundamental frequency, F_0, and harmonic frequencies called as formants, F_n. Pertaining to speech mechanism, vowels can be mapped using the relationship between lip opening width to the first formant frequency, F_1, and tongue constriction width to second formant frequency, F_2. In this study, samples of the *Rathana, KaraniyaMetta* and *Angulimala*Suttas recited by male monk chanters were recorded using a high precision microphone array and 25 samples of each Sutta were analysed. In the computational speech model, a pre-emphasis filter is applied to the sampled time series of voiced segments to cancel out the effect of the glottis. Then frame-by-frame analysis was used with hamming windows and linear predictive coding (LPC) and auto correlation to extract the formant values. Further, the vowel distribution reveals that the majority of vowels in the *AngulimalaSutta* and *KaraniyaMettaSutta* are closer to cardinal vowel [a] while the vowels of the *RathanaSutta* remains closer to cardinal vowels [u],[o],[ɔ] and [ɒ].

Keywords:*Cardinal vowels, Formant frequencies, Voiced to unvoiced ratio, Vowel distribution, Zero-Crossing rate.*

1. INTRODUCTION

Speech production process begins at the point of converting an idea developed in the speaker's mind to a language code. With the aid of articulatory motion and vocal tract movement, the phonemes which are lined up in a set of sequences propagate outside as an acoustic waveform. *Pirith* means protection from all aspects and this protection is to be obtained by reciting or listening to *Pirithsuttas*. The practice of reciting and listening to *Pirithsuttas* began very early in the history of Buddhist culture.

---

[*]Corresponding author: Email: shanthagamage@sci.sjp.ac

A famous Japanese researcher, Masaru Emoto had provided evidence that human thoughts can affect the molecular structure of water through words, ideas and human vibrational energy (Emoto, 2004). In the literature, a large majority of the studies carried out so far in this discipline have used a qualitative approach to tackle the problem. Instead, we chose a rigorous but quantitative approach which exploits state-of-the-art computer aided tools such as high-performance computing facilities to evaluate acoustic properties of a vast range of *Pirith*chants.

According to the acoustic theory of speech production, the vocal tract is modelled as a non-uniform tube closed at vocal folds and open at the lip end (Stevens and House 1955). Due to varying cross sections along the vocal tract, different resonance frequencies (harmonics) are generated in response to varying vocal fold vibrations. Consequently, the complex output voice signal is composed of several harmonics called formants (Fant,1973).

Voiced to unvoiced ratio (V/UV ratio) is an important parameter as it indicates the involvement of the speech production system with vibration of vocal codes. In voiced speech, the vibrating glottis generates periodic pulses, which resonate in the vocal tract. Therefore, when vowels are pronounced similar frequencies are generated. However, in unvoiced speech, vocal chords held open and a continuous air beam flows through them. The air beam turns into a turbulent flow because of narrowed vocal tract and it creates non-periodic, noise-like sounds (Lee and Yoo, 2003). Usually, in speech, silent regions exist in between voiced and unvoiced regions, yet without the existence of silent regions the speech will not be intelligible (Gunawardana and Gamage, 2018).

The zero crossing rate measures the number of intersections a given signal makes with the time axis per unit time in an amplitude-time plot. Voiced speech shows a low zero-crossing rate due to the excitation of vocal tract by the periodic air flow, whereas the unvoiced speech shows high zero-crossing count as it is produced by the turbulent airflow flowed through the narrowed vocal tract (Bachu*et al*., 2010). Additionally, the voiced part of the speech has high energy content because of its periodicity.

Vowels can be mapped using the relationship between lip opening width to the first formant frequency F_1 and tongue constriction width to second formant frequencyF_2.Cardinal vowels, which are not of any particular language but a measuring system in describing sounds of languages, are used as a set of reference vowels in this work. These vowel sounds demonstrate if the tongue is in an extreme position, either front or back, highor low. The cardinal vowel system wasmodified by Daniel Jones (Jones, 1953), based on the original idea proposed by earlier phoneticians, notably Ellis and Bell.Table 1 shows the basic description for 8 primary cardinal vowels using standard symbols presented in International Phonetic Alphabet (IPA). Figure 1 illustrates vowel space for the 8 primary cardinal vowels reported in Bruce(Bruce, 2010;Bruce and Engstrand, 2006).

The aim of this study is to develop a phonetic picture on Pirith chants and analyse acoustic properties using computer-aided tools. As reported by several other studies, characteristic vowels are identified in chanting, contrast to normal speaking. The motive of this study is to investigate vowel distribution of Pirith chants with the aim of special pattern recognition. Pertaining to speech mechanism, vowels can be mapped using the relationship between lip opening width to the first formant frequency, F_1 and tongue constriction width to second formant frequency, F_2. In this study, samples of *Rathana, KaraniyaMetta,*and *AngulimalaSuttas* recited by male monk chanters were recorded using a high precision microphone array and 25 samples of each Sutta were analysed.

Table 1: Description of Daniel Jones's 8 primary cardinal vowels in terms of height, back/front and roundedness using standard symbols presented in International Phonetic Alphabet(IPA)

	Tongue position front Lips unrounded	Tongue positioned back Lips rounded
Tongue positioned high	[i]	[u]
Tongue positioned upper mid	[e]	[o]
Tongue positioned lower mid	[ɛ]	[ɔ]
Tongue positioned low	[a]	[ɑ]
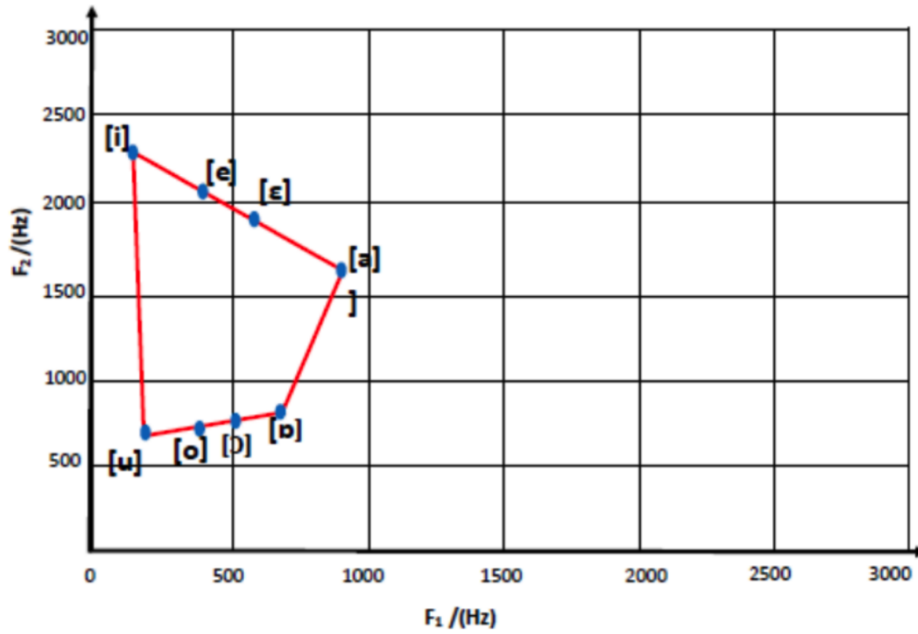
Figure 1: The vowel space of F_2 versus F_1. Formant chart showing the first two frequencies of 8 primary cardinal vowels i, e, ɛ, a, u, o, ɔ, and ɒreported in Bruce, 2010.

2.EXPERIMENTAL

In the analysing process,samples of *Rathana*, *KaraniyaMetta* and *AngulimalaSuttas* recited by male monk chanters were recorded using high precision microphone array and 25 samples of each *Sutta*were analysed. Recorded samples were then subjected to splitting of smaller voiced segments of frame length $10\ ms$ using a sampling rate of $44.1\ kHz$.This specific frame length was selected as the vocal tract has

fixed characteristics over a time interval of the order of 10 *ms*.

Fast Fourier Transformation (FFT) and Linear Predictive Coding (LPC) are techniques used in spectral analysis of the speech. Fast Fourier Transformation(FFT) develops a spectrum by decomposing a sound wave into sinusoidal components whereas Linear Predictive Coding (LPC) estimates formant frequencies associated with the vocal tract.

The formant frequency estimation was performed using a computational method as follows. A pre-emphasis filter is applied to the sampled time series of voiced segments to cancel out the effect of the glottis. Then frame-by-frame analysis was used with hamming windows and linear predictive coding (LPC) and auto correlation to extract the formant values. Speech signal has been modelled as a combination of a source and a filter. A source-filter separation model is used as a fundamental method for formant frequency estimation. The modelled system and its frequency resonances are only considerable in this estimation and Linear Predictive coding (LPC) is used to find the best matching system. The LPC filter is a function with a set of filter coefficients. Resonance of the filter is expressed by a pair of coefficient. In every 10 I the vocal tract parameters are changed, creating a new set of coefficients. When applying LPC, a speech sample is approximated as a linear combination of past speech samples. Minimizing the sum of squared differences over a 10 I frame between actual sample and linearly predicted sample, a set of predictor coefficients can be obtained.

According to the discrete-time model,

$$\frac{S(z)}{U(z)} = \frac{G}{1 + \sum_{k=1}^{p} a_k z^{-k}}$$

where $S($ = speech output, $U($ = excitation, G gain, and $\leftarrow$ predicted coefficients.

$$S(n) = \sum_{k=1}^{p} \alpha_k S(n-k) + GU(n)$$

where $S($ = estimated current value, ι = predicted coefficients, $S(n -$ = past samples and $U($ = excitation of vocal folds.

Between two pitch pluses $U($ is zero. Therefore, the nth speech sample can be written as a linear combination as follows:

$$S(n) = \alpha_1 S(n-1) + \alpha_2 S(n-2) + \alpha_3 S(n-3) \ldots \ldots + \alpha_p S(n -.$$

Figure 2 demonstrates how the prediction error ($e($) is defined. By minimizing the square of the error $\{e(n)$ filter coefficients can be generated. After finding the locations of the resonance to extract the formant frequencies from the filter, the filter coefficients were treated as a polynomial and solved for the roots of the polynomial.

In vowel analysis, frequency values regarding first formant, F_1, and second formant, F_2, were extracted from the recorded voiced track with the aid of mathematical modelling tools and the vowel distribution was obtained by plotting F_1 against F_2. In the analysis of vowel distribution, primary cardinal vowels introduced by Jones (1953) were used as a reference.
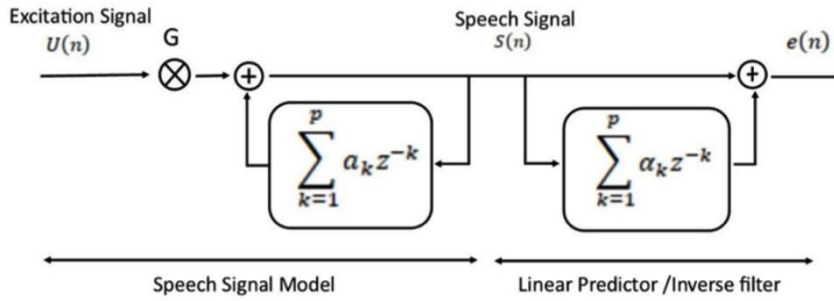
Figure 2: Linear Prediction model and speech signal model

3. RESULTS AND DISCUSSION

In the frame by frame analysis, speech signals are divided into a non-overlapping frame of samples. Figure 3, Figure 4, and Figure 5 show the vowel distribution for each of the 25 samples of *Rathana*, *KaraniyaMetta,* and *AngulimalaSuttas* respectively. Those figures offer a comparison of vowel distribution with primary cardinal vowels.
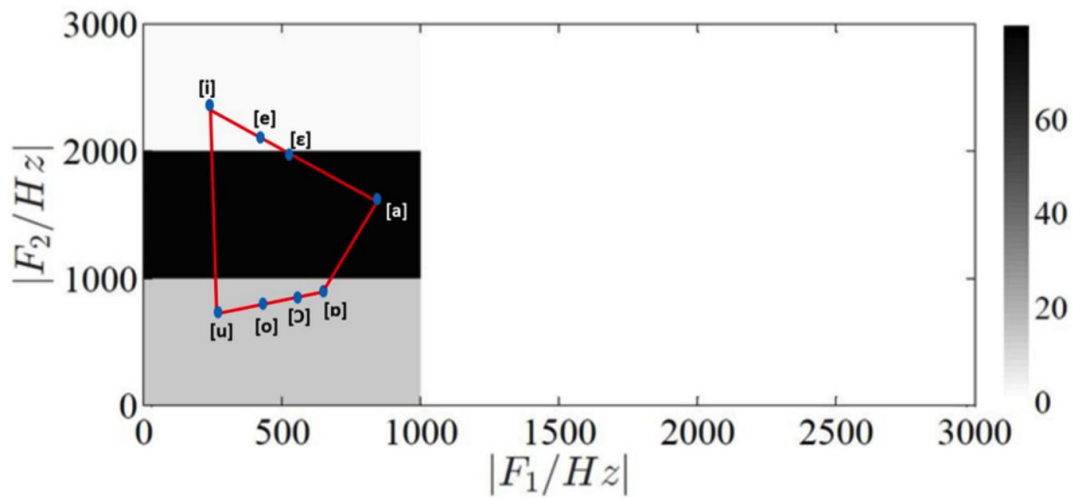

Figure 3 The comparison between vowel distribution of *Angulimala*sutta and primary cardinal vowels reported in Bruce, 2010.
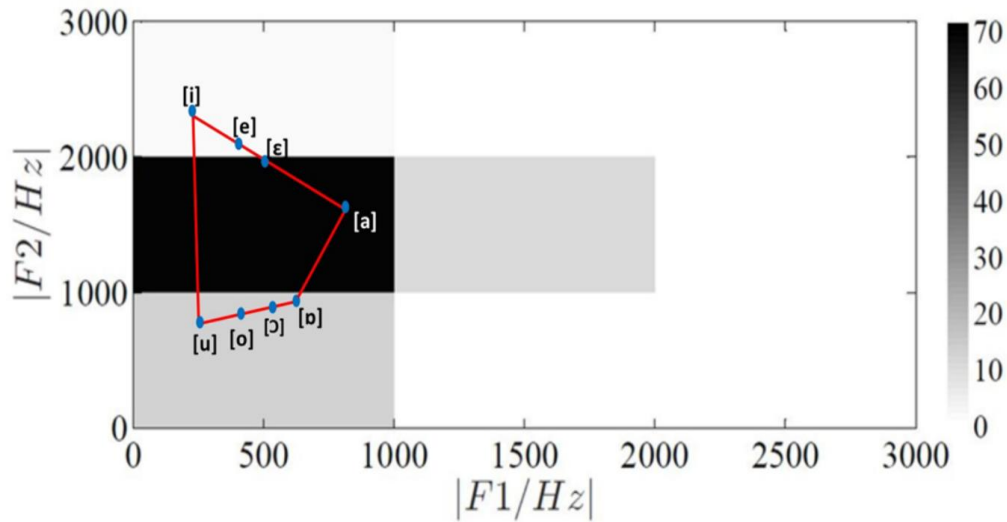
Figure 4 The comparison between vowel distribution of the *KaraniyaMettaSutta*and primary cardinal vowels reported in Bruce, 2010

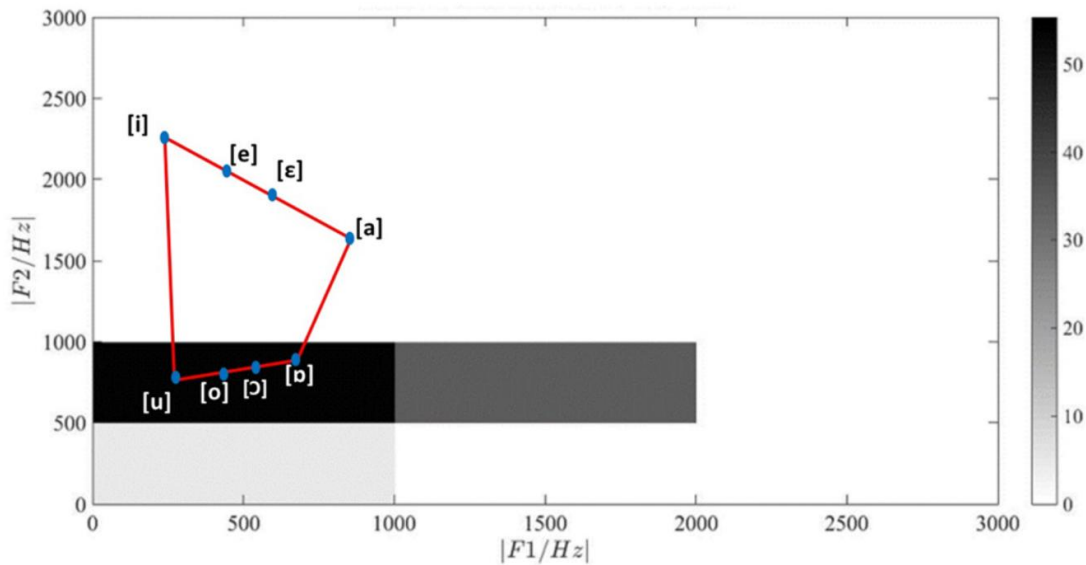**Figure 5**The comparison between vowel distribution of the*Rathanasutta*andprimary cardinal vowels reported in Bruce, 2010

A previous research study on formant frequency tuning in professional Byzantine chanters shows clear evidence that chanters have a special ability to use personal formant tuning at chanting (Fant, 1973). In this analysis, vowel distribution reveals that the majority of vowels inthe *AngulimalaSutta* and *KaraniyaMettaSutta* are vowels concentrated around the frequency range of $F_1, 0 - 1000\,Hz$ and $F_2, 1000 - 2000\,Hz$ as shown in Table 2, while the vowels of the*RathanaSutta*concentrate around the frequency range of $F_1, 0 - 1000\,Hz$ and $F_2, 500 - 1000\,Hz$. When comparing the results with the cardinal vowel chart, the densest vowel areas for the *AngulimalaSutta* and *KaraniyaMettaSutta*, show the qualities of cardinal vowel [a] as shown in Table 2, while the vowels of *RathanaSutta*remaincloser to cardinal vowels [u],[o],[ɔ], and [ɒ].

37

Table 2- Vowel distribution in all *Suttas* in percentage values

	Area		Vowel Percentage
	F1 range (Hz)	F2 range (Hz)	
AngulimalaSutta	0-1000	0-1000	11.98%
	0-1000	1000-2000	67%
KaraniyaMettaSutta	0-1000	0-1000	15.81%
	0-1000	1000-2000	77%
RathanaSutta	0-1000	500-1000	66%
	1000-2000	500-1000	20%

4. CONCLUSION

It can be concluded as when chanting the *AngulimalaSutta* and *KaraniyaMettaSutta*, the arrangement is inclined to be the tongue is low positioned in front levels while lips shaped unrounded. Vowels of *RathanaSutta* are show low back rounded vowel and high back rounded vowels. Besides, vowels generated with lower positioned tongue are called open vowels while high positioned ones are closed vowels. Therefore, it can be concluded that higher number of open vowels are articulated in *Pirith* chanting with totally disuse of closed vowels.

ACKNOWLEDGEMENT

REFERENCES

1. Bachu, R., Kopparthi, S. and Adapa, B. (2010). Voiced/Unvoiced Decision for Speech Signals Based on Zero-Crossing Rate and Energy. Advanced Techniques in Computing Sciences and Software Engineering. Springer, Dordrecht., pp.279-282.

2. Bruce, G. and Engstrand, O. (2006). The phonetic profile of swedish. Sprachtypologie und Universalienforschung,12–35.

3. Bruce, G. (2010) Vårfonetiskageografi: Om svenskansaccenter, melodiochuttal. Lund: Studentlitteratur.

4. Emoto, M., 2004. The True Power of Water: Healing and discovering our selves, Oregon,159pp, USA: Beyond world pub Co..

5. Fant, G. (1973). Speech Sounds and Features. 159 pp, Cambridge, MA: MIT Press.

6. Gunawardana, M.A.C.P. and Gamage, S.S.N. (2018), Evaluation of Acoustic Parameters for AngulimalaSutta using Voiced to Unvoiced Ration and Vowel Distribution, International Journal of multidisciplinary Studies-IJMS 2018, Vol 5(1): 1-8.

7. Jones, D. (1953). An English pronouncing dictionary. London: J.M. Dent. New York.

8. Lee, J. and Yoo, C. (2003). Wavelet speech enhancement based on voiced/unvoiced decision. In: Korea Advanced Institute of Science and Technology The 32nd International Congress and Exposition on Noise Control Engineering. pp.4149-4156.

9. Stevens, K. and House, A. (1955). Development of a Quantitative Description of Vowel Articulation. The Journal of the Acoustical Society of America, 27(3), pp.484-49

Light travel time effect of the binary orbit of SZ Lyn

J. Adassuriya,[1*] K.P.S. Chandana Jayaratne,[2] and S. Ganesh[3]

Astronomy Division, Arthur C Clarke Institute, Katubedda, Moratuwa, Sri Lanka

Department of Physics, University of Colombo, Colombo 03, Sri Lanka

Astronomy and Astrophysics Division, Physical Research Laboratory, Ahmedabad, India.

Abstract

SZ Lyncis, HD 67390 (RA=08^h 09^m 35.8^s, DEC=+44° 28' 17.6") is a high amplitude Delta Scuti type binary star of magnitude m_v= 9.1, which has pulsation period of 0.12053491 days and long orbital period of 1185 days. We determine fifty two new times of light maxima and collected all times of light maxima to calculate the orbital elements of SZ Lyn. The photometric observations were carried out in six nights at Mount Abu Infrared observatory, India. The difference of the observed times of light maxima and calculated times of light maxima is denoted by the O−C diagram of SZ Lyn. A total of 378 light maxima, including our observations of 20 light maxima of SZ Lyn, 32 of Wide-angle search for planets (WASP), 162 of American Association of Variable Star Observers (AAVSO) and 164 observations that have been published, were used for the O−C analysis. The non linear O−C diagram was approximated by secular change in pulsation period and the light-travel-time effect of the binary orbit. The fitting non-linear function of secular change and light-travel-time effect in the least square method determines the orbital parameters projected semi-major axis of the binary orbit $a \sin(i)$, eccentricity (e), longitude of the periastron passage (ω), orbital period (P_{orbit}) and secular change of the pulsation period (β). The Levenberg-Marquardt algorithm and trust-region-reflective algorithm were used in the least square sense to converge theoretical function to observations with the minimization parameter χ^2 of the best fit. The determined $a \sin(i)$ is 1.4±0.1×10^8 km and the eccentricity e is 0.18±0.07. The convergence of solution also approximated the orbital period to be 1187±15 days.

Key Words: SZ Lyn, orbital parameters, photometric, pulsation period

[*]Corresponding author: Email: adassuriya@gmail.com

1. INTRODUCTION

SZ Lyncis, HD 67390 (RA=08h 09m 35.8s, DEC=+44_ 280 17.600) is a high amplitude Delta Scuti type binary star, visual magnitude m_v= 9.1, spectral type of A7-F2, and has a pulsation period of 0.12053491 days and an orbital period of 1185 days (Soliman*et al*. 1986). The pulsating star is the brighter component while the faint component could not be observed in spectroscopy and is characterized as single line spectroscopic binary (Gazeas*et al.* 2004). The Delta Scuti stars are pulsators situated in the classical Cepheid instability strip on the main sequence or moving from the main sequence to the giant branch (Breger 2000). The main characteristic of Delta Scuti stars is the very short period pulsation time, ranging from 0.02 to 0.25 days. The orbital parameters of a binary system can be determined by spectroscopy if it were double line or by photometry if it were a transit system. SZ Lyn is neither double nor transit system. The pulsation property of SZ Lyn is used by observers, Van Genderen (1967), Moffett *et al.* (1975), Paparo*et al.* (1988), Li Lin-Jia*et al.* (2013), to determine orbital parameters with the use of O−C variations. The linear ephemeris of the time at maximum brightness for the pulsating stars is given as:

$$T_{max} = T_o + P \times E \tag{1}$$

where*E* denotes cycle number, *P* is the pulsation period, T_o is the initial epoch of maximum and T_{max} is the time at maximum brightness of the observation. According to the equation 1, the ephemeris of the intrinsic fundamental pulsation period of SZ Lyn was first determined by Binnendijk (1968) as:

$$T_{max} = 2439121.7003 + 0.12053188 \times E \tag{2}$$

and it was redefined by Gazeas*et al.* (2004) as:

$$T_{max} = 2452776.289 + 0.1205349 \times E \tag{3}$$

The star has been discussed a number of times in the literature for the periodic variations and the main pulsation period is found to change $(2.25\pm0.42)\times10^{-12}$ day per cycle (Paparo*et al*. 1988). Van Genderen (1967) reported that the linear ephemeris does not accurately predict the time of pulsation maximum. Barnes and Moffett (1975) suggested that this was due to the very long period orbital motion of SZ Lyn and hence the linear ephemeris deviated due to the light-travel time across the orbit.

The times of light maxima predicted by the linear equation 1 are known as calculated light maxima and denoted by C. The observed times of light maxima were taken by the light curve of SZ Lyn, denoted as 'O'. The assumption of constant pulsation period and linear ephemeris results in the O−C, the difference of observed and calculated times, being zero. The O−C diagram of SZ Lyn was previously studied by several authors, Moffett *et al*. (1988), Paparo*et al*. (1988) and showed a non-linear relation. The non-linearity of the O−C diagram can be explained by periodic variations of the main pulsation period and light-travel time across the binary orbit (Irwin 1952). The non-linear ephemeris is given by:

$$T_{max} = T_o + P \times E + \kappa + \tau \tag{4}$$

$$\kappa = \frac{\beta}{2}E^2 \tag{5}$$

$$\tau = \frac{a\sin(i)}{c}\left[\sqrt{1-e^2}\sin E^* \cos\omega + cosE^* \sin\omega - e\sin\omega\right] \tag{6}$$

Equations (5) and (6) are the periodic variation and light travel time effect of the orbit respectively. βis the secular change in the pulsation period, $a\sin(i)$ is the projected semi-major axis to the line of sight, e is the eccentricity, E^* is the eccentric anomaly, ω is the longitude of the periastron passage and c is the speed of light. The combination of the intrinsic pulsation and binary orbit produces a very complex O−C diagram for SZ Lyn. A comprehensive O−C analysis provides details of the orbital parameters and the pulsation properties. The times of light maxima from Mount Abu observations, WASP (Wide-angle search for planets), AAVSO, and all the observations that have been published were used for the classical O−C analysis method. This paper reports the photometric observations carried out at Mount Abu observatory in Section 2, detailed analysis of O−C diagram in Section 3 and discussion and conclusions in Sections 4 and 5, respectively.

2. EXPERIMENTAL

The observations were carried out at Mount Abu Infrared observatory. The observatory is located 1680 meters above the sea level in the western state of Rajasthan, India. Observations were made using a 50 cm, f/6.8 equatorial mount telescope equipped with an Andor 1024x1024 EMCCD thermoelectrically cooled to -80 °C. A set of 4569 frames in the V band obtained over six nights were subjected to basic reduction steps of bias and flat field correction, and the instrumental magnitudes extracted by defining an aperture of four times the FWHM of the star. Though the field of view of the imaging system, 13×13 arc seconds, is relatively large, there were no stars of similar magnitude to SZ Lyn to perform the differential photometry. Therefore to normalize the six day observations, all magnitudes were shifted to the highest magnitude of six days. A part of normalized light curve is shown in Figure 1. The entire light curve provides 20 light maxima. In addition, the WASP observation of SZ Lyn in the V band of a total of 2894 frames covering 32 light maxima, 162 maxima from AAVSO and 164 from all the previous observations brought together for a total of 379 times of light maxima for O−C analysis.
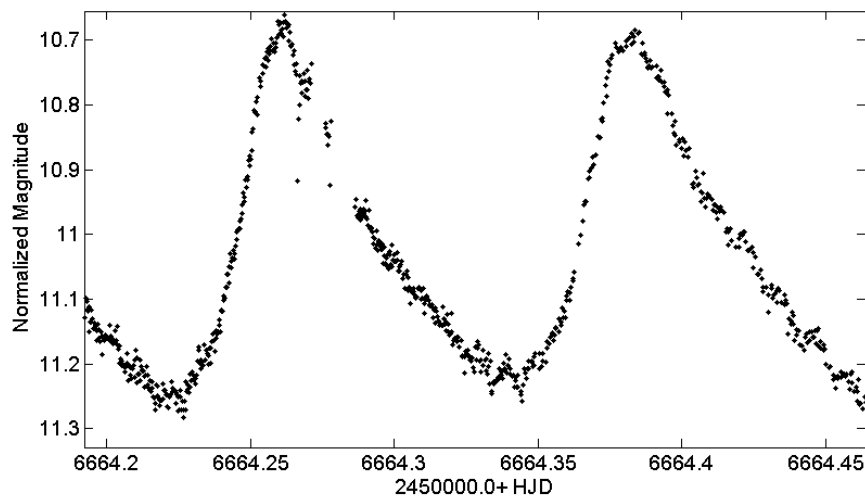

42

Figure1: Light curve of SZ Lyn taken on 6th January 2014 at Mount Abu observatory.

3. RESULTS & DISCUSSION

3.1 Observed times of light maxima (O)

The discrete magnitudes shown in Figure 1 were approximated by a continuous Fourier fitting and hence determine the first derivative of the function. The time equivalent to the zero point of the first derivative which is changing from negative to positive (Fig. 2) of the Fourier function was taken as the observed times of light maxima, 'O'.

3.2 Calculated times of light maxima (C)

The ephemeris given by Paparo et al. (1998) in equation 7 was used to calculate the calculated times of light maxima (C). The number of cycles, E, were taken from equation 7 for the observed times of light maxima (T_m) and assuming pulsation period 0.12053492 days. These calculated values were converted to integers to represent the cycle number. Thereafter calculated times of lightmaxima, T_{max}which is denoted by 'C' were taken from equation 7 by feeding the corresponding number of cycles which are calculated using the observed T_{max}.
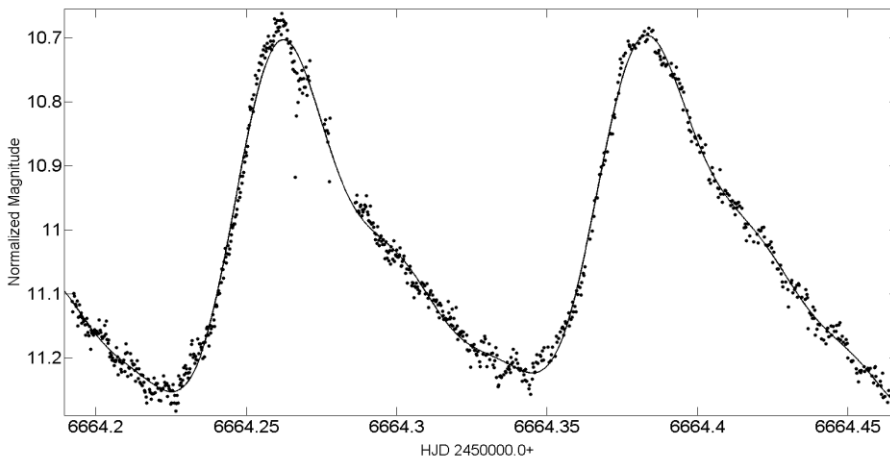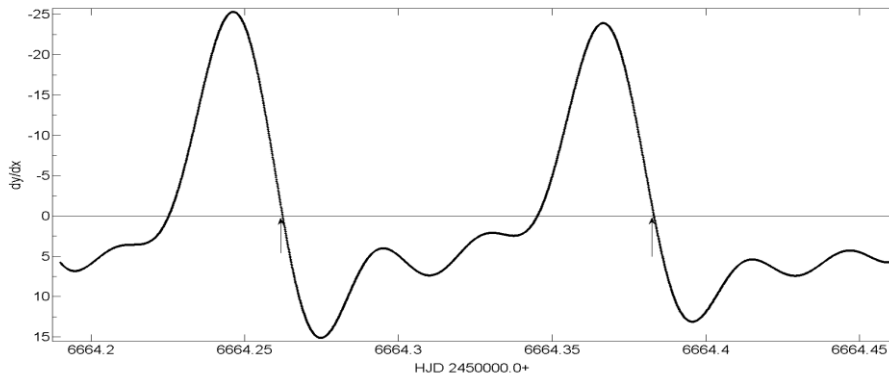

Figure 2 (a)

Figure 2 (b)

Figure 2: Fourier approximation of the light curve Figure 2(a). Note that the Y axis is reversed to get the correct magnitude scale. The first derivative of the Fourier function and the times of light maxima taken from zero points were marked with arrows Figure 2(b).

$$T_{max}(HJD) = 2438124.39955 + 0.12053492 \times E \tag{7}$$

Finally the difference of observed and calculated times of light maxima were calculated and denoted as O−C. The O−C value against the cycle number E is shown in Figure 3.
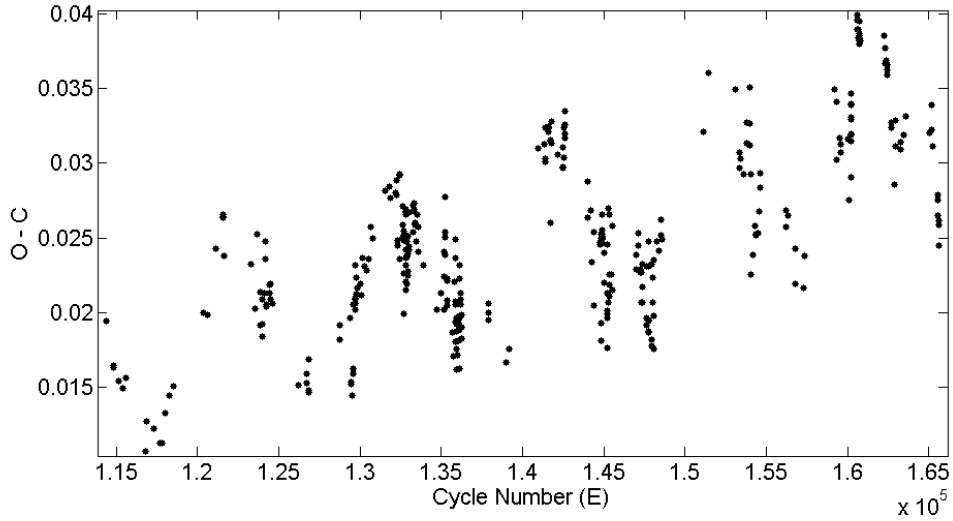

Figure 3: The difference of times of observed and calculated light maxima.

The O−C in Figure 3 is a non-linear distribution with an overall increase in O−C and some local variation. The non-linear behavior implied that there is a countable effect of light travel time in the binary orbit (Irwin 1952) as well as change in pulsation period. The overall increase is due to the change in pulsation period which is given by the quadratic equation in equation 5. The local variation is a sinusoidal function which is given by the light travel time effect of the binary orbit in equation 6. The introduction of light travel time effect to the O−C variation provides the orbital parameters to be included in the calculation. Therefore the equation 4 provides the unknown parameters for non-linear least square fitting to the O−C variation.

3.3 Non-linear curve fitting

The O−C diagram clearly shows that the O−C variation is not constant and it is non-linear. Therefore ephemeris in equation (1) is inadequate to explain the variation of O−C. The terms in equation 5 and 6 are additionally needed to explain the variation of O−C. The exponential term (κ) in equation 4 is resulted the overall increase of the O−C variation and the light travel time effect (τ) in equation 6 along the binary orbit is caused the sinusoidal variation. In order to fit the difference of observed and calculated times of light maxima, the equation of O−C should be included the correction values of T_o and P denoted by δT_o and δP respectively. Therefore O−C equation should be;

$$O - C = \delta T_o + \delta P \times E + \kappa + \tau \tag{8}$$

The light time travel effect of equation 6 is a function of eccentric anomaly (E*). The eccentric anomaly should be converted to the common independent variable of cycle number (E) in equation 8. Therefore the equation 4 was transformed to the independent variable (E) using equations 9 and 10.

$$M = E^* - e \sin E^* \qquad (9)$$

$$M = \frac{2\pi}{P_{orbital}}(T_{max} - T) \qquad (10)$$

where M is mean anomaly, $P_{orbital}$ is the orbital period of SZ Lyn, and T the time of passage through the periastron where E* is zero.

The parameters determined by Li Lin-Jia *et al*. (2013) given in Table 1 were used for initial calculations and estimations of δT_o and δP. The T_o and P values inTable 1 with the ephemeris given in equation 7 were used to calculate the δT_o and δP.

Table 1: Initial parameters of SZ Lyn used for optimization.

Parameter	Value
T_o (HJD)	2438124.39849
P (days)	0.120534908
β (days/cycle)	2.73×10^{-12}
a sin (i) (au)	1.002
e	0.17
ω (degrees)	117.6
P_{orbit} (days)	1182
T (days)	2445786.4

The optimization tool, *lsqcurvefit,* in MATLAB with two algorithms, 'trust-region-reflective' and 'Levenberg-Marquardt', was used iteratively to converge the solution. Equation 8 was fitted to the data points in the least square sense as shown in Figure 5 using *lsqcurvefit*solver. Two different optimization techniques given in table 2 determine the orbital parameters.
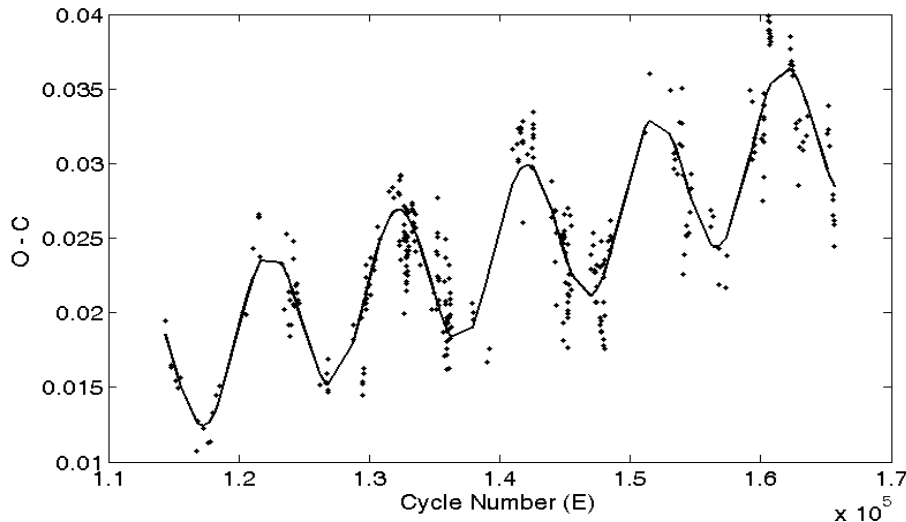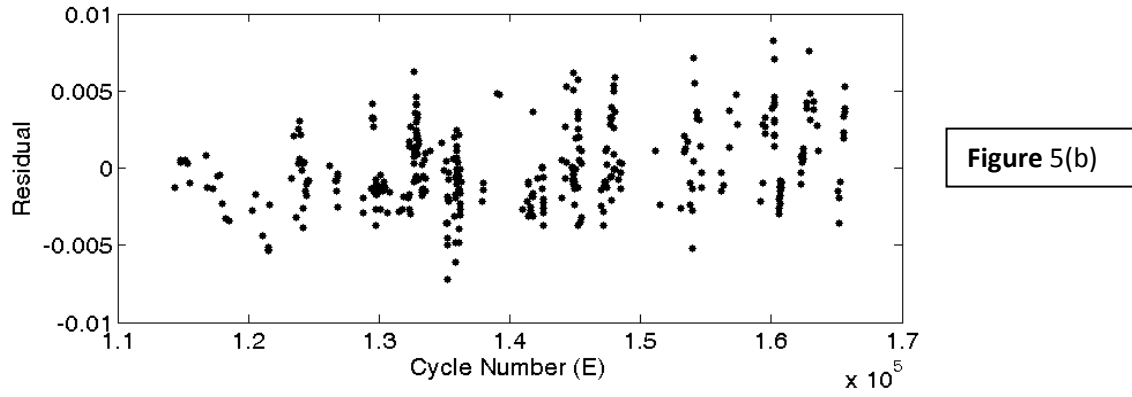

Figure 5(a)

Figure 5(b)

Figure 5: The least square fitting of equation 8 to the observed O−C data Fig 5(a) and the residual of the function Fig 5(b).

We fixed the values of δT_o, δP, P and T as 0.001, 2×10^{-9}, 0.12053491 and 2454786.4 respectively and consider $a\sin(i)$, eccentricity (e), longitude of the periastron passage (ω), orbital period ($P_{orbital}$) and secular change (β) as coefficients in the non-linear equation. In thelsqcurvefit approach, the initial values for those coefficients were assigned and the solution was converged to the minimum value of χ^2,0.0022, in both algorithms mentioned in Table 2. Figure 5 shows the approximation of the equation 8 to the observations. The continuous line is the equation 8 with the secular change in the pulsation period and the light travel time effect of the orbital motion of the SZ Lyn.

Table 2: Optimization parameters of *lsqcurvefit*

Algorithm	Trust-region-reflective	Levenberg-Marquardt
MaxIter	5000	5000
TolFun	4×10^{-18}	4×10^{-18}
TolX	1×10^{-17}	1×10^{-17}
MaxFunEvals	5000	5000

Table 3: The obtained orbital and pulsation parameters of SZ Lyn

Parameter	Trust-Region	Levenberg- Marquardt
Status of Convergence	Local minima possible	Local minima found
χ^2	0.0022	0.0022
a sin(i) (km)	$(1.4\pm0.1)\times10^8$	$(1.4\pm0.1)\times10^8$
e	0.17±0.05	0.18±0.07
ω (°)	106±11°	106±5°
β (days/cycle)	$(2.4\pm0.4)\times10^{-12}$	$(2.2\pm0.2)\times10^{-12}$
P_{orbit}(days)	1186±15	1187±15

The errors of the coefficient were estimated by the*nlparci*function in MATLAB. The parameters, residual, lambda, and Jacobian (J) produced by *lsqcurvefit*function were fed into the *nlparci*function to get the 95% confidence intervals of the coefficients, which are given as the *ci* matrix.

4. DISCUSSION

SZ Lyn, the short period binary variable star, has been observed for many years. This binary system is very complicated as the major star, SZ Lyn, is pulsating in radial and non-radial modes. The light curve has the binary variation as well as the intrinsic pulsation variations. However this intrinsic pulsation time scale is very much shorter than the extrinsic magnitude variations due to the binary. The orbital parameters were calculated several times with the addition of times of light maxima contributed by different observers. Li Lin-Jia*et al*. (2013) have investigatedthe SZ Lyn binary system with the 262 times of light maxima. This study includes the AAVSO data for the O – C analysis providing a total number of 378 data points, the highest number of data points for an orbital analysis. The higher number of data points are significant for this analysis because it provides many orbital and pulsation cycles and hence the solutions are accurately converged. However the convergence is also depended on the quality of the observations. The AAVSO data is a collection of different observes with different systems. Therefore some inconsistency is shown in AAVSO data as the residual increases in Figure 5.

We used two algorithms to get the solutions. In Trust-region-reflective algorithm the, local minima are not found while in Levenberg-Marquardt (LM), the solution was converged. Therefore coefficients determined by LM method were considered as the final results. The handling of underdetermined systems using trust-region is unreliable. The optimization parameters in Table 2 were changed in Trust-region-reflective algorithm for the convergence, but the local minimacould not be found. Therefore it can be concluded that the LM method is more appropriate for a least squares solutions with several unknowns.

Although the O–C variation of SZ Lyn is well explained theoretically, it is very difficult to combine the intrinsic pulsation properties with the orbital properties as given in equations 8, 9, and 10. The solutions of the Kepler equation (equation 9), can only be obtained by successive approximations using Newton's method (Danby 2003). For simplicity we assumed the orbit is circular and therefore eccentricity e is zero. With this initial assumption of $e = 0$, the non-linear equation can be transferred to a common independent variable of cycle number (E). In this way we eliminate the eccentric anomaly (E*) from equation 8. But the binary system is non-circular and has some eccentricity, so the sine function fitted to the data points is not smooth enough as shown Figure 5.

The determined orbital parameters were agreed with the previous observations. Particularly the eccentricity *'e'* which is very important parameter for binary orbit is consistence for all the observations. The average value of all the observation is 0.19±0.02.
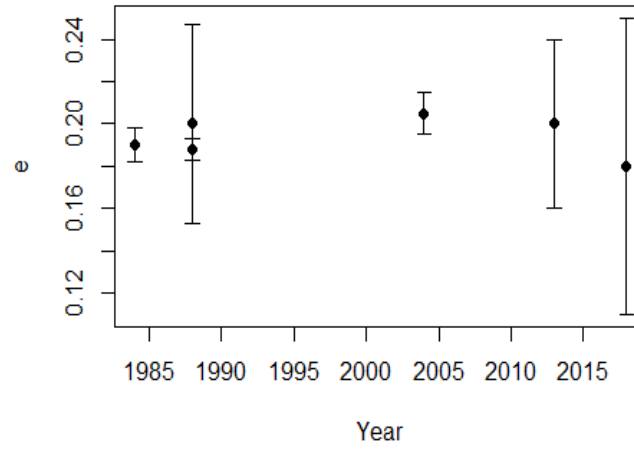
Figure 6: Thevariation of eccentricity of different observations.

The change in longitude of the periastron passage, also called apsidal motion in a binary system, has been observed for many years. This motion of the binary orbit can be caused by several effects such as general relativistic effect, tidal distortion, rotational flattening, a third component or combined effect (Li Lin-Jia*et al*. 2013). Li Lin-Jia (2013) proposed that ω is decreasing with time. In Figure 6, we found that the ω is inconsistently changing with the time.
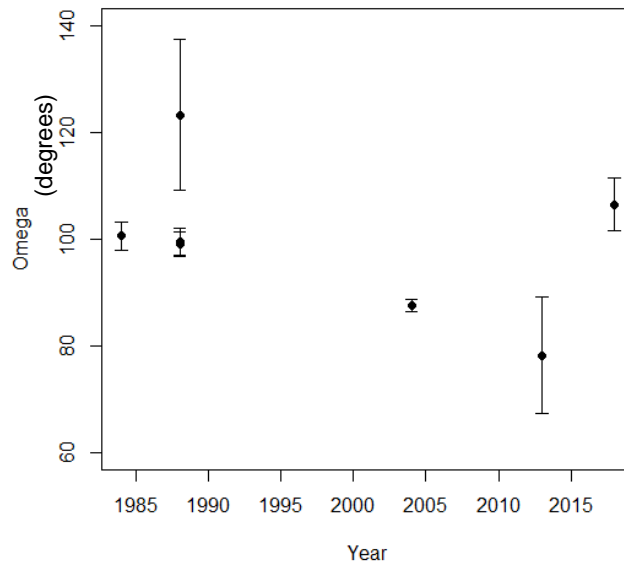

Figure 7: The variation of longitude of the periastron passage for seven different observers.

The dependency of the initial values and constants in the Table 1 to the determined orbital parameters was investigated. The value T, time of passage through the periastron where E*(T) = 0; determined by

previous observers were different. These different values were used in the optimization process and it was found that there is no significant change in the χ^2 value of 0.0022.

5. CONCLUSIONS

The orbital parameters were determined with the new photometric observations of SZ Lyn with a total number of 378 light maxima. The O−C analysis determined the projected semi-major axis a sin (i) as $1.4\pm0.1\text{x}10^8$ km and eccentricity, e is 0.18 ± 0.07. The orbital period is determined as 1187 ± 15 days. The orbital period is consistent within the above range, which does not deviate much from the previous determinations. The longitude of the periastron passage is highly uncertain as it is inconsistent in the previous determinations as well. Furthermore it can be concluded that the Levenberg-Marquardt least square algorithm is more appropriate for the convergence of a solution with several unknowns.

REFERENCES

1. Bardin, C., and Imbert, M., (1984). Orbital motion of the dwarf cepheid SZ Lyn.*Astronomy and Astrophysics*.57: 249.

2. Breger, M. (2000). *ASP Conference, San Francisco*.

3. Binnendijk, L. (1968). Photoelectric observations of SZ Lyncis.*Astronomical Journal*.73:29-31.

4. Gazeas, K., *et al.* (2004). SZ Lyn: New BVRI CCD observations and improved pulsational and orbital elements.*Communications in Asteroseismology*.144: 26-34.

5. Irwin, J. B., (1952). The Determination of a Light-Time Orbit.*Astrophysical Journal*. 116**:** 211.

6. Li Lin-Jia andQian Sheng-Bang. (2013). Observation and orbital analysis of high amplitude Delta Scuti star SZ Lyncis. *Publication Astronomical Society of Japan*.65: 116.

7. Moffett, J., *et al.* (1988). Orbital and photometric properties of SZ Lyncis.*The Astronomical journal*.95: 1534-1541.

8. Paparo, M., *et al.* (1988). The high amplitude Delta Scuti star SZ Lyncis revisited. *Astrophysics and Space Science*.149: 73-82

9. Soliman*et al*. (1986). Photoelectric Observations of SZ Lyncis.*Communications of the Konkoly Observatory*.88: 39-56.

10. Van Genderen, (1967). Variations in the period and in the light-curve of SZ Lyncis.*Bulletin of the Astronomical Institutes of the Netherlands*. 19: 74

Fabrication and characterization of rGO / PANI / TiO₂ compositeas an electrodematerial for supercapacitors

M.D.R. De Costa,[* 1,2] R.C.L. De Silva,[1] L.D.C. Nayanajith,[1] H.C.D.P Colombage,[1] S.R.D. Rosa,[2]and I.R.M. Kottegoda[1]

[1]*Materials Technology Section, Industrial Technology Institute, Colombo 07, Sri Lanka.*
[2]*Department of Physics, University of Colombo, Colombo 03, Sri Lanka.*

Abstract

Graphite is an important export product of Sri Lanka. However, little effort has been made to add value to the product. Graphene, synthesized from natural graphite, has a world market value more than 100,000 times that of natural graphite. A reduced graphene oxide (rGO)/Polyaniline (PANI)/Titanium Dioxide (TiO₂) composite has been synthesized by an *in situ* polymerization of PANI, with synthesis by a hydrothermal method. The preparation process is systematically investigated by Fourier transform infrared spectroscopy (FTIR) and X-ray diffraction (XRD). The morphology structure of the composite was examined by scanning electron microscopy (SEM). Electrochemical properties are characterized by cyclic voltammetry (CV), galvanostatic charge/discharge (GCD) and impedance spectroscopy. The specific capacitance of the rGO/PANI/TiO₂composite obtained was as high as 425 F g^{-1} at a current density of 1 mAg^{-1} showing potential for using as electrode in supercapacitors.The proposed work will attempt to develop economical and efficient methods to produce graphene based materials in commercial scalesand,in parallel,investigate high-tech applications, such as graphene based material for supercapacitors.

Keywords:*NaClO₄ electrolyte, rGO / PANI / TiO₂ composite,supercapacitors*

1. INTRODUCTION

Sri Lanka owns one of the best graphite sources in the world. However, it is being exported mainly as a raw material at a very low price. It is desirable to enhance our earnings from local graphite by at least partially converting natural graphite into value added forms, such as multi-layer grapheneand reduced graphene oxide (rGO). Graphene based materials have attracted worldwide attention due to a huge range of high-tech applications[1]. Sri Lanka has a great opportunity toobtain the maximum benefit by exporting high quality value added materials from graphite. The proposed work attempts to develop

---

[*]Corresponding author: Email: damithdecosta123@gmail.com

economical and efficient methods to produce graphene based materials on commercial scales.In parallel,investigation of high-tech applications, such as supercapacitors, can be constructed using graphene based composites.

Three dimensional (3D) reduced graphene oxide (rGO) has attracted extensive attention [2-4] due to its superior porous bulk structure [5], high specific capacitance [6], largespecific surface area [7], and excellent adsorption capacity [8-9].In recent years, the formation of functional three dimensionalgraphene/polymer composites by combining graphene with polymers has attracted much attention, which greatly expands theapplications of graphene[10-16].

TiO_2has been studied extensively due to its high chemical stability, large surface area, degradability and commercial availability[17-20]. However, the wide band gap (3.2 eV) and the nature of the powder limit the utilization efficiency of light and its applications [21].Transition metal oxides andconducting polymers with various oxidation states have attracted intense interest as potential supercapacitor materials. Among thevarious conducting polymers, polyaniline (PANI) is a promising candidate for practical applications due to its high capacitivecharacteristics, its environmental stability, low cost, commercialavailability, facile synthesis, and high conductivity [22-23]. However,poor stability during the charge-discharge process restricts itspractical application in supercapacitors. One of the ways to improvethe performance of PANI based supercapacitors in terms of stability is to combine PANI with transition metal oxides. Polymer-metaloxide composite electrodes have shown enhanced supercapacitiveproperties compared to the pristine electrode material [24-26].

Considering all the advantages of graphene, TiO_2, and PANI, in the present study, a novelrGO/ PANI/TiO_2 nano composite was synthesized and investigated as an electrode forsupercapacitors. In addition rGO was synthesized using local graphite,which would be a value addition to Sri Lankan graphite.

2. METHODOLOGY

Synthesis of the composite

Graphite was obtained from the Kahatagaha graphite mine in Sri Lanka. The reagents and chemicals NaOH, $NaNO_3$, H_2SO_4, HCl, $KMnO_4$, H_2O_2, TiO_2, Aniline, $(NH_4)_2S_2O_8$, L- ascorbic acid and ethanol were provided by Sigma–Aldrich Co, USA, and SuperchemProducts Ltd, England.

First, the graphite from Kahatagaha mine was converted into Graphite Oxide (GO) following the improved Hummers method [27]. Secondly, L-ascorbic acid (40 mg) was added into 4 mL of 4 mg mL^{-1} GO solution with ultrasonication for 40 min and heated at 95°C for 1.5 h to obtain the graphene hydrogel. Eight mg of PANI was added into 20 ml distilled water in separate beaker and it was sonicated for 2 h. Eight mg of TiO_2 were directly added into the PANI solution. Finally the pre-prepared graphene solution was added to the PANI/TiO_2 solution under ultra-sonication for 40 min. The resulting solution was placed in a water bath at 95 °C for 1.5 h. The resulting suspension was centrifuged, and the solid separated was washed 4 times with distilled water and four times with ethanol, by centrifugation. It was then dried in a vacuum oven at 70°C to obtain the rGO/ PANI/TiO_2 composite, which is the material for electrodes for the supercapacitor.

Fabrication of electrodes for supercapacitor

The synthesized material was used to fabricate electrodes for the supercapacitor as active material on stainless steel plates by spreading a slurry made of rGO / PANI /TiO$_2$ composite 85% (active material) with 5% acetylene black and 10% polytetrafluoroethylene (PTFE- 60 wt %) as the binder and leaving it to dry slowly. Filter paper (50 μm) placed as the separator was soaked with the electrolyte consisting of a 1 M solution of NaClO$_4$ in propylene carbonate. Electrical contacts were firmly made to touchthe electrodes to avoid any voltage drop. A bubble of soldering material located on either jaw of each crocodile clip was used for this purpose.
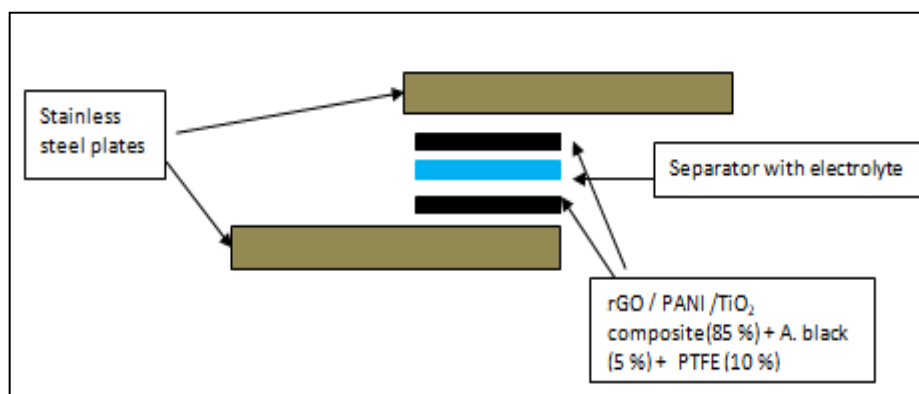

Figure 1: Schematic diagram of fabrication of electrodes for supercapacitor

The specific capacitance of the electrode was calculated from the CV curve according to the formula: $C_{sc} = 2\int I(V)dV/m\upsilon\Delta V$, where C_{sc} is the specific capacitance (F g^{-1}) based on the mass of electroactive materials, m is the weight of active material (g), υ is the scan rate (V s^{-1}), ΔV is the potential window (V) and I is the response current density (A).

Measurements/Characterization Analysis

X-ray diffraction (XRD) analysis was conducted by using aRegakuultima VI X-ray Diffractometer using Cu Kα (λ= 1.542 Å) radiation to analyze the structure of the sample. Crystallographic information was obtained with the aid of the ICDD data base. Scanning electron microscopic tests (LEO 1420 vp) were carried out to study the formation of cathode material with maximum enabled instrument resolution. Fourier Transform Infrared spectroscopy (FTIR) (Bruker Tensor 27) was carried out to determine the type of the atomic bonding in the composites.

Electrochemical Performance

Charging / discharging tests and cyclic voltammetric measurements were performed (Biologic sp150) to find the charge retention of the developed rGO/PANI/TiO$_2$ based supercapacitor. Impedance spectroscopic measurements were made to find the impedance of the active material and to construct equivalent circuit matching with the impedance data.

3. RESULTS AND DISCUSSION

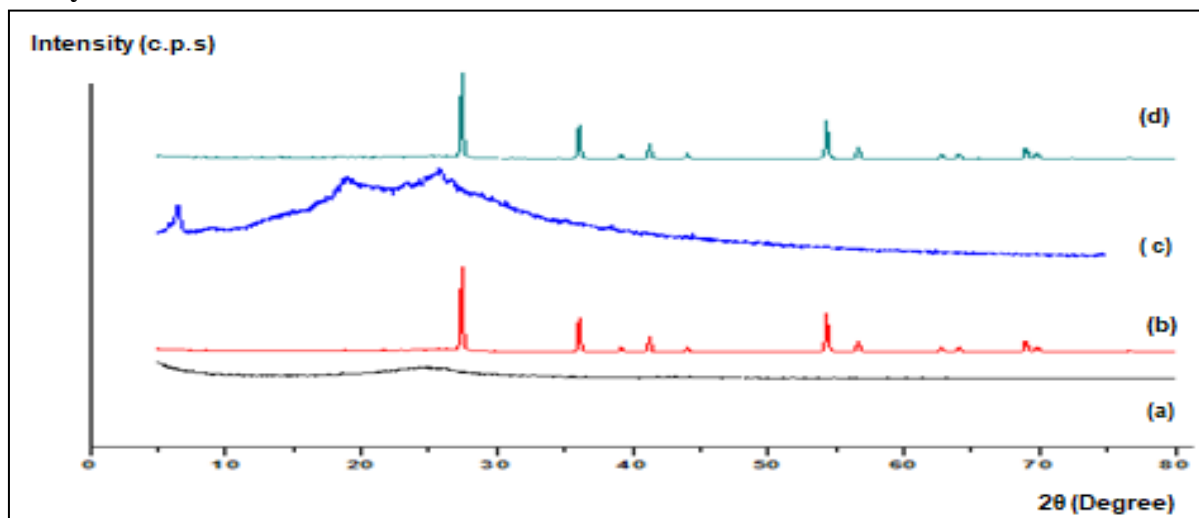**Characterization Analysis**

XRD Analysis

Figure 2: XRD spectrums of rGO (a), TiO_2 (b), PANI (c), andrGO / PANI / TiO_2composite(d)

XRD analysis was used to investigate the crystalline structureand phase purity of the as-prepared samples. As shown in fig. 2 (c), diffraction peaks of PANI indicated that PANI mainly existed inamorphous form. The width peaks were mainly concentrated at2θ= 20°, 26° with crystal planes of (0 2 0) and (2 0 0) which is the peak of Bragg diffraction characteristic of PANI [28]. Diffraction peaks at 25° are the (110) face of PANI,which is attributed to the periodicity parallel to the polymer chainsof PANI [29]. There was a broad peak at ~26° for the diffractionpeaks of rGO in fig. 2 (a). The XRD pattern of TiO_2 could be observed at 2θ = 27.40°, 37.1°,42.3°, 44.8°, 54.9°, 56.1°, 64.1°, 65.2°, 70.3° with crystal planes of (1 0 1),(0 0 4),(2 0 0), (1 0 5), (211), (204), and (2 1 5) respectively in fig. 2 (b). The peak of rGO and PANI did not appear in rGO / PANI / TiO_2 composite in fig. 2 (d), obviouslydue to the high intense of peaks corresponding to TiO_2.

FTIR Analysis

The FTIR spectrum of prepared rGO / PANI / TiO_2 composite was shown in Fig. 3. The peak at about 1310 cm^{-1} and at 1268 cm^{-1}can be assigned to the C–N of intrinsic PANI [30]. The peak at about 760 cm^{-1}corresponds to Ti–O–Ti of TiO_2[31]. The FTIR results show that the rGO / PANI / TiO_2composite was successfully synthesized [32].

SEM Analysis

To confirm the nonporous nature of the rGO / PANI / TiO_2 composite the sample was examined using an SEM with1000 magnification. The crystals could be seen as clusters of smaller particles.
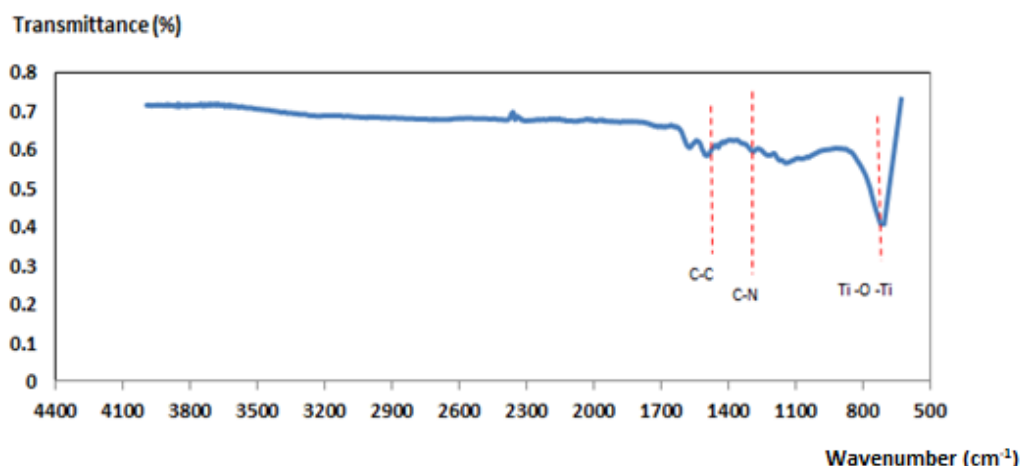
Figure 3: FTIR spectrum of rGO / PANI / TiO$_2$composite

Fig. 4 shows that the TiO$_2$particles in the rGO / PANI / TiO$_2$ complex arewell-distributed on the surface of rGO and PANI and closely relatedto each other. The micron size cavities can be visualized clearly which obviously results in high surface area which gives possibilities to use the composite in applications like supercapacitors, sensors and batteries.
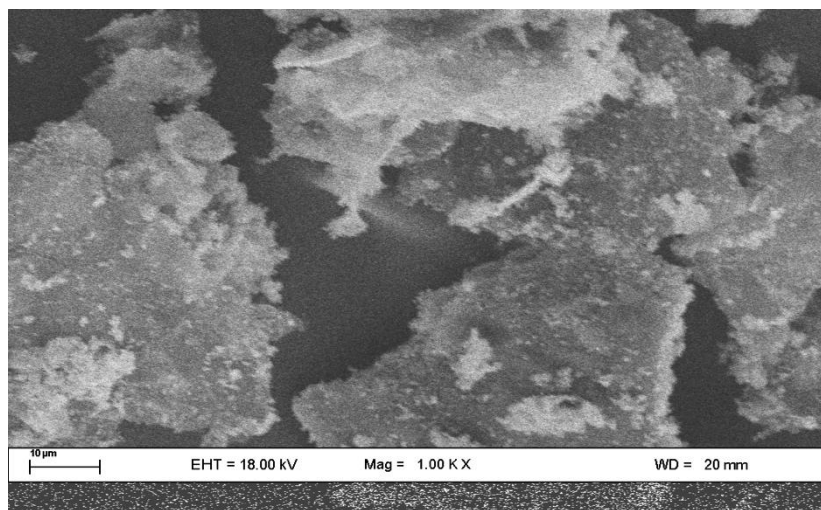

Figure 4: SEM image of rGO / PANI / TiO$_2$ composite

Electrochemical Performance /Charging / discharging test

Figure 5shows the charging / discharging curve of rGO / PANI / TiO$_2$ composite at 0.1 mA constant current for both charging and discharging. The shape of the charge / discharge curve is in typical triangular shape, which again indicates that there is no pseudo capacitance distortion behavior. It is also noted from Fig. 5. A voltage of 0.34 V was reported as the open voltage (no load) at the beginning and the supercapacitorwas kept for more than 25 charge-discharge cycles. An average of a 0.358 V was recorded as the maximum at charged voltage, which highlights the fact that after 26th charge/discharge cycle it still possesses the ability to hold the same amount of chargeas before. Nevertheless this was a

positive indication of the retention of charges without considerable draining. The voltage was still maintained at an average of above 0.12 V.
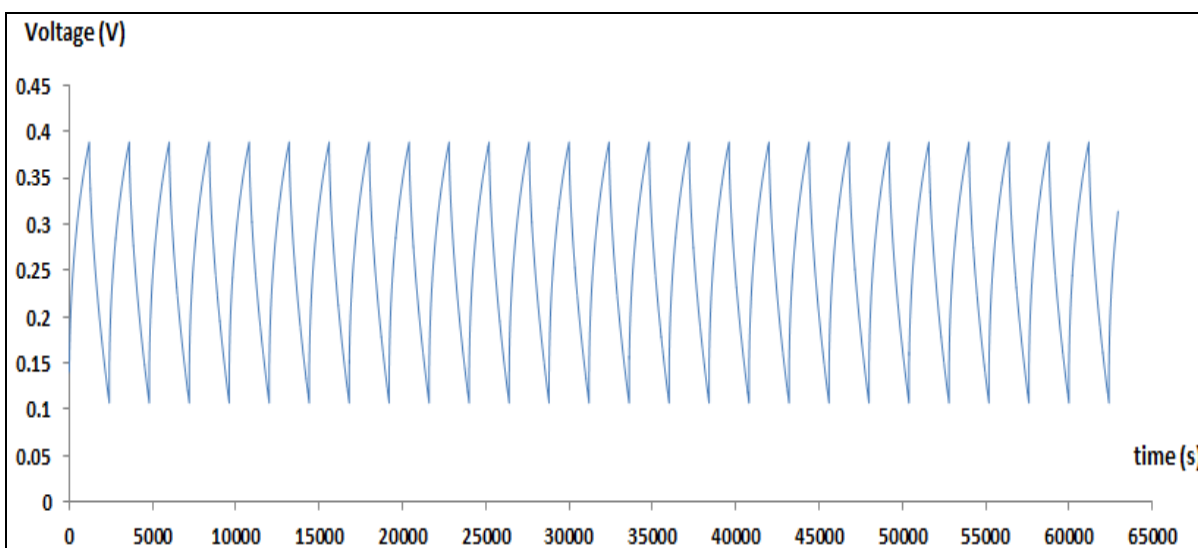

Figure 5: Charging / discharging curve of rGO / PANI / TiO$_2$ composite

Figure 6 depicts the 1st discharge behavior of rGO / PANI / TiO$_2$ composite electrode at different current densities. The specific capacitance can be calculated by the formula: $C_{sc} = I\, t/\Delta V\, m$, where $C_{sc}(Fg^{-1})$ is the specific capacitance of the electrode, I (A) is the discharging current, t (s) is the discharge time, ΔV (V) is the potential window and m (g) is the mass of the active materials.
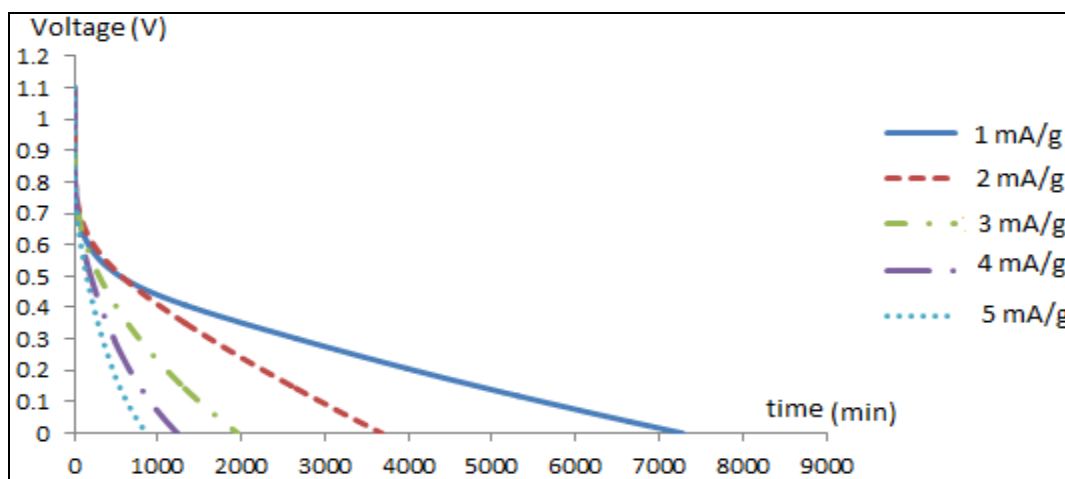

Figure 6: 1st discharge curves of rGO / PANI / TiO$_2$ composite for different current densities

The specific capacitance of the rGO / PANI / TiO$_2$ composite electrodewas 425, 402, 320, 270, and 236 Fg^{-1}at the current densities 1, 2, 3, 4, and 5 mAg^{-1}, respectively.

Cyclic Voltammetry (CV) analysis

Figure. 7 (a), (b) and (c) shows the cyclic voltammograms of supercapacitorsfabricated with rGO, rGO / TiO$_2$ and), rGO / TiO$_2$ composite (b) and of rGO / PANI / TiO$_2$ composite respectively at various scan rates. In fig 7 (a) and fig. 7 (b), CV tests were performed between -1 to 1V at a scan rate of 1 mVs^{-1}. The specific capacitance of rGO is 12.8 Fg^{-1} and rGO/ TiO$_2$ composite is 242 Fg^{-1}. The specific capacitance of rGO / PANI / TiO$_2$ composite are359 Fg^{-1}, 348 Fg^{-1},285 Fg^{-1} and 268Fg^{-1}at 5 mVs^{-1}, 10 mVs^{-1}, 15 mVs^{-1} and 20 mVs^{-1}scan rate with -1 to 1 V, -1.7 to 1.7 V, -2 to 2 V and -2 to 2 V potential windows respectively. It can be seen that as the scan rate increases from 5 to 20 mVs^{-1}, specific capacitance values decrease from 359 to 268 Fg^{-1} respectively.The CV curves of rGO / PANI / TiO$_2$ composite shows the pseudocapacitive behavior distinctfrom the electric double layer capacitance,which produces a CV curve close to the ideal reactangular shape[33]. The high capacity is attributable to the unique performance of the combination of rGO, PANI and TiO$_2$ such as high surface area, good electrical conductance and efficient ion and electron transport.
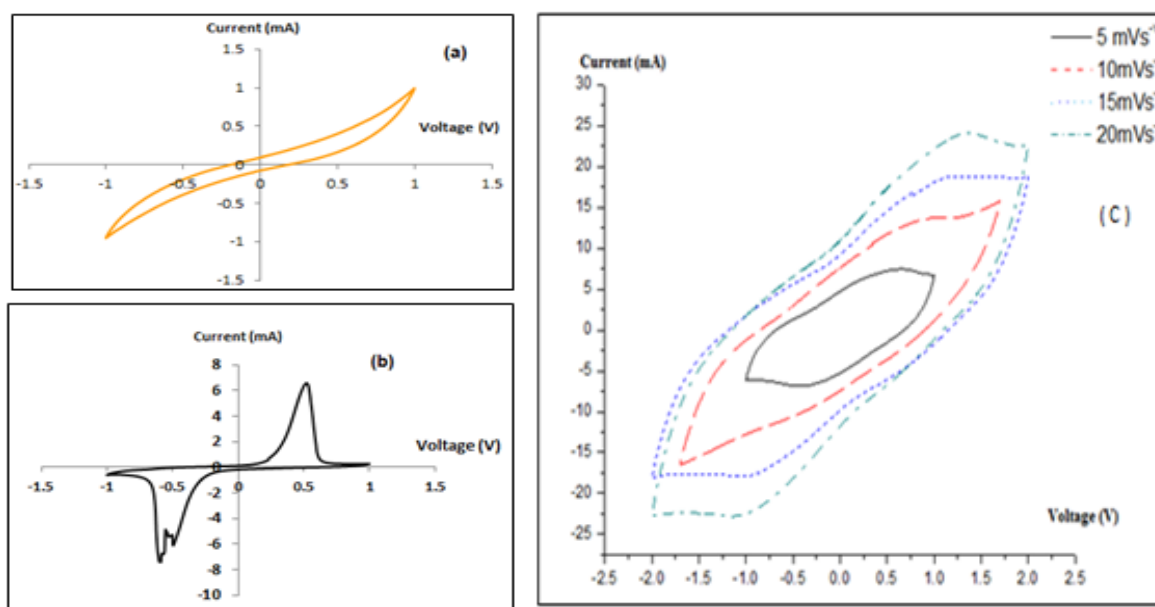

Figure 7: The CV curves rGO (a), rGO / TiO$_2$ composite (b) and of rGO / PANI / TiO$_2$ composite at various scan rates

Impedance analysis

Electrochemical impedance spectroscopy (EIS) is also used to characterize the composite electrode. Fig. 8(a) shows the Nyquist plots of the rGO / PANI / TiO$_2$ compositeelectrodes, represent common features with a semicircle at high frequency and a straight line at low frequency. The semicircle in the high frequency region is attributed to "charge transfer". The numerical value of the diameter of semicircle on the real axis gives an approximate indication of charge transfer resistance (R$_{ct}$) [34]. The possible fitted line for the original curve represented in solid line. The equivalent circuit of the rGO / PANI / TiO$_2$composite is shown in Fig. 8 (b).
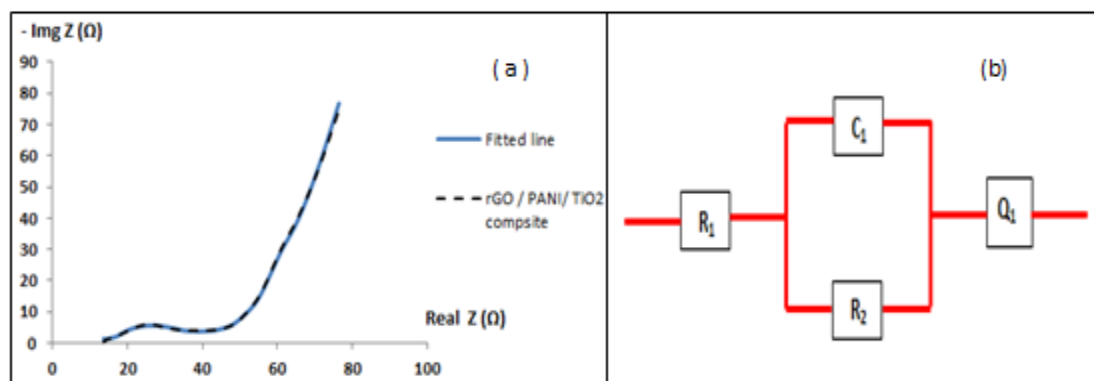
Figure 8: (a) Nyquist plot   and (b) Equivalent circuit of supercapacitorofrGO / PANI / TiO_2 composite electrodes

R_1 = 5.78 Ω which represent ohmic resistance. R_2 = 41.66 Ω represents the charge transfer resistance. Q_1 = 9.501 $Fs^{(a-1)}$ represents the double layer charge of the rGO / TiO_2 supercapacitor, where a = 0.23. C_1= 59.07 F represent capacitance of active material.

4. CONCLUSION

The rGO/PANI/TiO_2 composite with a well-ordered structureis prepared by one-step *in situ* polymerization of aniline in the presence of rGO and TiO_2particles. The specific capacitance of the composite was as high as425 Fg^{-1}, and it also showscharge/discharge stability as an electrode material. Our study demonstrated that the rGO/PANI/TiO_2nanocomposite was a potentialelectrode material forsupercapacitors.

ACKNOWLEDGEMENT

REFERENCES

1. Lokhande, C.D.,Dubal,D.P., and Joo,O.S., (2011).*Curr. Appl. Phys.*, 11, 255.

2. Ma,Y.F., and Chen,Y.S.,(2014),Three-dimensional graphene networks: synthesis, properties, and applications,*Natl. Sci. Rev.2,* 40–53.

3. Li,X., Yu, J.G.,Wageh,S., Al-Ghamdi,A.A., and Xie,J.(2016),Graphene in photocatalysis: A review,*Small,*12, 6640–6696.

4. X
    iang, Q.J., Yu, J.G., and Jaroniec, J.(2012),Graphene-based semiconductor photocatalysts, *Chem. Soc. Rev.*,41,782–796.

5. Z
    hang,X.T.,Sui,Z.Y., Xu, B., Yue, S.F., Luo,Y.J., Zhan, W.C., and Liu,B.(2011), Mechanically strong and highly conductive graphene aerogel and its use as electrodes for electrochemical power sources,*J. Mater. Chem.,*21, 6494–6497.

6. S
    ong, W.L., and Song, K., (2015),A versatile strategy toward binary three-dimensional architectures based on engineering graphene aerogels with porous carbon fabrics for supercapacitors,*ACS Appl. Mater. Interfaces,*7, 4257–4264.

7. X
    u, Z., Zhang, Y., and Li,P.G. (2012), Strong conductive lightweight neat graphene aerogel fibers with aligned pores, *ACS Nano.*,6 ,7103–7113.

8. C
    heng, C.S., and Deng, J. (2013),Toward 3D graphene oxide gel based adsorbents for high-efficient water treatment via the promotion of biopolymers, *J. Hazard.Mater.,*263 ,467–478.

9. L
    iang, W.Q., and Cui, H. (2017).Highly efficient removal of bisphenol A by a three-dimensional graphenehydrogel-AgBr@rGO exhibiting adsorption/photocatalysis synergy, *Appl. Catal,* 217, 65–80.

10. M
    iao, J.,Xie,A.J.,Li,S.K.,Huang,F.Z., Cao,J., and Shen,Y.H. (2016),A novel reducing graphene/polyaniline/cuprous oxide composite hydrogel with unexpected photocatalytic activity for the degradation of Congo Red, *Appl. Surf. Sci.,*360, 594–600.

11. L
    i.,X., Li, Q.,Wageh,S.,Al-Ghamdi,A.A., and Yu,J. (2015), CdS/graphenenanocompositephotocatalysts,*Adv. Energy Mater.,*5,1500010.

12. Z
    hang, Q.,Xu,X., Li, H., Xiong,G.P.,Hu,H., and Fisher, T.S. (2015), Mechanically robust honeycomb graphene aerogel multifunctional polymer composites,*Carbon*, 93, 659–670.

13. M
    u,C.F.,Zhang,Y., Cui, W.Q., Liang, Y.H., and Zhu,Y.F. (2017),Removal of bisphenol A over a separation free 3D Ag$_3$PO$_4$–graphene hydrogel via an adsorption-photocatalysis synergy, *Appl. Catal. B: Environ.,*212, 41–49.

14. C
    hen,X.J.,Chen,Q.,Jiang,W.J., Jiang, Z., Wei, Y.F., and Zhu,Y.(2017), Separation-free TiO$_2$–graphene hydrogel with 3D network structure for efficient photoelectrocatalytic mineralization, *Appl. Catal. B: Environ.,*211,106–113.

15. Low,J.X., Yu, J.G., and Ho,W.K.(2015),Graphene-based photocatalysts for CO_2 reduction to solar fuel, *J. Phys. Chem. Lett,* 6, 4244–4251.

16. Li,X.,Yu,J.G., and Jaroniec,M.(2016),Hierarchicalphotocatalysts,*Chem. Soc. Rev.,* 45, 2603–2636.

17. Kondamareddy, K.K., and Liu,M.,(2017),Two-dimensional TiO_2-based nanosheets co-modified by surface-enriched carbon dots and Gd_2O_3 nanoparticles for efficient visible-light-driven photocatalysis, *Appl. Surf. Sci.,*396, 185–201.

18. Liang,H.J.,Jia,Z.C.,Zhang,H.C.,Wang,X.B., and Wang,J.J. (2017),Photocatalysis oxidation activity regulation of Ag/TiO_2 composites evaluated by the selective oxidation of rhodamine B, *Appl. Surf. Sci.,* 422, 1–10.

19. Wen, J.Q.,Li,X., Liu, W., Fang, Y.P.,Xie,J., and Xu,Y.H. (2015),Photocatalysis fundamentals and surface modification of TiO_2nanomaterials, *Chin. J. Chem.,*36, 2049–2070.

20. Low, J.X.,Yu, J.G.,Jaroniec,M., and Wageh,S.(2017),Heterojunctionphotocatalysts, *Adv. Mater.,*29, 1601694.

21. He,D.,Li,Y.L.,Wang,I.S., Wu, J.S., and Yang,Y.L.(2017),Carbon wrapped and doped TiO_2mesoporous nanostructure with efficient visible-light photocatalysis for NO removal,*Appl. Surf. Sci.,*391,318–325.

22. Tong, Z.,Yang,Y.,Wang,J., Zhao, J.,Suc,B.L., and Li, Y.(2014),*J.Mater. Chem. A* 2, 4642.

23. Jaidev,R.I.,Jafri,A.K., and Ramaprabhu, M.(2011),*J. Mater. Chem.,* 21, 17601.

24. Zang,L.J., and Wang, M.X., (2003),*J. Phys. Chem.,*107, 6748.

25. Margelefsky,E.L.,Zeidan,R.K., and Davis,M.E.(2008),*Chem. Soc. Rev.,* 37, 1118.

26. Zheng,Y.Z.,Xue,W.,Zheng,S.L.,Tong,M.L.,Chen,X.M.(2008), *Adv. Mater.,* 20 ,1534.

27. Alemany,A.,Lu,L. B., and Tour, J.M.(2011),Improved synthesis of graphene oxide,*ACS Nano,*4, 8.

28. Chen,X.,Li,H.K.,Wu,H.S., Wu, Y.X., and Shang,Y.Y.,(2016),Fabrication of TiO_2@PANI nanobelts with the enhanced absorption and photocatalytic performance under visible light, *Mater. Lett.,*172, 52–55.

29. Jiang,W.J., Liu, Y.F.,Wang,J., Zhang,M.,Luo,W.J., and Zhu, Y.F. (2016),Separation-free polyaniline/TiO$_2$ 3D hydrogel with high photocatalytic activity,*Adv. Mater. Interfaces,*3,1–9.

30. Luo, J.,Jiang,S.S.,Wu,Y.,Chen,M.L., and Liu,X.Y.(2012),Synthesis of stable aqueous dispersion of graphene/polyaniline composite mediated by polystyrene sulfonic acid,*J. Polym. Sci. A: Polym. Chem.,*50,4888–4894.

31. Kumar,K.D., Kumar,G.P., and Reddy,K.S. (2015),Rapid microwave synthesis of reduced graphene oxide-supported TiO$_2$ nanostructures as high performance photocatalyst,*Mater. Today,*2,3736–3742.

32. Wei,W.Q.,Liu,D.,Wei,Z., and Zhu,Y.F.,(2016)Short-range stacking assembly on P$_{25}$ TiO$_2$ nanoparticles for enhanced visible-light photocatalysis,*ACS Catal.,*7, 652–663.

33. Sun, L.J., and Liu, X.X.(2008),*European Polym. J.,* 44, 219.

34. He,B.,Tang,Q., and Liang, T. (2014),*J. Mater. Chem. A,* 2, 3119.

Prime graph of non-commutative rings: An investigation of prime graphs and the chromatic number of prime graph of non-commutative rings

D.B.V Kolombage[*] and G.S.Wijesiri

Department of Mathematics, University of Kelaniya, Kelaniya 11600, Sri Lanka

Abstract

Prime graph, $PG(R)$ is a graph associated to a ring R such that in the graph $G(V, E)$, $V = R$ and $E = \{\overline{xy} | xy = 0 \text{ or } yx = 0, \text{ and } x \neq y\}$. The zero divisor graph of the ring R is the simple undirected graph, $\Gamma(R)$, associated to vertices $Z(R)$, the set of zero-divisors of R, and for distinct $x, y \in Z(R)$, the vertices are adjacent if and only if $xy = 0$. In this paper we investigate the characteristics of prime graphs and zero divisors. We have also studied some fundamental results for prime graphs and have found the chromatic numbers of prime graphs of several non-commutative rings using a Mathematical software.

Key words: Prime graphs, prime rings, zero divisor graphs, chromatic number.

1. INTRODUCTION

This paper discusses prime graph of a ring and use Mathematical software to find the chromatic number of prime graph of several non-commutative rings. The paper is divided into four sections. In the section 1, we collect necessary definitions and results from literature. In section 2 we provide the methodology we used to find the chromatic number. In section 3(A) we prove several theorems on zero-divisor graphs and prime graphs. In section 3(B), we discuss the chromatics number of prime graph of non-commutative rings. In the last section we conclude our results and potential future work.

Useful definitions and notations

Definition 1.1.

[*]Corresponding author:Email:bhagyak192@gmail.com

An ordered pair $G = \langle V, E \rangle$ where V, a finite set and $E = \{\{u,v\}|u,v \in V\}$, a set of two elements subsets is called a *graph*. The set V is called the vertex set and the set E is called the edge set.

Note 1.2.
The cardinality (number of elements) of V and E are called *order* and *size* of the graph respectively.

Definition 1.3.
A *walk* is defined as a sequence of alternating vertices and edges. A walk is *closed* if it begins and ends at the same vertex.

Definition 1.4.
A *directed graph* is a graph that is a set of vertices connected by edges, where the edges have a direction associated with them.
An *undirected graph* is one in which edges have no orientation. In an undirected graph the edge (v_1, v_2) is identical to the edge (v_2, v_1).

Definition 1.5.
A *complete graph* is a simple undirected graph in which every pair of distinct vertices is connected by a unique edge. The complete graph on n vertices is denoted by K_n.

Definition 1.6.
A *clique* is defined as a complete sub graph of a graph.

Definition 1.7
The *distance* between two vertices in a graph is the number of edges in a shortest path connecting them. The distance between two vertices x and y is denoted by $d(x, y)$.

Definition 1.8.
The *diameter* of a graph G is the maximum of the distances between pairs of vertices in the graph.

Definition 1.9.
A *proper coloring* of a graph G is an assignment of k colours to the vertices of G such that no two adjacent vertices are assigned the same colour.

Definition 1.10.
The *chromatic number* of a graph G is the minimum value of k for which G has a k colouring.

Definition 1.11.
A *group* $(G, \bullet)$ is a non-empty set G together with an operation $\bullet$ that combines any two elements a and b to form another element, denoted $a \bullet b$ or ab satisfying the following axioms,

- for $\forall x, y \in G, x \bullet y \in G$
- for $\forall x, y, z \in G, x.(y.z) = (x.y).z$
- $\exists e \in G$ such that $\forall x \in G, e \bullet x = x \bullet e = x$
- For each $x \in G, \exists y \in G$ such that $x \bullet y = y \bullet x = e$ where $y = x^{-1}$ and e is the identity element.

Definition1.12.

A *ring*$(R, +, \ .)$ is a set R together with two binary operation $+$ and $.$satisfying the following axioms,

- $(R, +)$ is an abelian group
- for$\forall x, y, z \in R, x.(y.z) = (x.y).z$
- $x.(y + z) = (x.y) + (x.z)and(x + y).z = (x.z) + (y.z)$for $\forall x, y, z \in R$

Note 1.13.

- For simplicity, we have written $x.y$ asxy.
- A ring R is said to be *commutative* if $xy = yx, \ \forall \ x, y \in R$ and if this property does not hold, then such a ring is called a*non-commutative* ring.

Definition 1.14.

A subset $S \subseteq R$ of a ring R is called a *subring* of R if it is itself a ring with the same operations as R.

Definition 1.15.

For a ring R, an additive subgroup $I \subseteq R$ is called an *ideal* of R if for every $r \in R, rI \subseteq I$and $Ir \subseteq I$. The ideal I is said to be *proper*if $I \neq R$.

Definition 1.16.

A ring is said to be a *prime ring* if the product of any pair of ideals is zero only if one of the two ideals is zero.

Definition 1.17.

For a ring R, a nonzero element $r \in R$ is said to be a *zero divisor* if there exists a nonzero $s \in R$ such that $rs = 0$ or $sr = 0$.

Definition 1.18.

The*Prime graph,*$PG(R)$of a ring R for some graph $G(V, E)$ holds the property $V = R$ and $E = \{\overline{xy} | xy = 0 \ or \ yx = 0, and \ x \neq y\}$.

Definition 1.19.

A *field* is defined as a ring whose nonzero elements form an Abelian group under multiplication.

Definition 1.20.

The *zero divisor graph* of the ring R is the simple undirected graph $\Gamma(R)$, associated to vertices $Z(R)$, the set of nonzero zero-divisors of R, and for distinct $x, y \in Z(R)$, the vertices are adjacent if and only if $xy = 0$.

Definition 1.21.

A *quotient ring* is a ring that is the quotient of a ring R and one of its ideals I, denoted byR/I. For example, when the ring R is $\mathbb{Z}$ (the set of integers) and the ideal is $6\mathbb{Z}$ (multiples of 6), the quotient ring is $\mathbb{Z}_6 \cong \mathbb{Z}/6\mathbb{Z}$.

Definition 1.22.

The *adjacency matrix* $A = (a_{ij})_{n \times n}$ of the graph $G(V, E)$ is a square matrix of order n defined by

$$A = (a_{ij}) = \begin{cases} 1 \; ; (i,j) \in E \\ 0 \; ; otherwise \end{cases}$$

2. METHODOLOGY

In this work, we prove several preliminary theorems which represents some characteristics of prime graphs and zero divisor graphs by considering the features of graphs and rings. Then we concentrate on non-commutative rings and we will find the chromatic number of prime graphs of several non-commutative rings. Due to the unpredictable behavior of non-commutative rings, in order to find the chromatic number, we write a programmein computer software to find the adjacent matrix of the ring, which consists of matrices. Then using this adjacent matrix as the input file for another programme, which has been coded to find the chromatic number, we demonstrate the color map of the prime graph associated to its chromatic number. In some cases, for simplicity, we find the chromatic number of the zero divisor graph of a given ring and thus obtain the chromatic number of the relevant prime graph. This is because any vertex representing any element of a ring, which is not a zero divisor, connects only with the zero element in the ring. This allows us to paint the vertex with any colour already used in the map other than the colour used to paint the zero element.

3(A). RESULTS AND DISCUSSION: PRIME GRAPHS AND PRIME RINGS

Lemma-01

If $PG(R)$ is a prime graph and K_n is any complete graph of order n, then K_n is a clique of $PG(R)$ if and only if at least $(n-1)$ elements of $V(K_n)$ are in $Z(R)$.

Proof

Suppose K_n is a clique of (R) .

Then, $V(K_n) \subseteq V(PG(R))$.

$\forall x, y \in V(K_n), xy = 0$ or $yx = 0$ **(1)**

Now, if $0 \in V(K_n), 0 \notin Z(R)$.

Since K_n is of order n, and by equation (1), $(n-1)$ elements of $V(K_n)$ are in $Z(R)$.

If $0 \notin K_n$, by equation (1),

$V(K_n) \subseteq Z(R)$.

As $|V(K_n)| = n$, we have the result.

Suppose that at least $(n-1)$ elements of $V(K_n)$ are in $Z(R)$.

We have $|V(K_n)| = n$.

Since at least $(n-1)$ elements of $V(K_n)$ are in $Z(R)$,

$\exists\ (n-1)$ number of nodes in $Z(R)$.

$\therefore$ there $\exists$ at least a clique of order $(n-1)$ in $PG(R)$.

But $\forall x \in V(K_n),\ 0x$ is an edge in $PG(R)$.

Thus K is a complete graph of order n.

Q.E.D.

Theorem-02

If $A \subseteq Z(R)$, then A is a ring and $PG(A)$ exists if and only if for $A \neq \phi$ and $x, y \in A \Rightarrow x - y,\ xy \in A$.

Proof

We have $A \subseteq Z(R)$.

Since $Z(R) \subseteq R,\ A \subseteq R$.   (1)

Suppose A is a ring and $PG(A)$ exists.

Since A is a ring, conditions $A \neq \emptyset$ and $x, y \in A \Rightarrow x - y,\ xy \in A$ are trivial by the definition of a ring.

In the other way suppose that $\forall x, y \in A \Rightarrow x - y,\ xy \in A$.

Then, A is a group under addition.

Since $xy \in A, \forall x, y \in A, A$ is closed under multiplication.   (2)

Since multiplication is associative in R and by (1), $A \subseteq R$, with the result in (2), multiplication is associative in A.

Again by (1), and since R is a ring, A obeys the distributive laws.

$\therefore A$ is a ring.

$PG(A)$ exists.

Q.E.D.

Theorem-03

For $A \in M_{n \times n}(F)$ where F is a field, A is a zero divisor if and only if $\det(A) = 0$.

Proof

Suppose A is a zero divisor.

Then, $\exists\ B \neq 0 \in M_{n \times n}(F)$ such that $AB = 0$.

$det\ (AB) = 0$,

i.e., $det(A) . det\ (B) = 0$.

Since F is a field, $det(A) = 0$ or $det(B) = 0$.

Assume $det\ (A) \neq 0$.

Then, A^{-1} exists.

$A^{-1}(AB) = 0$ implies $B = 0$, but $B \neq 0$.

$\therefore det(A) = 0$.

Now, in the other way, suppose that $det(A) = 0$.

Then, by linear algebra, $\exists\ \underline{x} \neq \underline{0} \in F^n s.t\ A\underline{x} = \underline{0}$.

Consider $B = [\times \ \times \ \times \ .... \ \times]$, where each column of the matrix denoted by $\times$ is the column vector $\underline{x}$. Thus $B \neq 0$.

Then, $AB = 0$, but $B \neq 0$.

$\therefore A$ is a zero divisor.

Q.E.D.

Theorem-04

$diam\big(M_{n \times n}(F)\big) \geq 2$

Proof

Claim: For any $A, B \in Z\big(M_n(F)\big), AB \neq 0, \exists C \in M_n(F)$ such that $AC = 0$ and $CB = 0$.

Since $A, B \in Z\big(M_n(F)\big)$,

$det(A) = 0$ and $det(B) = 0$.

$\Rightarrow A^{-1}$ does not exist.

Now, apply row operations to get Reduced Row Echelon Form (RREF).

If RREF is I_n, then A is invertible.

But A is not invertible.

Hence, at least one row is entirely zero.

Suppose all entries of the first row in $(E_k \dots E_2 E_1)A$ is all zero, where E_i represents the elementary matrix.

Take $P = E_k \dots E_2 E_1$.

Then, P is invertible.

A^T is also not invertible.

Hence, $\exists Q \ s.t. QA^T$ has all zero in the last row.

$\Rightarrow (QA^T)^T$ has all zero in the last column.

$\Rightarrow AQ^T$ has all zero in the last column.

Hence, for any $A, B \in Z\big(M_n(F)\big)$, there exist invertible matrices P and Q such that AP has all zero in the last column and QB has first row all zero.

Let, $C = P \begin{pmatrix} 0 & 0 \cdots 0 & 0 \\ \vdots & \ddots & \vdots \\ 1 & 0 \dots 0 & 0 \end{pmatrix} Q$.

Then, $AC = AP \begin{pmatrix} 0 & 0 \cdots 0 & 0 \\ \vdots & \ddots & \vdots \\ 1 & 0 \dots 0 & 0 \end{pmatrix} Q = 0$.

Similarly,

$CB = P \begin{pmatrix} 0 & 0 \cdots 0 & 0 \\ \vdots & \ddots & \vdots \\ 1 & 0 \dots 0 & 0 \end{pmatrix} QB = 0$.

Therefore, $\exists C \ s.t. AC = 0$ and $CB = 0$.

$\Rightarrow d(A, B) = 2$.

$diam\big(M_n(F)\big) \geq 2$.

Q.E.D.

Corollary-05

If $M_{n \times n}(F)$ is a prime ring, $det(A) \neq 0$ for

$A \neq 0$ where $A \in M_{n \times n}(F)$. $diam(PG(R)) = 2$ where $R = M_{n \times n}(F)$ for nonzero vertices of R with

$|R| > 2$.

Proof

The first part is obvious by definition of a prime ring.

For second part, suppose that A and B are two non-zero distinct vertices.

Now, if $d(A, B) = 1$, $AB = 0$.

This is a contradiction.

$\therefore d(A, B) \neq 1$.

Since $d(A, 0) = 1$, $d(0, B) = 1$ and by the fact that $M_{n \times n}(F)$ is a prime ring, $d(A, B) = 2$.

As this is the case for all nonzero vertices in a prime ring, and by definition of diameter, $diam\left(PG(M_{n \times n}(F))\right) = 2$.

Q.E.D.

Corollary-06

The following statements are equivalent.

(i). $R = M_{n \times n}(F)$ is not a prime ring.

(ii).   There exists at least one clique of order 3 in $PG(M_{n \times n}(F))$.

(iii).   There exists $A, C \in M_{n \times n}(F)$ s.t. the length of the walk from A to C is greater than two.

Proof

(i) $\Rightarrow$ (ii):

Suppose that R is not a prime ring.

Then, $\exists A, B \in M_{n \times n}(F)$ s.t. $A \neq B \neq 0$ and $AB = 0$.

$\Rightarrow d(A, B) = 1$.

Since $d(A, 0) = 1$ and $d(0, B) = 1$, $A0B$ forms a triangle.

$\Rightarrow \exists$ a clique of order 3.

(i) $\Rightarrow$ (iii):

Suppose R is not a prime ring.

Then for $A, B \in R$ with $A \neq B \neq 0$, $d(A, B) = 1$.

$\Rightarrow \exists$ a triangle.

Now let $C \in R$ s.t. $C \neq A$ or $C \neq B$ and $C \neq 0$.

Then, $d(0, C) = 1$.

Now, $\exists$ a path $A \to B \to 0 \to C$ which is,

$d(A, B) + d(B, 0) + d(0, C) = 1 + 1 + 1 = 3$.

But, if a walk is considered from A to C, $\exists$ a walk of length ≥ 3.

(ii) $\Rightarrow$ (iii):

Let $\exists$ at least one clique of order 3 in $PG(M_{n \times n}(F))$.

Since $\exists$ a clique of order 3,

$\exists A, B \ s.t. A \neq B \neq 0$ with $d(A, B) = 1$.

This is $d(A, B) + d(B, 0) + d(0, A) = 3$.

This is a closed walk of length 3.

Now if $\exists C \in R \ s.t. C \neq 0$,

then $\exists$ a walk from $A \rightarrow C$ with the length ≥ 3.

(ii) $\Rightarrow$(i):

Suppose there exists at least one clique of order 3 in $PG\big(M_{n \times n}(F)\big)$.

By definition of a clique, there exists a triangle.

$\Rightarrow \exists A, B \in R \ s.t. A \neq B \neq 0$ but $d(A, B) = 1$.

$\Rightarrow AB = 0, A \neq B \neq 0$.

$\Rightarrow R$ is not a prime ring.

(iii) $\Rightarrow$(ii):

$\exists A, C \in R$ such that the length of the walk from $A \rightarrow C \geq 3$.

If $\{A, C, 0\} = V(R)$,

then, the maximum length from $A \rightarrow C = 2$.

$\Rightarrow \exists$ at least one element different from $A, C,$ and 0.

Now take $B \in M_{n \times n}(F)$.

If $d(A, B) \neq 1$ or $d(B, C) \neq 1$,

then, the maximum length from $A \rightarrow C = 2$.

But if $d(A, B) = 1$ or $d(B, C) \neq 1$.

then $\exists$ a triangle.

$\Rightarrow$ there exists a clique of order 3.

(iii) $\Rightarrow$(i):

Since $3 \leftrightarrow 2 \leftrightarrow 1$, we have $3 \rightarrow 1$.

Q.E.D

3 (B). RESULTS AND DISCUSSION: CHROMATIC NUMBER

Consider the ring of upper triangular 2×2 matrices over $\mathbb{Z}/3\mathbb{Z}$. Then, the prime graph of the ring is as in Figure 1 whereas Figure 2 represents its corresponding colour map.
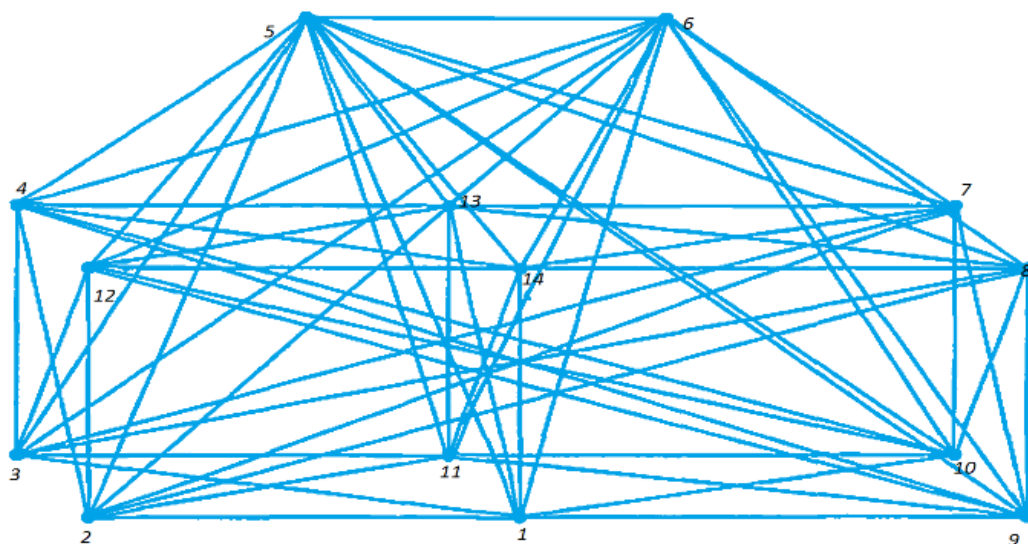
Figure1:$\Gamma(R)$ *where* $R = \left\{ \begin{bmatrix} a & b \\ 0 & c \end{bmatrix} \mid a, b, c \in \mathbb{Z}_3 \right\}$

The chromatic number of $\Gamma(R)$ is six.

In *Figure 2*, we have numbered each node with similar colours with the same number for the recognition. Since we have found the chromatic number of zero divisor graph, and as we know that all the vertices in the ring adjoin with the vertex representing zero matrix, the chromatic number should be increased by one. Therefore, the chromatic number of $PG(R)$ where $R = \left\{ \begin{bmatrix} a & b \\ 0 & c \end{bmatrix} \mid a, b, c \in \mathbb{Z}_3 \right\}$ is seven.
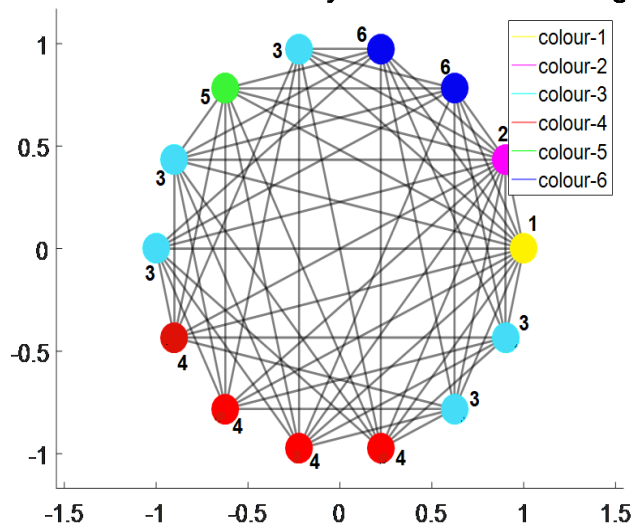
Figure 2 :*Color map of* $\Gamma(R)$

Table 1 represents few more prime graphs and their corresponding chromatic numbers.

Prime Graph	Chromatic Number
$PG(R)$, where $R = \left\{ \begin{bmatrix} a & b \\ 0 & c \end{bmatrix} \mid a, b, c \in \mathbb{Z}_2 \right\}$	4
$\Gamma_0(R \times M_2(\mathbb{Z}_2))$, where $R = \left\{ \begin{bmatrix} a & b \\ 0 & c \end{bmatrix} \mid a, b, c \in \mathbb{Z}_2 \right\}$	5
$PG(R)$ where $R = \left\{ \begin{bmatrix} a & b \\ 0 & c \end{bmatrix} \mid a, b, c \in \mathbb{Z}_3 \right\}$	7
$PG(M_{2 \times 2}(\mathbb{Z}_2))$	5
$PG(R)$ where $R = \left\{ \begin{bmatrix} a & b \\ 0 & 0 \end{bmatrix} \mid a, b \in \mathbb{Z}_2 \right\}$	3
$PG(R)$ where $R = \left\{ \begin{bmatrix} a & b \\ 0 & 0 \end{bmatrix} \mid a \in \mathbb{Z}_4, b \in 2\mathbb{Z}_4 \right\}$	4
$PG(R)$ where $R = \left\{ \begin{bmatrix} a & b \\ 0 & 0 \end{bmatrix} \mid a \in 2\mathbb{Z}_4, b \in \mathbb{Z}_4 \right\}$	7

Table 1: Prime graphs and their chromatic numbers

4. CONCLUSION

With the above results we have expanded the limits of our knowledge on prime graphs of non-commutative rings and have discussed the chromatic number of several cases. This study can be carried out for matrices with higher dimensions. The study can also carried out for rings of matrices containing decimal values as elements.

REFERENCES

1.   Satyanarayana, B., Prasad, K. S., and Nagaraju, D. (2010). Prime graph of a ring. *Journal of Combinatorics, Information and System Sources,35*(1), 27-42.

2.   Patra, K., and Kalita, S. (2014). Prime graph of the commutative ring Zn. *MATEMATIKA,30*(1), 59-67.

3.   Redmond, S. P. (2001). *Generalizations of the zero-divisor graph of a ring* (Unpublished Doctoral Dissertations).

4.   Anderson, D.D. and Naser, M. (1993). Beck's Coloring of a Commutative Ring,*Journal of Algebra* (159), 500-514.

5.   Anderson, D.F.,and Livingston, P.S. (1999). The Zero-Divisor Graph of a Commutative Ring, *J. Algebra* (217) 434-447.

6.   Akbari S., and Mohammadian A.(2006) Zero-divisor graphs of non-commutative rings, *Journal of Algebra* (296), 462–479.

7.	Kolombage, K.A.D.D.B.V., and Wijesiri G.S, (2016) Investigation of characteristics of prime graph of a ring. (Unpublished Undergraduate Dissertation).

Effects of the polymethine chain length on the spectral response of dye sensitized devices

P.K.D.D.P. Pitigala,[a, b.c ,*] M. M Henary,[d] and A.G.U. Perera[c]

[a]Department of Physics, University of Sri Jayawardenepura, Gangodavila

[b] Center for Advanced Material Research, University of Sri Jayawardenepura, Gangodavila

[c]Department of Physics and Astronomy, Georgia State University, Atlanta GA, USA.

[d]Department of Chemistry, Georgia State University, Atlanta GA, USA.

Abstract

In a dye sensitized (DS) devices, the working principle is based on the excitation and injection of electrons in the dye molecules. Due to the narrower spectral response of the dyes used as the sensitizer in the DS devices, the efficiency of the DS solar cells remains low, which is a major drawback in popularizing and commercializing DS solar cells. Therefore, the study of spectral response broadening methods applicable to DS devices is vital. In general, when synthesizing novel dyes, long carbon chains have been used to absorbed infrared radiation. In this study, cyanine dye molecules containing carbon chains of different chain lengths were used to observe the variations in the spectral response of the DS structures. Four cyanine dye derivatives, with different carbon ligands were investigated under the configuration, n-D-p structure. TiO_2 was used as the n-type semiconductor, and the CuSCN was used as the p-type semiconductor, representing the n and p in the above configuration respectively. The device sensitized with the dye containing the longest central polymethine chain have shown a red shift in the spectral response threshold, extending up to ~900 nm. Additionally, the other dye molecules with shorter carbon ligands have a lesser extension in the spectral response.

Keywords: *Cyanine, dye-sensitized, polymethine, spectral response*
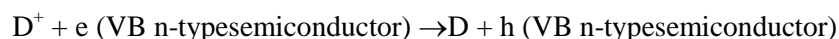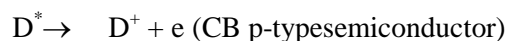
1. INTRODUCTION

The importance of developing novel highly efficient renewable energy conversion devices is obvious due to the ever increasing demand for energy, and safety issues, environmentally unfriendly operation, and the limited availability of widely utilized energy resources. Development of solid/quasi-solid state dye sensitised solar cells (DSSCs) based on nano-crystalline semiconductors is important due to their low

---

production cost. It is equally important to identify and understand the possible effects of different ligands attached to the dyes on the performance of the device in order to implement modifications to enhance the device performance.

Extensive work has been conducted in the area of dye-sensitization introducing original solar cell and photon detector device concepts. Dye-sensitized (DS) and bulk heterojunction (BHJ) solar cells, organic light emitting diode (OLED) and organic field effect transistors (OFET) are the prototype organic electronic devices that greatly encourage further research in the area of organic optoelectronics [1-3]. The main difference between the dye sensitized solar cell and p-n junction solar cells is in the photon energy absorber. In p-n junction solar cells, photon energy is absorbed directly by the semiconductor at the junction, but in dye sensitized solar cells, the light is absorbed by the dye chromospheres and the electron-hole pair is generated in the dye molecule. In a DS solar cell, the excited dye molecules, anchored to a high-band gap semiconductor surface, inject carriers to an energy band, thereby separating charges and driving a current in an external circuit [4]. The whole electron transfer process of the DSSC heterojunction structure can be summarized by the following three reactions, where the excited dye molecule is denoted as D^*.

$$h\nu + D \rightarrow D^*$$

$$D^* \rightarrow D^+ + e \text{ (CB p-typesemiconductor)}$$

$$D^+ + e \text{ (VB n-typesemiconductor)} \rightarrow D + h \text{ (VB n-typesemiconductor)}$$

Similarly, the operative principle of BHJ solar cell is based on decomposition of photo-generated excitons at an interface between donor (p-type) and acceptor (n-type) phases, and transfer of separated carriers to the electrodes along percolative paths [2-4]. Although many technical hurdles were initially encountered in fabrication of stable cells, the efficiency of DS solar cells still remains well below that of the silicon cell. One reason for lower efficiency results from the narrower spectral response of DS solar cells compared to that of the silicon cell. Different alterations such as the use of multiple dye layers and other modifications to support strong bonding to the semiconductor have been introduced into the dye molecules, in order to extend the spectral response of the DS solar cell [5-8]. Another factor affecting the efficiencies is the rate of injection of the carriers to the bands of the semiconductor and the slow back reaction. Strong electronic coupling of the dye molecule onto the semiconductor surface can cause fast and efficient injectionof carriers.

This paper discusses the effects on the spectral response of four different newly synthesized cyanine dyes, having different carbon chain lengths and different ligands.

2.METHODOLOGY

A schematic of the typical layered structure of a DSSC is shown in tFigure 1. Here a thin film of TiO_2 was grown on a fluorine doped tin-oxide (FTO) coated glass. The TiO_2 (1×1 cm^2) films were deposited on the FTO glass plates (1×1.5 cm^2) by hydrolysis of titanium isopropoxide (5 ml) in the mixture of 75% propan-2-ol (15 ml) and acetic acid (5 ml) to form a colloidal TiO_2 suspension. The hydrolyzed product is mixed with Degussa P25 TiO_2 powder and the viscous slurry formed was spread over the FTO plate. The plate is heated to 120 °C for 10 min and after blowing off the loose crust of TiO_2 particles not

73

adhered to the FTO surface, film is sintered at 425 °C for 10 min. By repetition of the process, TiO$_2$ film has been grown to a desired thickness of ~8 ▯ m.
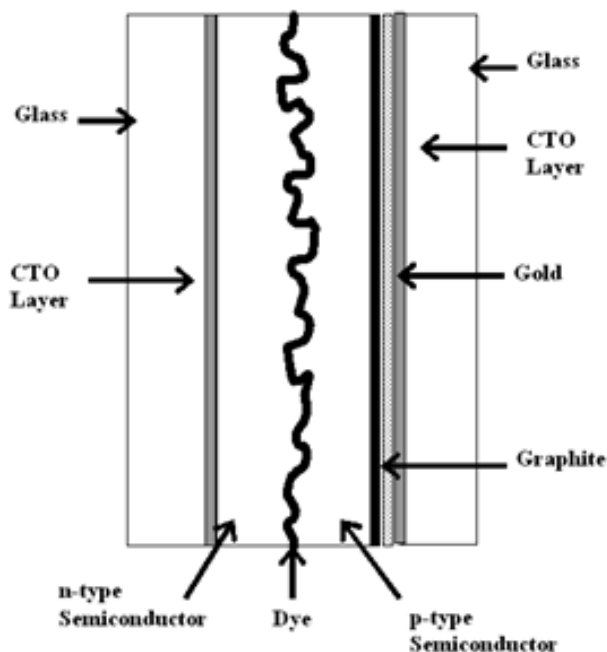

Figure 1: Schematic diagram illustrating the cross section of Dye sensitized photovoltaic cell of heterostructure configuration of n-type semiconductor / Dye / p-type semiconductor.

Newly synthesized cyanine dyes named QBN1, T-23, ES-21 and SP-2-56 were coated on the TiO$_2$ electrodes. The structure of the dye molecules that were studied are shown in Fig.2. These dyes were separately coated over the TiO$_2$ films after thoroughly cleaning the TiO$_2$ films with alkaline 50% propan-2-ol followed by water and 99% propan-2-ol and then drying at 120 °C. Then a dried plate is positioned vertically at the bottom of a glass tube and immersed in the dye solution (in 90% ethanol) at a constant temperature (20°C) for 24 hrs to adsorb and form the dye layer. In general a monolayer of dye will be attached on the TiO$_2$ film.

The film is then dried in air at ambient temperature and a thin layer of p-CuSCN is deposited over the dye coated surface from a solution in n-propyl sulfide, by keeping the dye coated TiO$_2$ sample on top of a hot-plate at ~120 °C. A layer of graphite is painted over the CuSCN surface to improves the back contact. And the back electrode is formed by pressing a FTO glass plate to secure the external electrical contacts.

The thickness of the dye film was estimated by extracting the dye molecules from sample films and spectrophotometric estimating of the dye content. Briefly, the process first generated a set of calibration data using known concentrations of the dye solutions and measuring the relative absorbance. Then the dye molecules on the TiO$_2$ film were stripped off the film by dipping the dye coated TiO$_2$ film in a dilute KOH solution. Then the absorbance of this solution is measured and the concentration estimated by interpolating or extrapolating the calibration date. Using the estimated concentration of the extracted dye molecules, the number of dye molecules are estimated. Using the estimated area of the dye molecule and

the effective surface area of the TiO_2 film (500×projection area) the thicknesses of the dye layers were estimated to be about one monolayer (0.8 - 1.1 monolayers).

—

Figure 2. Structures of the dye formula QBN1, T-23, ES-21 and SP-2-56

The I-V characteristics of the cells were recorded using a KETHLY 2400 source meter under a 1000 W/m^2 light source and a monochromator set-up coupled with the KETHLY 2400 was used to measure the photocurrent action spectra of each device.

3.RESULTS AND DISCUSSION

The normalized spectral response of the dyes are shown in Fig.3. The QBN-1, with the longest polymethine chain, hasa response threshold extending to ~900 nm; the SP2-56 hasthe next longest threshold at ~850 nm, and the threshold of the other two dyes, the ES-21 and T-23, are around 750 nm and 760 nm respectively. It is interesting to note that, both the ES-21 and T-23 have the same number of carbon atoms in the central polymethine chain,*i.e*., an equal polymethine chain length. But the T-23 has a CH_3 ligand attached on the pyrrolidinium ring, while the ES-23 has a CH_3CH_2ligand which is longer. The extra length in this ligand has resulted in the red shift observed in the response spectra, at peak maxima and at the threshold, as can be observed in Fig 3. Again the SP-2-56 has a much longer ligand $((CH_3)_2N(CH_2)_3)$ compared to the ES-21 and T-23, hence the response spectra is further red shifted in SP-2-56 compared to the other two. In contrast the QBN-1 has the longest center polymethine chain out of the four dyes, and it has the longest red shift in the spectral response. Even though the other ligands attachedto the dye molecule can influence the shifts observed in the spectral response, these results imply the dominance of the polymethine chain length in extending the spectral response.
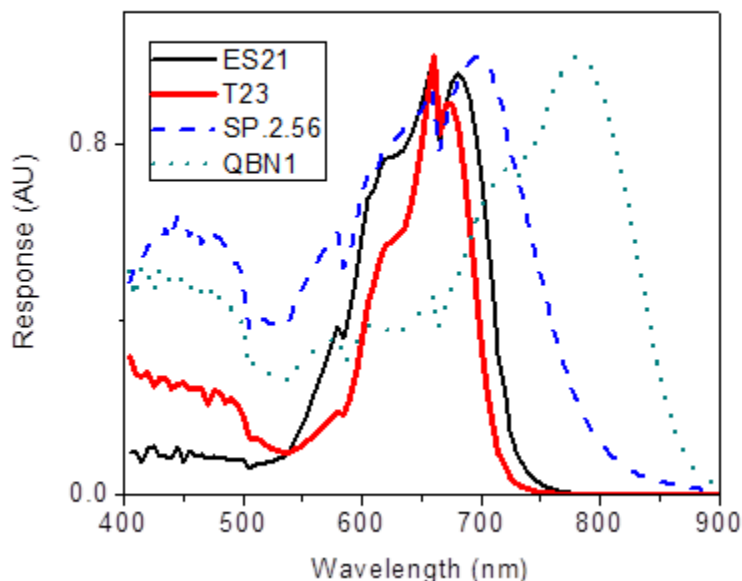
Figure3 Normalized spectral responses (given in arbitrary Units) of theTiO$_2$/Dye/CuSCNheterojunction configuration structures coated with the dyes QBN1, T-23, ES-21 and SP-2-56.

The I-V characteristics of the devices are shown in Fig 4. Here the device sensitized with QBN-1 has the highest short-circuit photocurrent and ES 21, T-23 and SP2-56 have their short-circuit currents decreasing in the given order. Here, no clear relation between the polymethine chain length and the short-circuit photocurrent was found. Clearly the chain length does not show a major influence on the photocurrent, similar to the way it affects the broadening or red shifting of the spectral response or response threshold. The differences in the photocurrent of the devices are due to a combined effect of the additional ligands attached to the dye molecule, but not the sole effect of the polymethine chain length itself on carrier injection rate. It can be concluded that the T-23, with two highly electronegative fluorine atoms attached, has a lower photocurrent compared to the ES-21. The electron affinity of the other ligands attached to the dye molecule can affect the charge injection rate as well as the strength of the chelation between the dye and the semiconductor surface, which has affected the total photocurrent of the device. It was not clear which effect had the most influence in limiting the carrier transitions, affecting the photocurrent of the device.

In contrast, the open-circuit voltage (V$_{OC}$) shows a dependence on the polymethine chain length, as can be seen in Fig. 4. The polymethine chain length of ES-21 and T-23 are similar, so is the open circuit voltage. QBN-1 hasthe lengthiest polymethine chain length and also the lowest V$_{oc}$. But the electron affinity of the other ligands attached to the molecule has also affected the V$_{oc}$ of each device; hence SP2-56 has the lowest V$_{oc}$ in the three dyes with the same polymethine chain length.
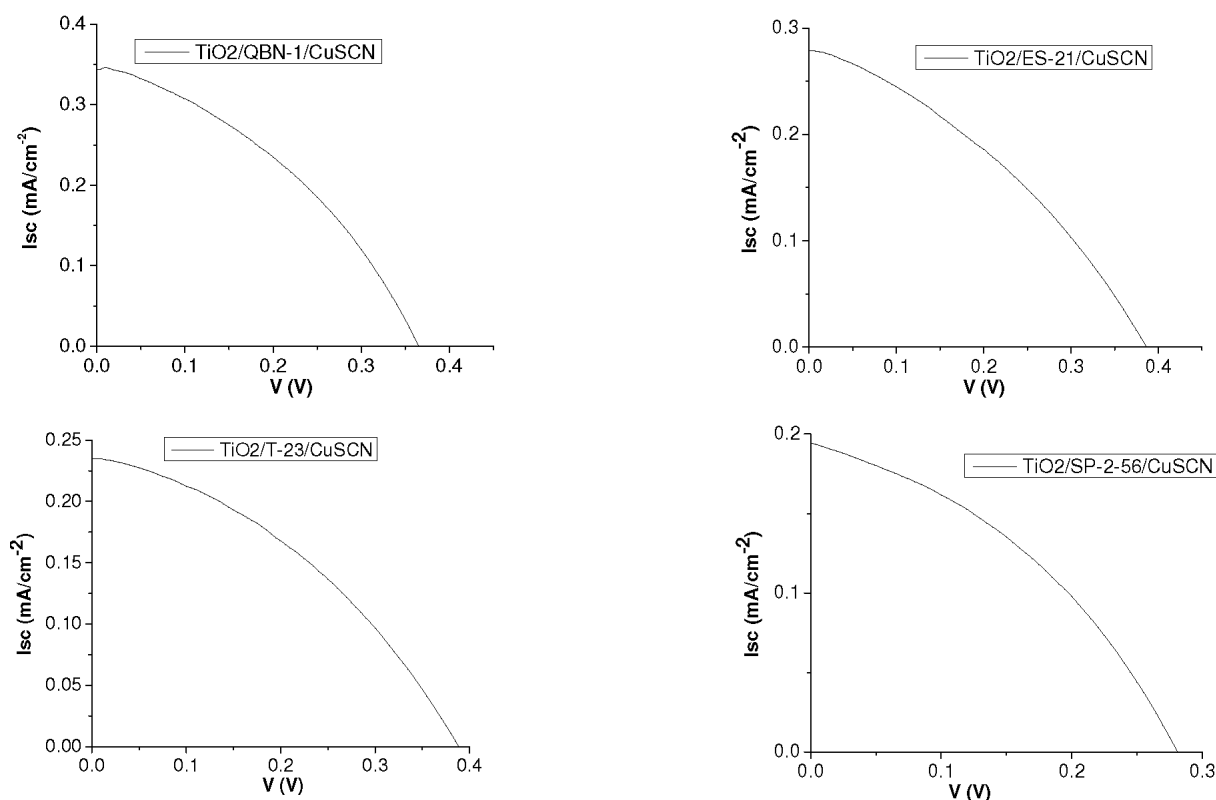
Figure 4. I-V characteristics of theTiO$_2$/Dye/CuSCNheterojubction configuration structures coated with the dyes QBN1, T-23, ES-21 and SP-2-56.

The effects of electron affinity of the other ligands are not within the scope of this paper, and additional exclusive theoretical and experimental work are needed to combine the effects of the other ligands and justify the effect of these ligands, in the molecules, on the photocurrent and the voltage of the dye sensitized devices. Current results on response broadening and shifting can also be further refined by excluding the additional effects.

4. CONCLUSION

The result shows the effects of the carbon chain lengths in cyanine dye molecules on the spectral response when the dye is used as the sensitizer in the DS device. In the cyanine dyes, the length of the centralpolymethine chain is more critical in the process of extending the spectral response into the infrared region. Furthermore, the length of the other carbonic ligands attached to the cyclic structures, is also contributing to the broadening of the spectral response of the DS devices and longer ligands have shown a greater red-shift in spectral response. The direct effects of the chain length on the photocurrent and the voltage were inconclusive due to the combined effects of the other legends in the system.

ACKNOWLEDGEMENTS

REFERENCES

1. Aswal, D.K., Yakami, V., Eds. (2010). *Molecular and Organic Electronics*, Nova Publishers, New York.
2. Franky, S., (2010). Organic Electronics: *Materials, processing, devices and applications*, CRC Press, New York.
3. Brabec, C.J., Dyakonov, V., Paris, J., Saricifti, N.S., (2003). *Organic Photovoltaics: Concepts and Realization*, Springer, Heidelberg.
4. Regan, B.O., Gratzel, M., (1991) A low cost and high-efficiency solar cell based on colloidal TiO_2 films.*Nature* **353** 737-740.
5. Senevirathne, M. K. I.,Pitigala, P. K. D. D. P., Sivakumar, V., Jayaweera, P. V. V.,Perera, A. G. U., and Tennakone, K. (2008) Sensitization of TiO_2 and ZnOnanocrystallinelms with acriflavine. *J. Photochem. Photobiol. A-Chem*., **Vol. 195**, 364.
6. Seneviratne, M., Pitigala, P., and Tennakone, K. (2005) Chromophore linked conducting polymers attached to semiconductor surfaces: A strategy for development dye sensitized solar cells.*J. Phys. Chem. B*, **109** 16033.
7. Jayaweera, P. V. V.,Perera, A. G. U.,and Tennakone, K. (2008) Whygratzel cell works so well. *Inorg. Chim. Acta,***361**, 707.
8. Perera, V. P. S.,Pitigala, P. K. D. D. P.,Jayaweera, P. V. V.,Bandaranayake, K. M. P.,and Tennakone, K. (2003) Dye-sensitized solid-state photovoltaic cells based on dye multilayer-semiconductor nanostructures. *The Journal of Physical Chemistry* B, **107**, 13758.

I. GENERAL INSTRUCTIONS

1) Research presented in the manuscript could be in any field of science. 2) The research work should not have been published or submitted for publication elsewhere. 3) A corresponding author who will be responsible for all communications with the SLAAS Office should be identified. 4) Submission of manuscripts: Manuscripts can be submitted by e-mail or regular mail to the Editor – SLAAS on or before 31st July, 2018. In case of submissions made through regular mail, The authors should forward three (03) hard copies of the manuscript and an electronic copy on a compact disc (CD) along with all other required documents. Authors are advised to mail the documents at least three (03) weeks prior to the deadline. 5) Certificate of authenticity: Declaration form attached hereto should be duly filled, signed by all authors and sent along with the manuscript. The authors who transfer the documents electronically should send the Certificate of Authenticity by regular mail. 6) Information of corresponding author: Duly filled form should be sent by regular mail. 7) Submissions that involve human or animal trials should provide evidence of approval obtained by an ethics review committee.

II. SPECIFIC INSTRUCTIONS TO AUTHORS

1. Documentto be submitted ! Manuscript in MS Word (2003 or 2007 for Windows or later)format. ! A compact disk (CD) containing an electronic copy of the manuscript (for submissions by regular mail only). ! Duly filled and signed 'Certificate of Authenticity' form. ! Duly filled 'Information of Corresponding Author' form.

2. Format for typesetting
   - Paper size: A4 (210 x 297) typed single sided only.
   - Margins: Top, bottom and right margins of 25 mm and a left margin of 30 mm. 2
   - Line spacing: 1.5 (18 points) throughout the text.
   - Length: Length of the manuscript including text, tables, figures and references should not exceed I5 typed pages.
   - Page and line numbering: All pages should be sequentially numbered using Arabic Numbers. All lines should also be numbered sequentially starting from the top to the bottom of each page.
   - Font: Arial font, size 12. ! Language/spelling: UK English only.
   - Software: Authors may use either MS Word 2003 or 2007/2011 for Windows or the Macintosh equivalent.
3. Title Page: Title page should include the following Information;
   - Title and running title (less than 25 Characters). They should be in bold faced letters
   - Name/s and affiliation/s of author/s
   - Email address, mailing address and contact numbers of the corresponding author. Note: Identified the corresponding author by placing an asterisk after the name.
4. Abstract
   Should be limited to a maximum of 250 words.
   Up to a maximum of the five (05) key word should be identified, arranged in alphabetical order, included immediately after the abstract.
   Abstract should be typed in italics. Scientific names in the abstract should be underlined.

No reference, tables, or figures should be included in the abstract.

5. Body
   - Introduction: Justification of the research work, objectives and hypotheses should be included in the introduction.
   - Methods and Materials/ Methodology: All materials, chemicals, clinical, subjects and samples used should be identified. Analytical, survey and statistical method should be explained concisely. Common analytical methods need not be elaborated.
   - Results and Discussion: Can be combined.
   - Conclusions: Should be concise.
   - Headings: All headings should be in bold capital and centered, e.g., INTRODUCTION
   - Subheadings: All subheadings should be in bold and in title case, e.g., Preparation of Land.
   - Non-English terms: All non-English terms should be italicized, e.g., et al., i.e., viz., except "etc."
   - References: Use APA style 3
6. Table and Figures
   - Should be included in the exact place within the text
   - Tables should be numbered sequentially using Arabic numerals. The titles should be selfexplanatory and placed above the tables.
   - Tabled should not contain any vertical lines
   - Illustration, Line drawing and photographs, if any, should be clear, properly numbered and captioned and ready for reproduction. They should be of high and resolution such as minimum of 300 dpi and saved in .tif or .bmp formats. Please do not use .jpeg or similar formats that do not reproduce well.
   - All lettering, graph lines and points on graphs should be sufficiently large and bold faced to permit reproduction for inclusion in the Journal.
   - Artworks and illustrations should be of appropriate thickness. Please note that thin lines do not reproduce well. Please note that the illustrations, line drawings and photographs should be placed in the appropriate location of the electronic file and numbered sequence with other figures.
7. Units
   - SI units should be used.
   - A single space should be left between the numerical value and the unit.
8. Acronyms and Abbreviations
   - All acronyms should be written in full at the first time of appearance. Abbreviations can be used subsequently.
   - The full stop should not be included in abbreviations. Where abbreviations are likely to cause ambiguity or may not be readily understood by readers, the units should be mentioned in full.
9. On being informed of the acceptance, the manuscripts should be revised as per the reviewers' suggestions and re-submitted to the Editor – SLAAS. The accepted manuscripts will be published in the inaugural Journal of the SLAAS. Manuscripts that do not confirm to the above guidelines will not be accepted.
10. Acknowledgements Only the essential individuals and/or organizations/institutes should be included.

Journal of the Sri Lanka Association for the Advancement of Science

Volume 1

Contents

Research Articles

9771391025002